

DEVELOPMENT OF MODELS TO ESTIMATE EMI FROM
SWITCHED-MODE POWER SUPPLY

Part II/II

by

Gian Lorenzo Giuliattini Burbui

A DISSERTATION

Presented to the

UNIVERSITY OF BOLOGNA

In Partial Fulfillment of the Requirements for the Degree

DOCTOR OF PHILOSOPHY

in

ELECTRICAL ENGINEERING

2006

Copyright 2006
Gian Lorenzo Giuliani Burbui
All Rights Reserved

ABSTRACT

This dissertation describes algorithms and techniques developed at the University of Bologna to estimate radiated EMI from Switched-Mode Power Supply (SMPS) .

The first chapter presents some basic ideas when dealing with radiated EMI from SMPS and briefly describes the principal sources of EMI.

The second chapter describes the theory, the construction and calibration of an optically-linked triple loop antenna system (TLS) to measure electric and magnetic field from SMPS. The TLA has been built and calibrated in the EMC laboratory of the University of Bologna. The TLS is used as reference receiver and to validate the proposed model.

The third chapter presents a resistance-inductance-capacitance (RLC) model for estimating current waveforms in digital CMOS circuits. The model is based on parameters that are readily derived from information available in board layout files and component data sheets or IBIS files. Compared with the simpler triangular waveform traditionally used to approximate current in CMOS circuits, the RLC model more accurately estimates the shape of the current waveform in the time domain and the amplitudes of the upper harmonics in the frequency domain. This chapter has been developed in collaboration with Dr. Todd H. Hubing and Yan Fu at the University of Missouri-Rolla and submitted for publication to IEEE Tansaction on Electromagnetic Compatibility.

The fourth chapter describes an algorithm based on analytical formulas to estimate radiated EMI from SMPS. The model is based on parameters that are readily derived from information available in board layout files, component data sheets and geometry dimensions. The EMI voltage and current noise sources are described by simple models: the trapezoidal waveform model and the RLC model presented in the previous chapter. The electric and magnetic coupling mechanisms between the sources and the victim are described by equivalent circuits. Their validation is pursued by using the TLS.

The last chapter describes the application of the proposed model to a commercial SMPS for personal computer. The proposed model shows a very good agreement with measurements.

ACKNOWLEDGMENTS

I would like to express my sincere gratitude to Prof. Ing. Ugo Reggiani my graduate advisor, for valuable discussions and direction during my pursuit of Ph.D. degree at University of Bologna. I learned most aspects of doing research activity, presenting and publishing my work from my advisor. I would also like to thank to Dr. Leonardo Sandrolini for his helpful discussions and instructions. Special thanks to Dr. Todd H. Hubing for his teaching in classes and beneficial discussions regarding research activity at the University of Missouri-Rolla. It is a pleasure to acknowledge all the students in the UMR-EMC lab, Andrea Albertini technicians of the University of Bologna for their support and teamwork.

I am most appreciative to my wife Costanza for supporting me these three years and especially during the period I spent at the University of Missouri-Rolla.

Equation Chapter 4 Section 1 Chapter 4

Proposed model to estimate electric and magnetic fields from Switched-Mode Power Supplies

I. Noise voltage sources

Typical voltage source of electric/electronic system are trapezoidal periodic waveforms and for the aim of this model some of the parameter need to be known.

A rigorous Fourier computation can be performed to sort out the frequency spectrum of the voltage and current waveform [1]. For EMC aims, the Fourier envelope method can be simply used for voltages and current requiring only some parameters. The Fourier envelope is the locus of the maximum harmonics without considering their phase. For a trapezoidal voltage waveform the following parameters must be known:

1. the peak amplitude A
2. the pulse width τ
3. the period of the signal T
4. the rise time t_r at 10% to 90% crossings. If fall and rise times are different, select the shortest of the two as t_r .

The typical trapezoidal waveform and its spectrum envelope are shown in Figs.1,2.

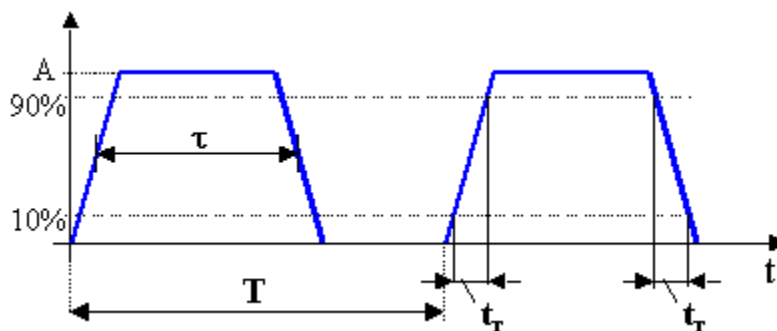


Fig. 1 Trapezoidal waveform and its parameters.

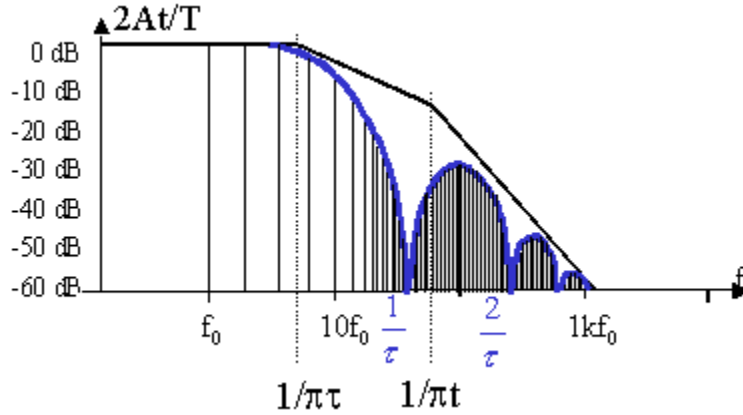


Fig. 2 Fourier envelope for narrowband spectral amplitude trapezoidal pulse train.

Besides the fundamental frequency $1/T$, the two key frequency in constructing the envelope are F_1 and F_2 :

$$F_1 = \frac{1}{\pi\tau} \text{ and } F_2 = \frac{1}{\pi t_r}.$$

Above F_1 the spectrum envelope roll off with -20 dB/decade while above F_2 decreases abruptly with -40 dB/decade. Once the envelope is drawn, the worst case amplitude of any harmonic can be found.

There is a deep relationship between the n-continuity of a waveform in $t=0^+$ and the spectrum behaviour when $f \rightarrow \infty$ described by Theorem of initial value for Laplace transform [2]. For ideal trapezoidal waveform this predict the spectrum rolling off at -40 dB/decade. Due to the continuity of derivates in $t=0^+$ of actual waveform, this theorem predict the spectrum rolling off more than -40 dB/decade. Depending on the symmetry of the waveforms even or odd harmonic can take place.

If the duty cycle of the voltage waveforms is not exactly 50%, even harmonics will take place. Although their level is lower than the odd ones, their amplitude is constant when f increases up to the maximum spectral envelope, and then they roll off at -40 dB/decade like the odd terms.

The voltage spectrum of trapezoidal waveforms with different duty cycle and rise time is shown in Figs.3-4.

The Fourier spectrum can be simply calculated using

$$V(f) = \frac{2A\tau}{T} \left| \frac{\sin(\pi f \tau)}{\pi f \tau} \right| \left| \frac{\sin(\pi f t_r)}{\pi f t_r} \right| \quad [\text{V}] \quad (1.1)$$

Beside the fundamental frequency $1/T$, the envelope of the spectrum can be drawn using the following points in spectral density/frequency plot:

$$(F_{min}; 2A\tau), (F_1 = \frac{1}{\pi\tau}; 2A\tau), (F_2 = \frac{1}{\pi t_r}; 2At_r), (F_3 = \frac{10}{\pi t_r}; 2At_r/100) \quad (1.2)$$

respectively corresponding to the minimum frequency to be visualized, the first corner frequency, the second corner frequency, and the maximum frequency to be visualized. Some example of the envelope of the spectrum for different duty cycle and rise time are presented in Figs.5-7.

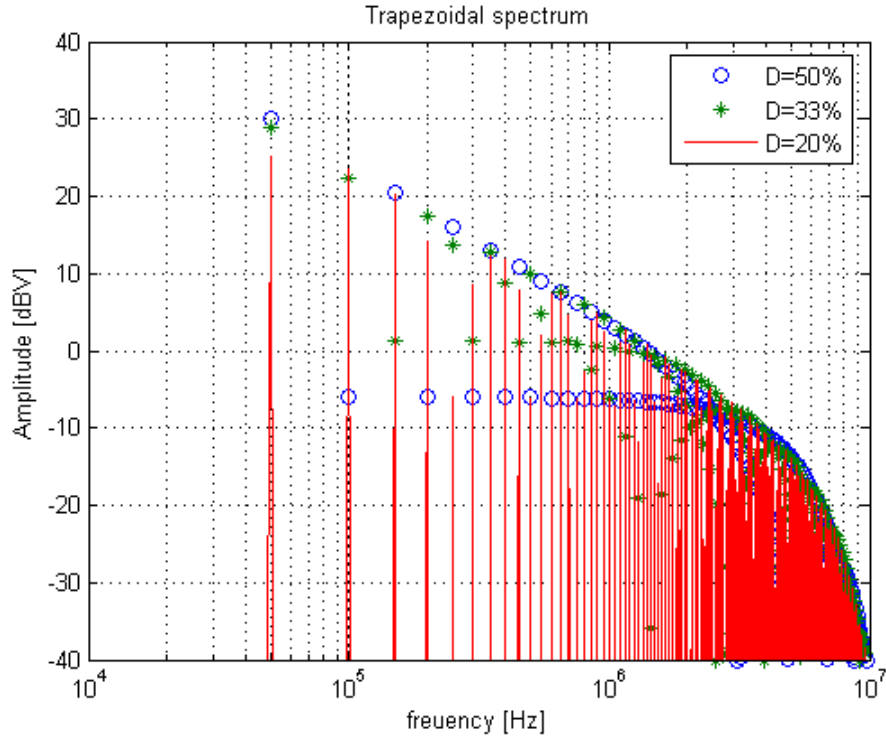


Fig. 3 Voltage spectrum of trapezoidal waveform with different duty cycle.

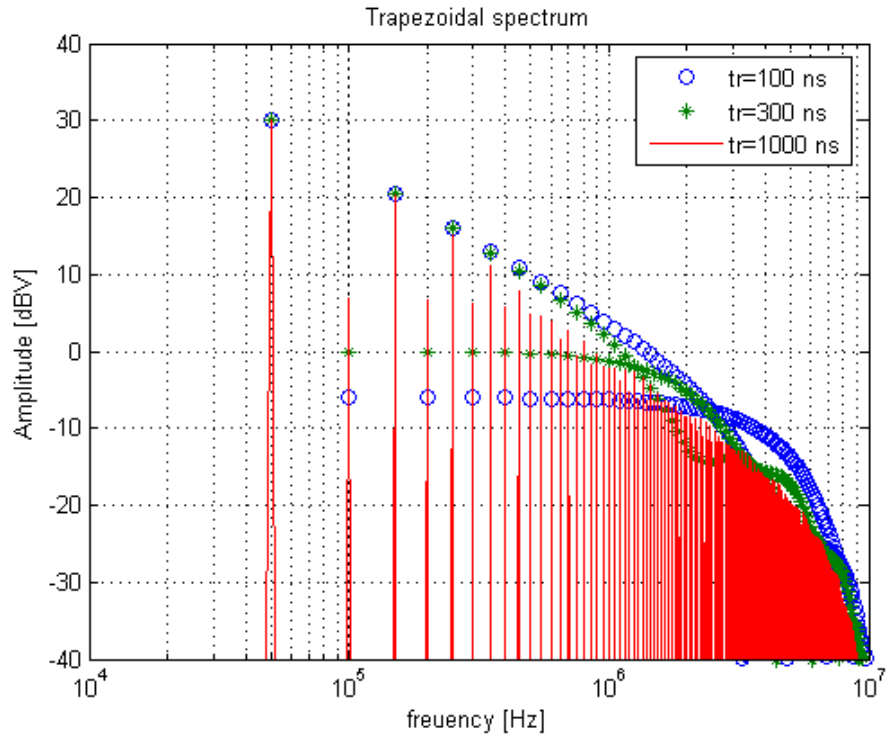


Fig. 4 Voltage spectrum of trapezoidal waveform with different rise time.

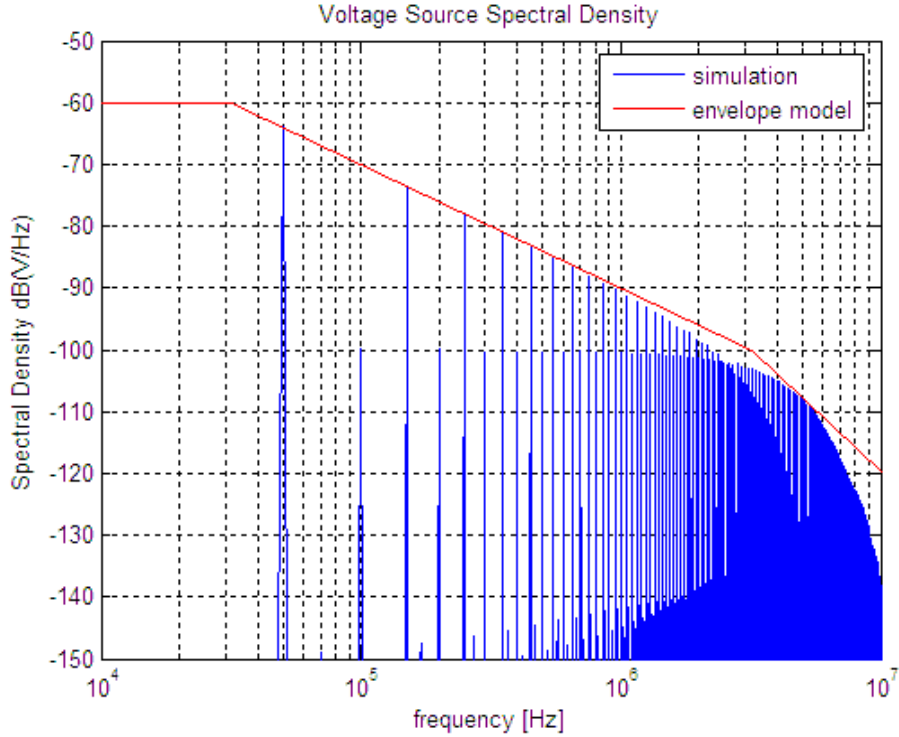


Fig. 5 Voltage spectral density for trapezoidal waveform with 50% duty cycle and 100 ns of rise and fall time.

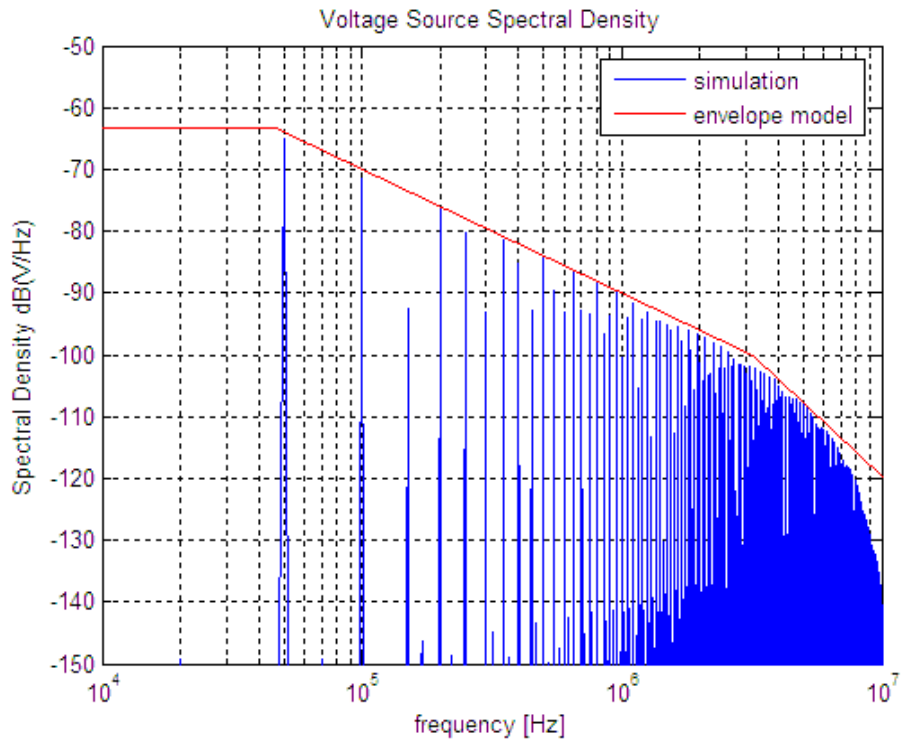


Fig. 6 Voltage spectral density for trapezoidal waveform with 35% duty cycle and 100 ns rise and fall time.

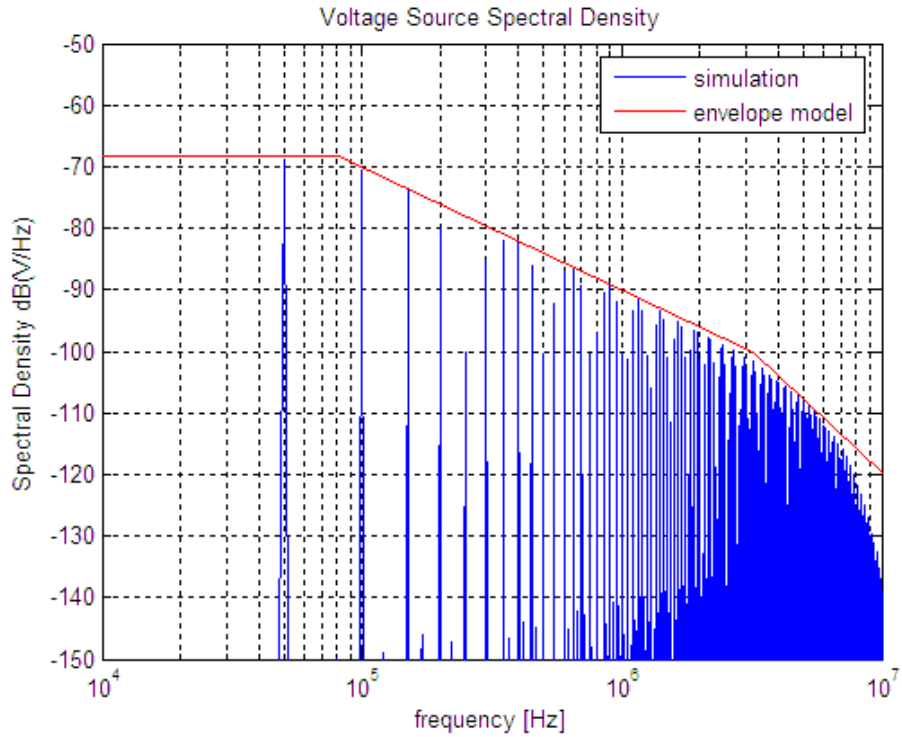


Fig. 7 Voltage spectral density for trapezoidal waveform with 20% duty cycle and 100 ns of rise and fall time.

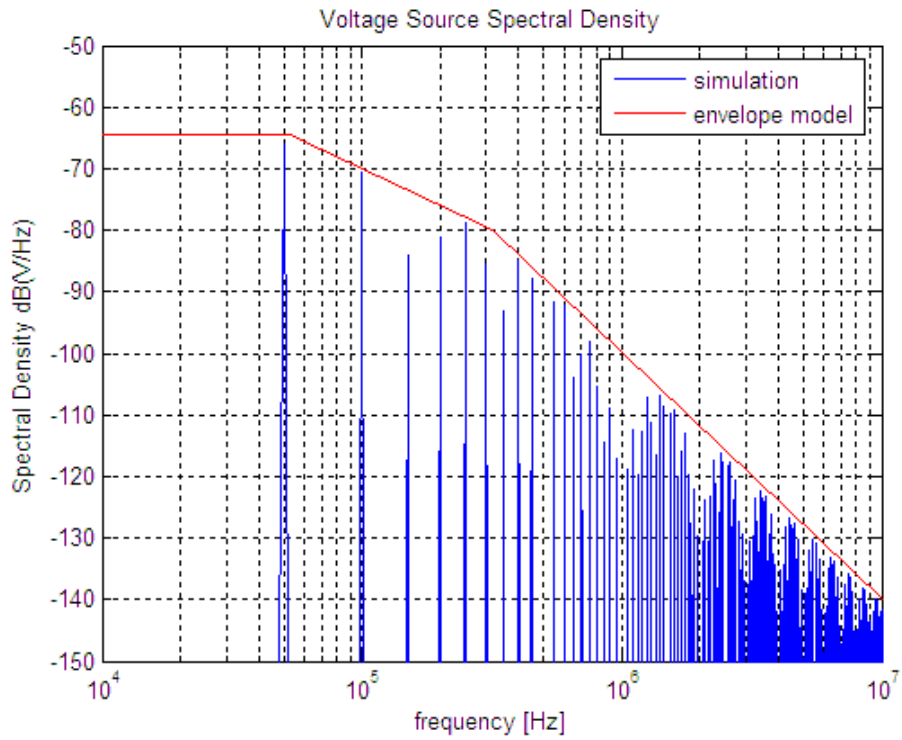


Fig. 8 Voltage spectral density for trapezoidal waveform with 35% duty cycle and 1 μ s of rise and fall time.

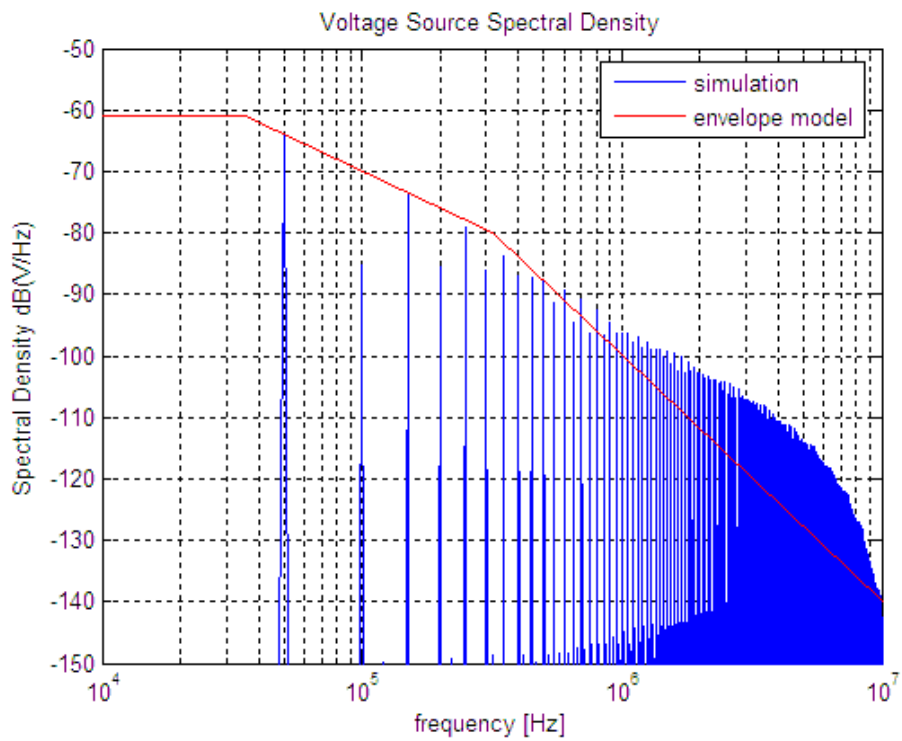


Fig. 9 Voltage spectral density for trapezoidal waveform with 50% duty cycle and 1 μ s rise time and 100 ns fall time.

With the same rise and fall time, the envelope model of the spectrum shows a very good agreement with simulations for any duty cycle; when rise and fall time are different the envelope of the spectrum shows some discrepancies with the simulated one in the upper part of the spectrum.

The comparison between the Fourier spectrum (1) and the envelope model (2), applied to different trapezoidal waveform, are shown in Figs. 10-14. Eq. (1) predicts generally a spectral density 10 dB lower than the envelope model (2). In case of EMC prediction the use of envelope model is reasonable taking into account that an EMC model need to predict the worst case of emission.

Therefore the envelope model (2) can be simply applied to the prediction of a *voltage driven source* in different circuits.

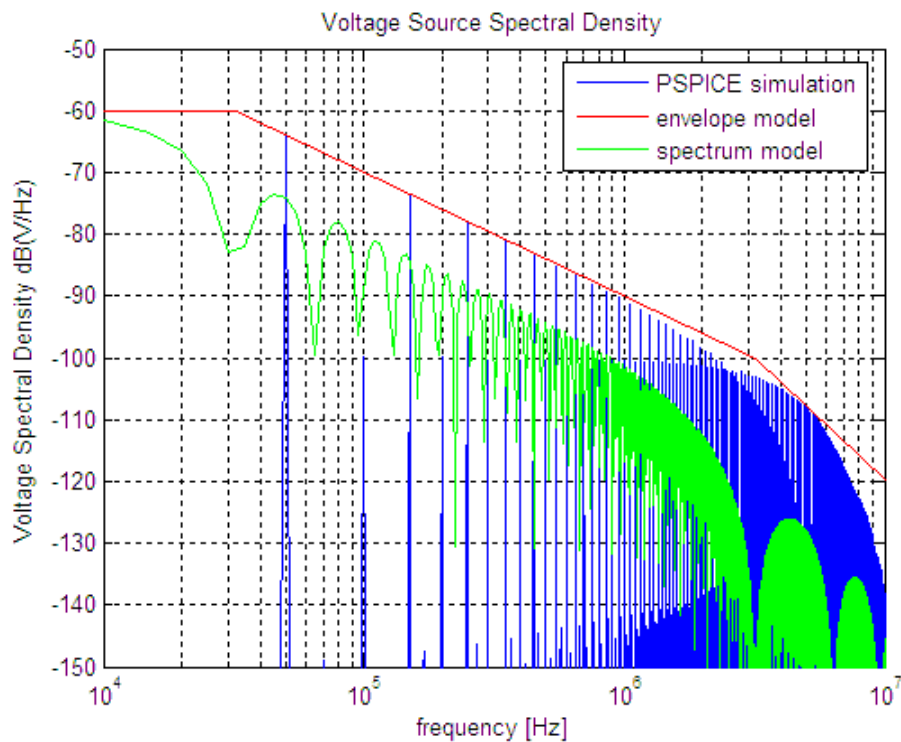


Fig. 10 Comparison between the envelope model and Fourier spectrum.

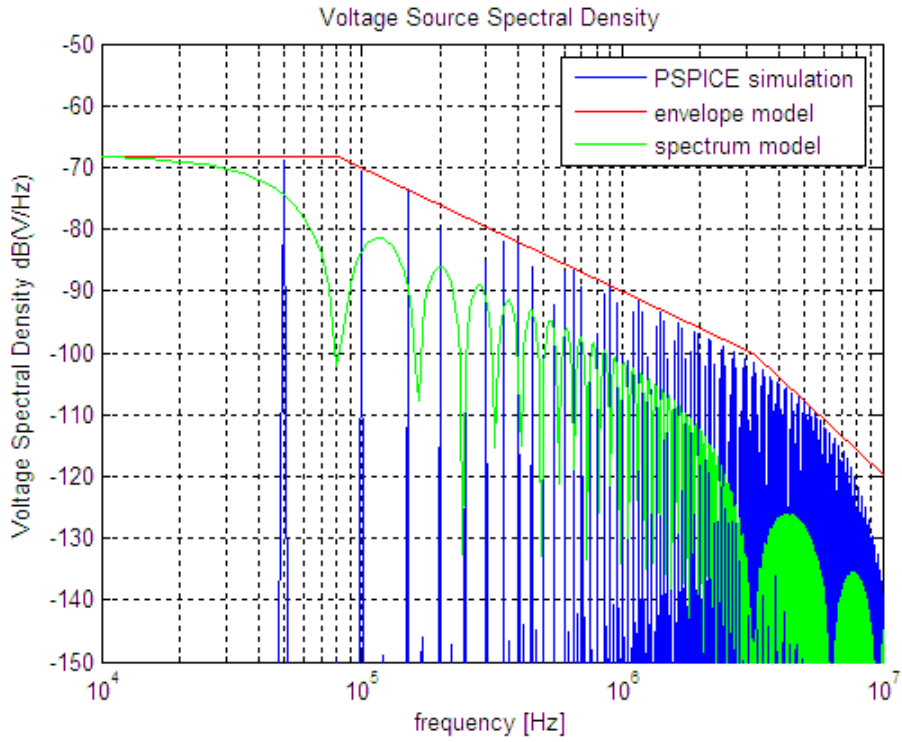


Fig. 11 Comparison between envelope model and Fourier spectrum.

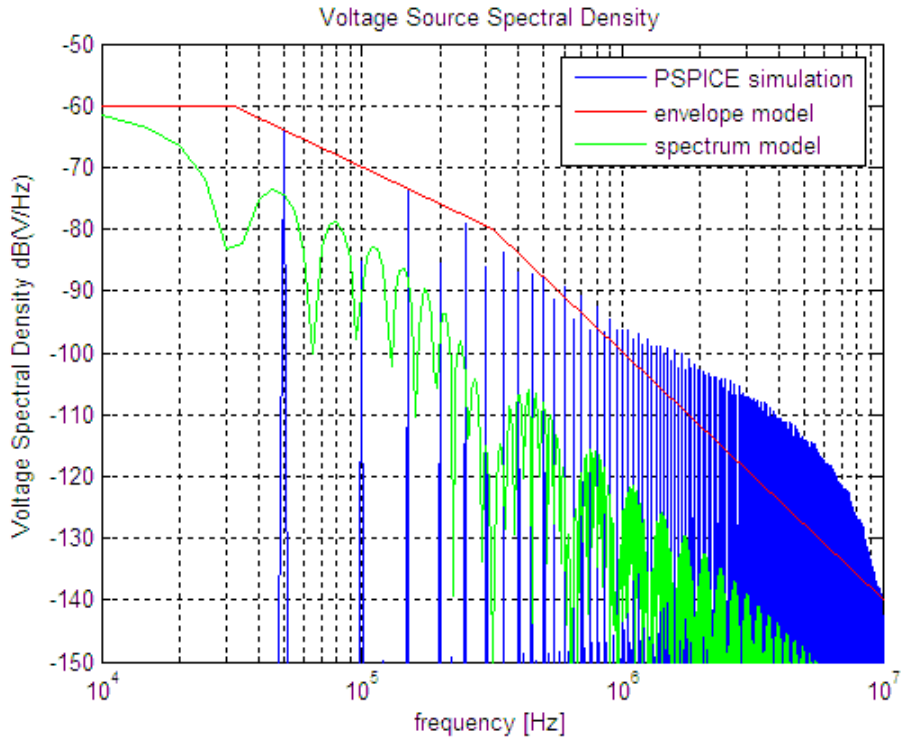


Fig. 12 Comparison between envelope model and Fourier spectrum.

In real circuits, transistor, mosfet or any other active device are generally bounded to heatsinks. Two different case can be highlighted depending on the connection between the active components and the heatsinks as shown in Figs. 13-14:

1. component can be directly connected to the heatsink (for the low voltage side) and the heatsink is grounded (Fig.13),
2. component can be capacitive coupled to the heatsink (for the high voltage side) and the heatsink is not grounded (Fig.14).

Two different equivalent circuits can be drawn as in Figs 15-16 and the following equation used to calculate the voltage between the heatsink and a ground reference point of the circuitry

$$V_{H1}(f) = V_{S1}(f) \tag{1.3}$$

$$V_{H2}(f) = V_{S2}(f) \frac{C_{TH}}{C_{TH} + C_{Heq}} \tag{1.4}$$

$$v_{S2}(t) = \frac{N_2}{N_1} \cdot abs(v_{S1}(t)) \tag{1.5}$$

being C_{TH} the capacitance between source and heatsink, C_{Heq} the capacitance between the heatsink and a ground reference point.

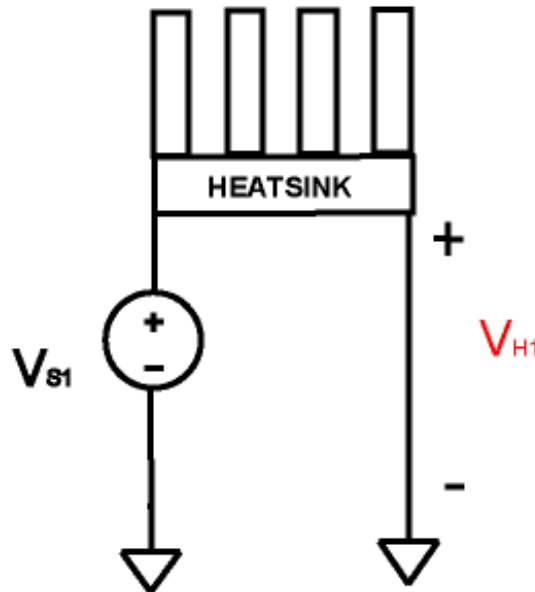


Fig. 13 Voltage driver mechanism with the heatsink grounded.

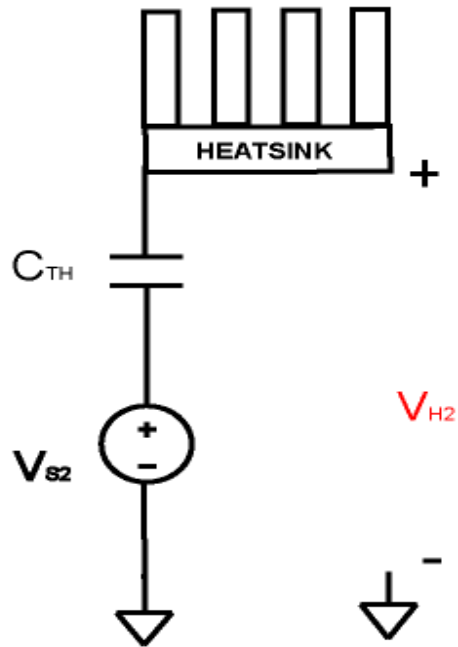


Fig. 14 Voltage driver mechanism with a not grounded heatsink.

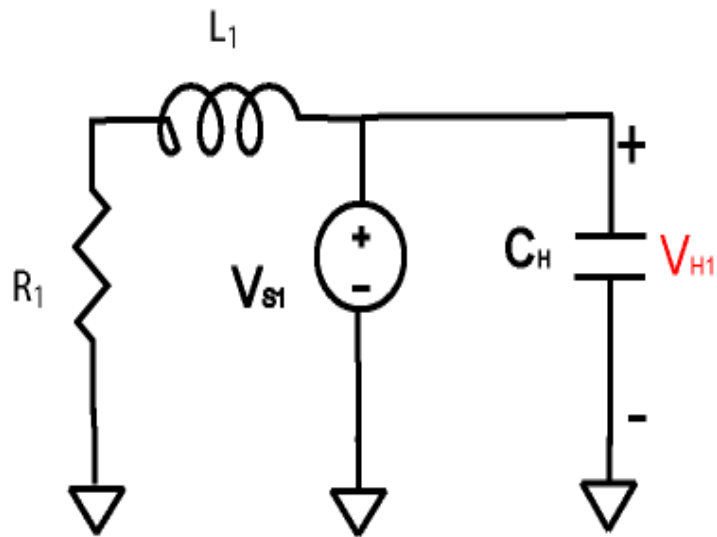


Fig. 15 Equivalent circuit for voltage driver mechanism with heatsink grounded.

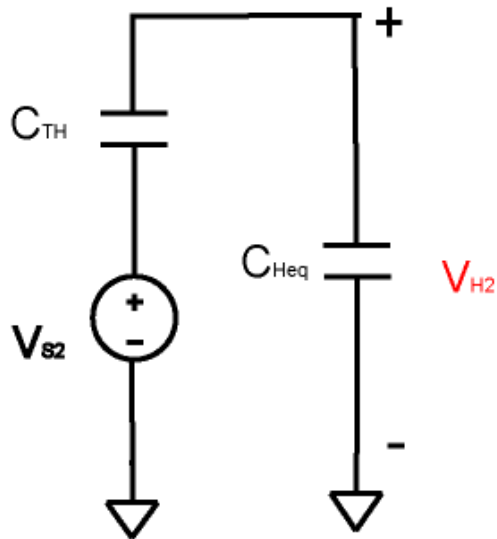


Fig. 16 Equivalent circuit for voltage driver mechanism with a not grounded heatsink.

Referring to an actual SMPS with a grounded heatsink on the primary side and a not grounded heatsink on the secondary side, the equivalent circuit is shown in fig.17.

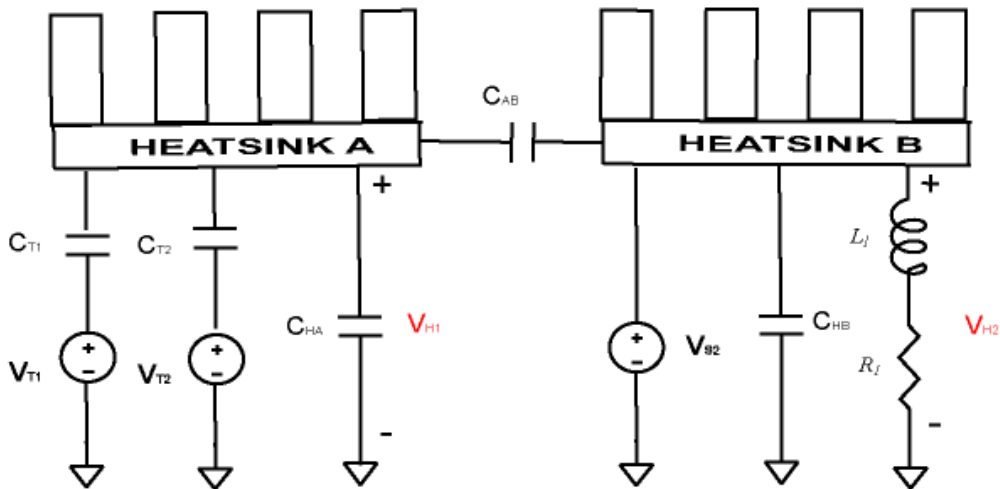


Fig. 17 Equivalent circuit for voltage driven mechanism of an actual SMPS.

V_{T1} and V_{T2} are the sources (transistors connected to the heatsink through a mica foil), C_{T1} and C_{T2} the capacitances between the sources and the heatsink, C_{HA} and C_{HB} the self-capacitance of the heatsinks itself, C_{AB} the capacitance between them and R_1, L_1 the resistance and the self-inductance of the wire connecting the heatsink B to a ground point reference. Each of them can be computed using some approximation as follows

$$C_{Ti} = \frac{\epsilon_{ri} \epsilon_0 S_i}{d_i} \quad (1.6)$$

$$C_{AB} \approx \frac{\epsilon_0 S_H}{d_{AB}} \quad (1.7)$$

$$C_{Hi} \approx 4\pi\epsilon_0 r_{eqi} \quad (1.8)$$

$$L_{wire} \approx \frac{\mu l_w}{2\pi} \left[\ln\left(\frac{2l_w}{r_w}\right) - 1 + \frac{r_w}{l_w} \right] + \frac{\mu \cdot l}{8\pi} \quad (1.9)$$

$$R_{DC} = \frac{l_w}{\gamma_{cu} S_w} \quad (1.10)$$

being S_i, d_i the surface and thickness of mica foils, ϵ_{ri} the permeability of mica, S_H, d_{AB} the fronted surface of the heatsinks and the distance between them, r_w, l_w, S_w the radius length and cross section of the wire connecting the heatsink to the ground point, r_{eq} is the equivalent radius of a sphere with the same surface of the actual heatsink (see chapter 4). Referring to (4) $C_{TH} \approx C_{Hi}$ and $C_{THeq} \approx C_{H1} + C_T + C_{AB}$, some of the parameter values are calculated and measured as shown in Tab.1.

Parameters	Calculated	Measured	Accuracy
C_{T1} [pF]	16.7	16.0	$\pm 0.15\%$
C_{T2} [pF]	16.7	16.0	$\pm 0.15\%$
C_{AB} [pF]	0.5	1.0	$\pm 0.15\%$
C_{H1} [pF]	3.0	3.1	$\pm 0.15\%$
C_{H2} [pF]	3.0	3.1	$\pm 0.15\%$
R_1 [Ω]	4.5	4.6	$\pm 0.15\%$
L_1 [nH]	10	12	$\pm 0.30\%$
$\frac{C_{TH}}{C_{TH} + C_{Heq}}$	0.37	0.32	0.32%

N_1/N_2	6	6	/
-----------	---	---	---

Tab. 1 Calculated and measured parameter for (4).

Model (2) and eq. (3-5) are applied to a real power supply to compute the voltage driven source and the results are presented in Figs.18-22.

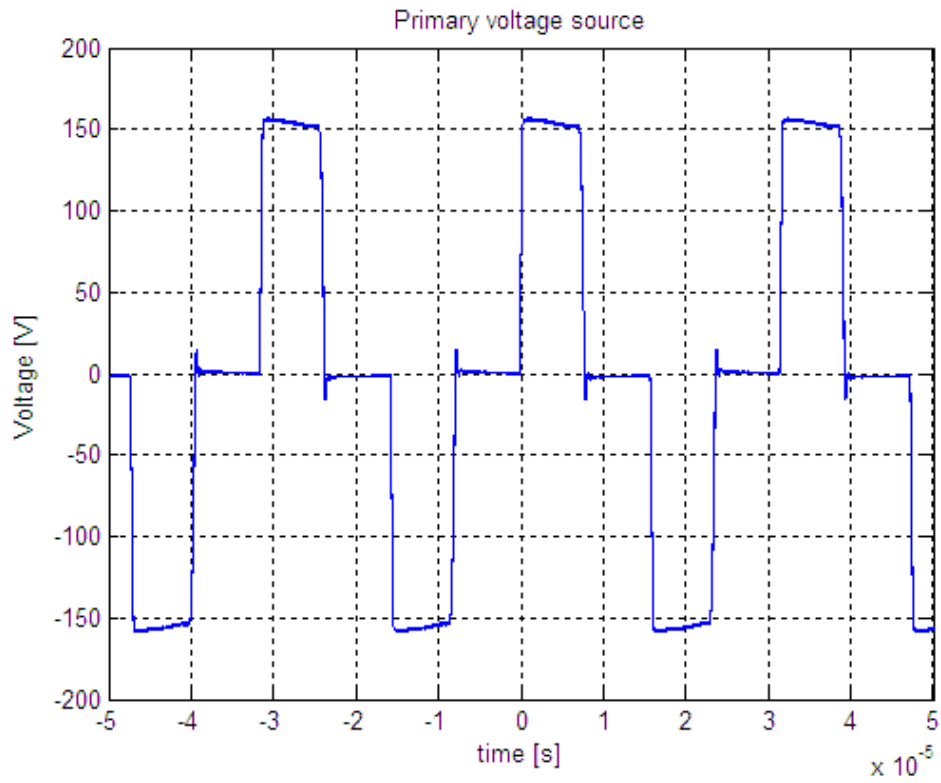


Fig. 18 Primary voltage source.

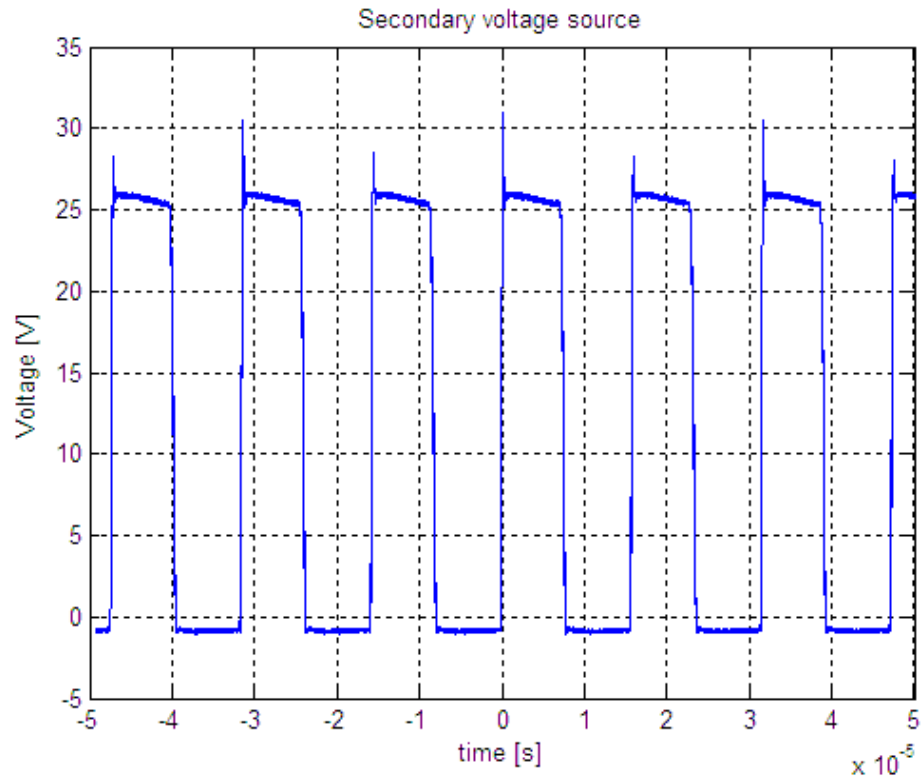


Fig. 19 Voltage waveform across the secondary of the transformers.

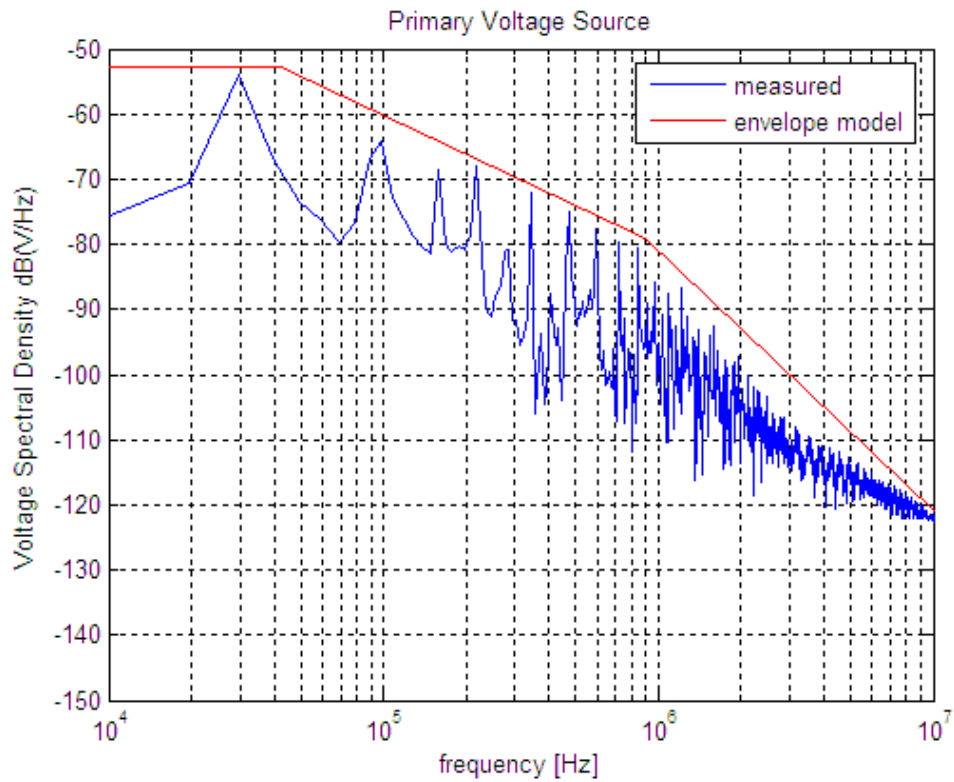


Fig. 20 Measured and predicted primary voltage source spectral density.

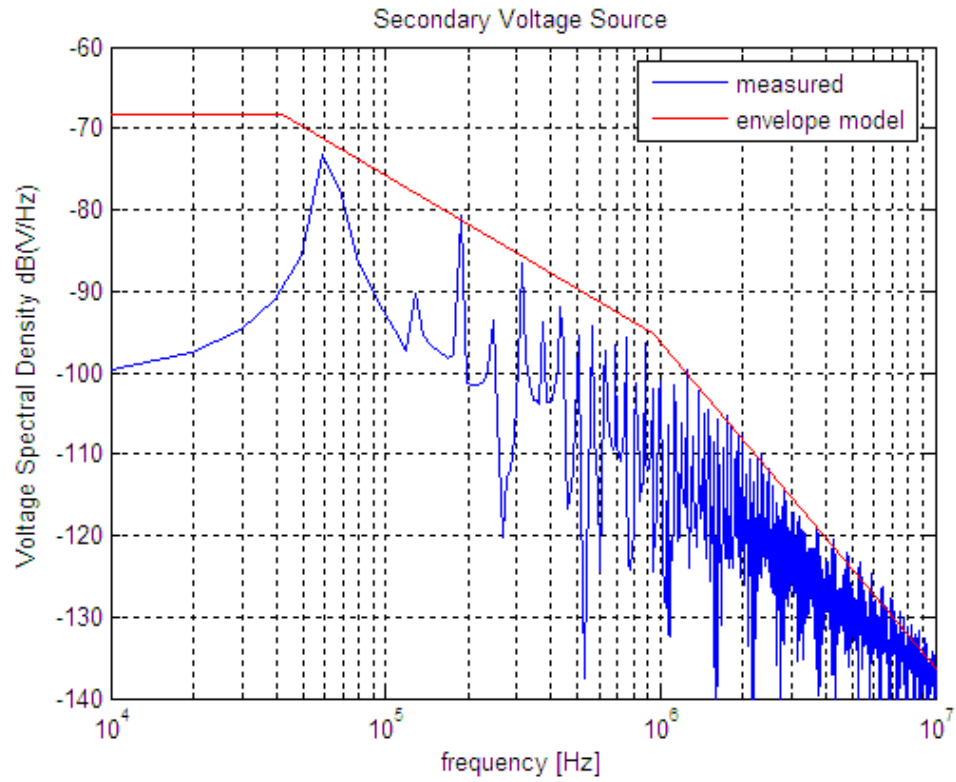


Fig. 21 Measured and predicted secondary voltage source spectral density.

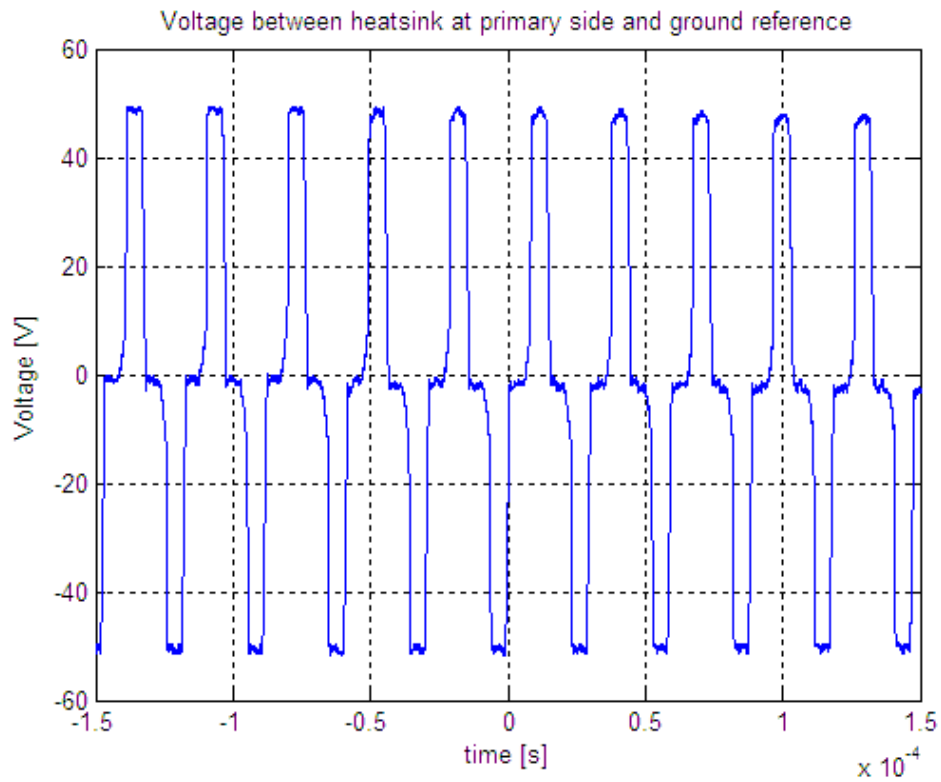


Fig. 22 Measured voltage between heatsink A and a round reference point.

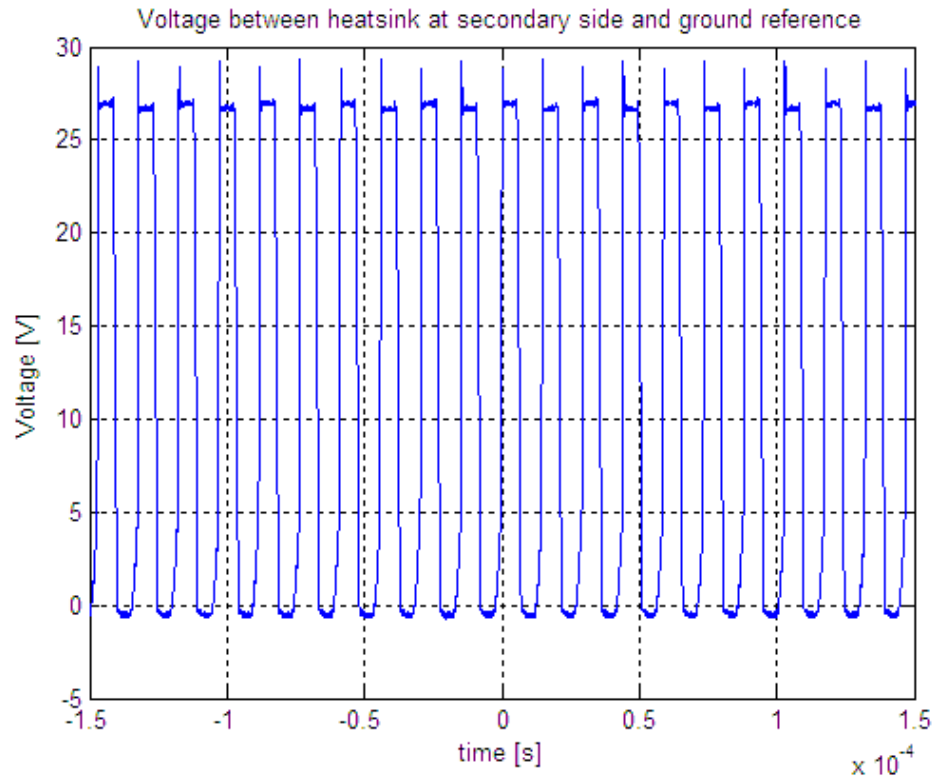


Fig. 23 Measured voltage between heatsink B and a voltage reference point.

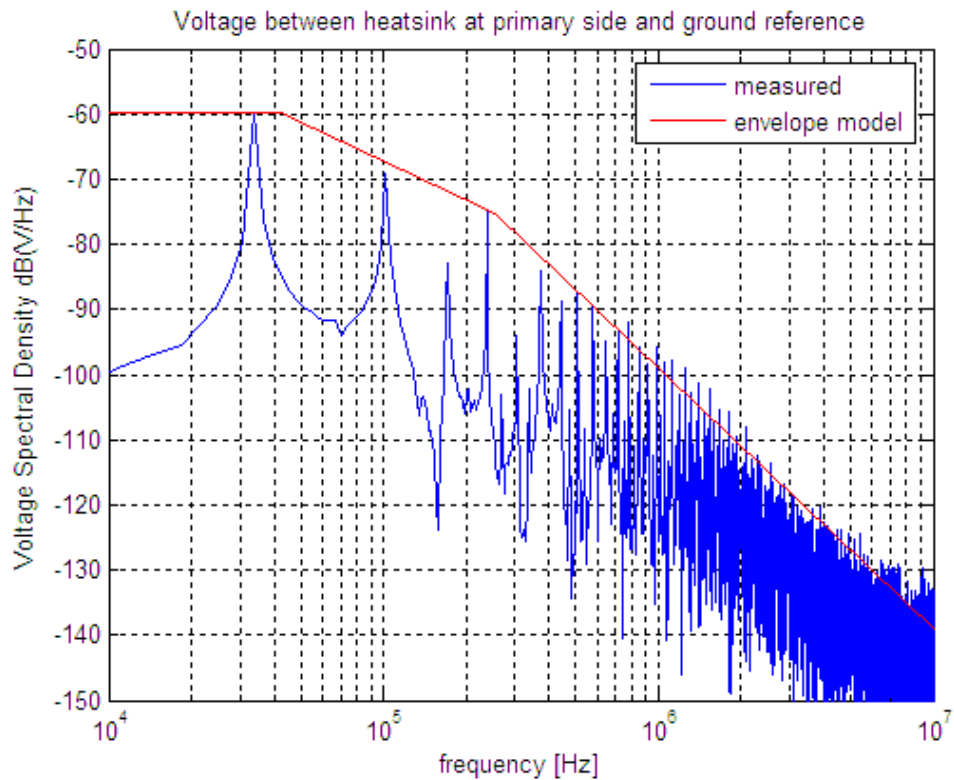


Fig. 24 Measured and predicted voltage driven source at heatsink A.

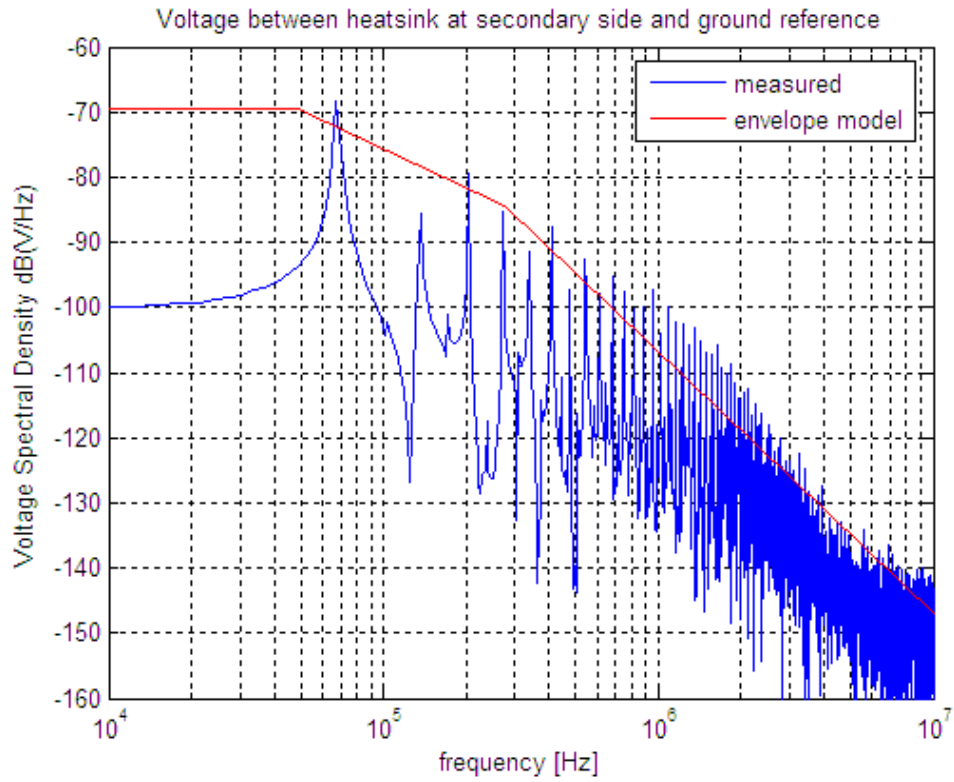


Fig. 25 Measured and predicted voltage driver source at heatsink B.

The results show a very good agreement between the measurements and the envelope model. The accuracy for the measurements is in the order of ± 2 dB all over the frequency range.

Equation Chapter 4 Section 2

II. Noise current source

As already highlighted in chapter 1, in a SMPS current loops are primary EMI sources. Two different current loop in DC/DC block of SMPS can be EMI sources:

1. the time varying current in the primary loop that comprises the switching transistor T_A and T_B , the transformer or the storage inductor and the primary capacitor C_A and C_B .
2. the time varying current in the secondary loop comprise the transformer secondary, the rectifiers D_A and D_B , the inductor and the load.

Typical schematic of DC/DC block of a SMPS is shown in Fig.1.

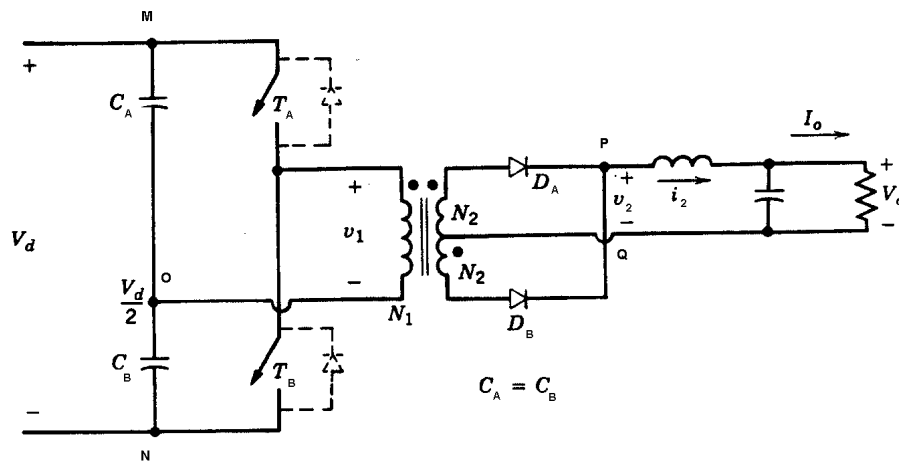


Fig. 26 Typical SMPS with primary and secondary loop.

Current Spectrum Model

In chapter 3 a resistance-inductance-capacitance (RLC) model is described for estimating current waveforms in digital CMOS circuits. The model is based on parameters that are readily derived from information available in board layout files and component data sheets or IBIS files and can be applied also to power converter to estimate current waveform. The model estimates the shape of the current waveform in the time domain and the amplitudes of the harmonics in the frequency domain.

Simple formulas are derived for the current based on parameters that are normally available or readily estimated for power circuits.

The transient current in a DC/DC power converter can be estimated using an RLC series equivalent circuit as shown in Fig.2. What the parameter represent will be described in details in the next section.

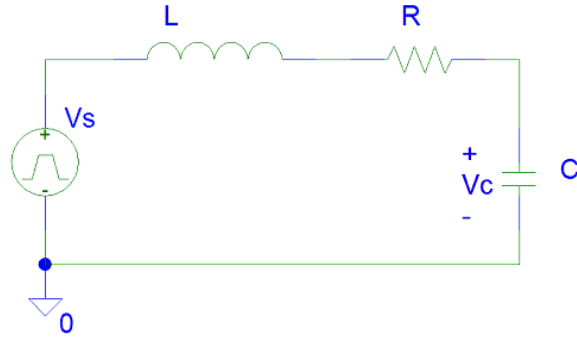


Fig. 27 Equivalent RLC circuit for DC/DC power converter and its load.

The current spectrum envelope when estimating current for EMC calculations is

$$|I(f)| = \frac{|V_s(f)|}{\left| R_1 + j2\pi fL_1 + \frac{1}{j2\pi fC_1} \right|} \quad (2.1)$$

$$|V_s(f)| = \begin{cases} \frac{2\Delta V\tau}{T}, & f < \frac{1}{\pi\tau} \\ \frac{2}{T} \frac{\Delta V}{\pi f}, & \frac{1}{\pi\tau} \leq f \leq \frac{1}{\pi t_r} \\ \frac{2}{T} \frac{\Delta V}{(\pi f)^2 t_r}, & f > \frac{1}{\pi t_r} \end{cases} \quad (2.2)$$

Flyback and half-bridge converter

To understand how these converters work, let us consider a simple Flyback converter as in Fig.3.

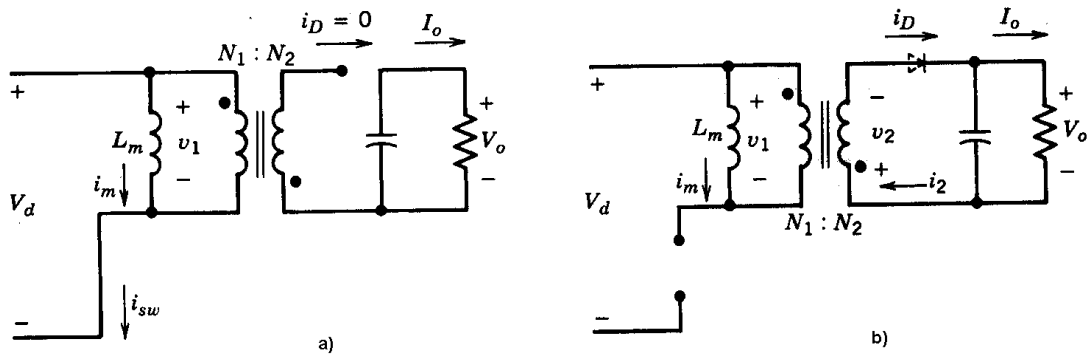


Fig. 28 Typical flyback converter: a) turn on state, b) turn off state.

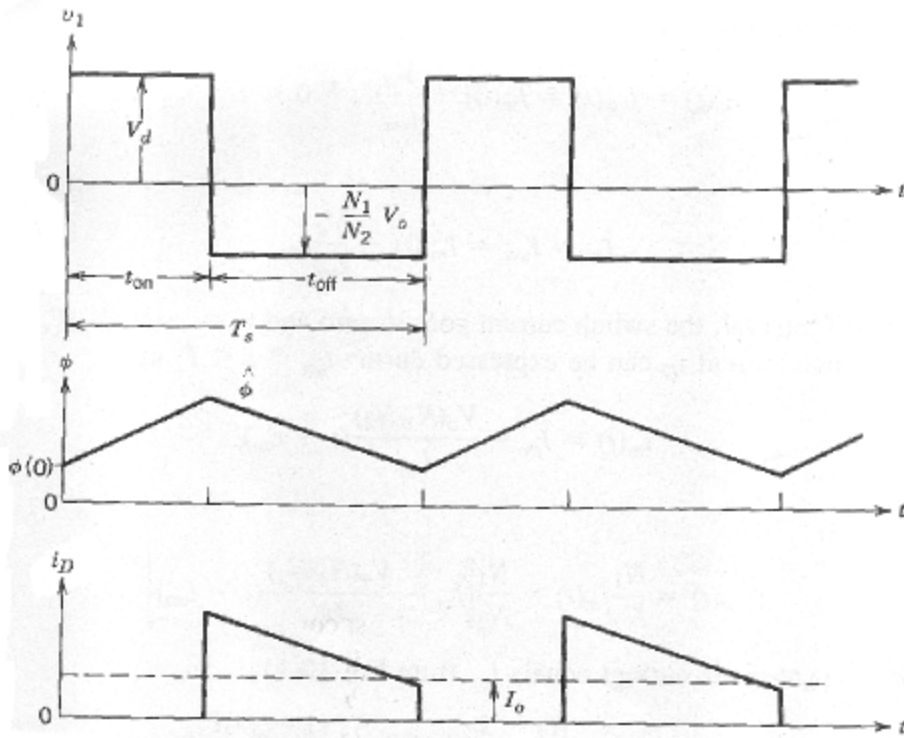


Fig. 29 Typical waveforms in a flyback converter.

When the switch is on (Fig.3a), the diode became reverse biased, the transformer core flux increase linearly from its initial value

$$\phi(t) = \phi(0) + \frac{V_d}{N_1} t \quad 0 < t < t_{on} \quad (2.3)$$

After t_{on} , the switch is turned off and the energy stored in the core causes the current to flow in the secondary winding through the diode as shown in Fig.3b . During t_{off} the flux decrease linearly from its previous value and the current can flow through the load.

$$\phi(t) = \phi(t_{on}) - \frac{V_o}{N_2}(t - t_{on}) \quad t_{on} < t < T_s \quad (2.4)$$

Since the net change of flux through the core over a period must be zero in steady state $\phi(T_s) = \phi(0)$ the voltage output/input relationship is

$$\frac{V_o}{V_d} = \frac{N_2}{N_1} \frac{D}{1-D} \quad (2.5)$$

In practical converter the transformer magnetizing current must be taken into consideration for a proper converter operation.

The half-bridge converter in Fig.1 is based on the same principle of operation and its voltage output/input relationship is

$$\frac{V_o}{V_d} = \frac{N_2}{N_1} D \quad (2.6)$$

The capacitors C_A and C_B after a transient are charged and establish a voltage mid point between the input DC voltage. The switches T_A and T_B are turned on alternatively, each for an interval t_{on} in order to achieve a constant duty cycle and DC output voltage.

The advantages of two transistors topology is that voltage rating of the switches is one-half of a single-transistor version.

In this kind of converters a high frequency transformer is required to provide electrical isolation between primary and secondary side and to provide energy storage for a proper converter operations. For the transformer is desirable to minimize the leakage inductances by providing a tight magnetic coupling between the two windings. For this topologies of converter is also desirable to make the magnetic inductance high to store energy during t_{on} .

Primary Current Loop

In steady state condition and due to the symmetry of topology, of passive elements of the actual circuit (Fig.1), the equivalent circuit for the primary side of the converter is shown in Fig.5. The equivalent voltage source between terminal MO-NO (Fig.1) causes the same voltage and current to occur in the primary winding of the transformer.

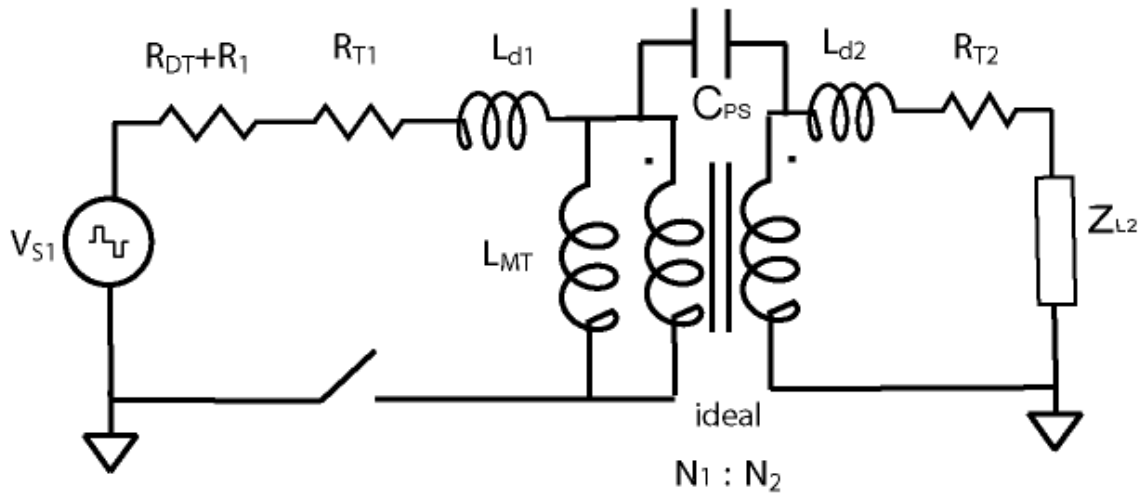


Fig. 30 Equivalent circuit at the primary side of transformer for current calculation.

The ideal voltage source V_{S1} is an alternative trapezoidal waveform which parameter are reported in Tab.1.

Referring the all parameter to the primary side of the transformer, the equivalent circuit for the calculation of the current is shown in Fig.6.

Tab.1 reports the parameter values as they can be calculated with simple formulas or reported from datasheet. These parameters are compared with the measured ones.

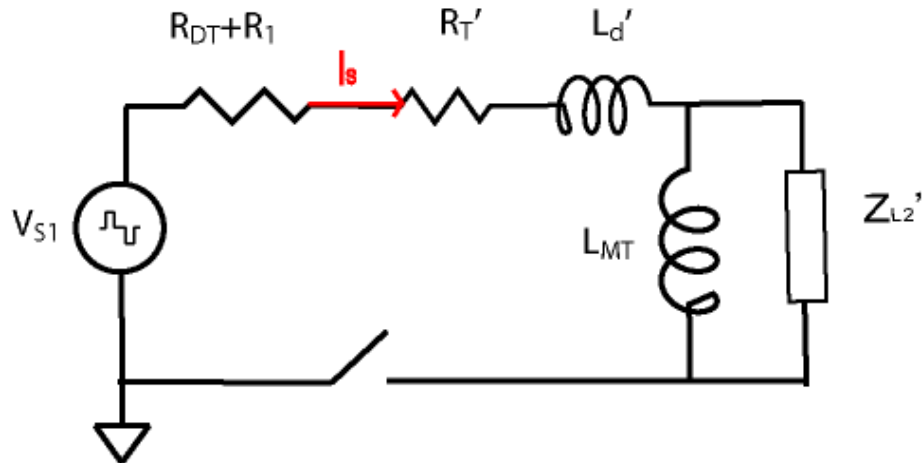


Fig. 31 Equivalent circuit referred to the primary side of the transformer.

Parameters	Measured	Accuracy	Computed/Datasheet
R_{L2} [Ω]	7.542	$\pm 0.15\%$	7.546
L_{L2} [μH]	63.31	$\pm 0.30\%$	68.12
N_1/N_2	6		6
R_{T2} [Ω]	200	$\pm 0.15\%$	220
R_{T1} [Ω]	100	$\pm 0.15\%$	109
$L_{d1} + L_{d2'}$ [μH]	6.75	$\pm 0.30\%$	/
$Z_{L2'}$ [Ω]	$279 + j\omega 2.28\text{m}$	$\pm 0.20\%$	$280 + j\omega 2.45\text{m}$
L_{MT} [mH]	0.955	$\pm 0.30\%$	1.005
C_{PS} [pF]	65	$\pm 0.15\%$	/
R_1 [Ω]	50	$\pm 0.15\%$	53
R_{DT} [Ω]	/		0.40

Tab. 2 Parameter values for the equivalent circuit for the primary side of the transformer.

R_{L2} and L_{L2} are the load at the secondary of the transformer as computed in the following section, N_1/N_2 the transformer winding turns ratio, R_{T1} and R_{T2} account for the ohmic losses in the windings, L_{d1} and L_{d2}' the leakage inductances for coils at the primary side, R_1 the connecting trace resistance, L_{MT} the magnetizing inductance and C_{PS} the inter-winding capacitance and R_D the equivalent series resistance for the transistor device during t_{on} . In circuit Fig.6, R_T' , L_d' and Z_{L2}' are the total transformer winding resistance, the total leakage inductance of coils and load respectively all referred to the primary side. The following formulas can be used to calculate the parameter values:

$$R_{r,l} = \frac{l_w}{\gamma_{cu} S_w} \quad (2.7)$$

for wires and trace and winding turns,

$$L_{MT} = \frac{N_1^2}{\mathfrak{R}_c} \quad (2.8)$$

$$\mathfrak{R}_c = \sum_k \frac{l_k}{\mu_k A_k} \quad (2.9)$$

$$R_D = \frac{V_{CEsat}}{I_C} \quad (2.10)$$

$$Z_{L2} = (R_{L2} + j\omega L_{L2}) \quad (2.11)$$

being \mathfrak{R}_c the magnetic reluctance in the path of magnetic flux lines, V_{CEsat} the collector-emitter saturation voltage and I_C the collector current of the transistor. Since $j\omega L_{MT} \gg I/j\omega C_{PS}$, $R_{L2}' \gg j\omega L_{L2}'$ and $L_d' \ll L_{MT}$ the equivalent circuit in Fig.6 can be simplified as in Fig.7.

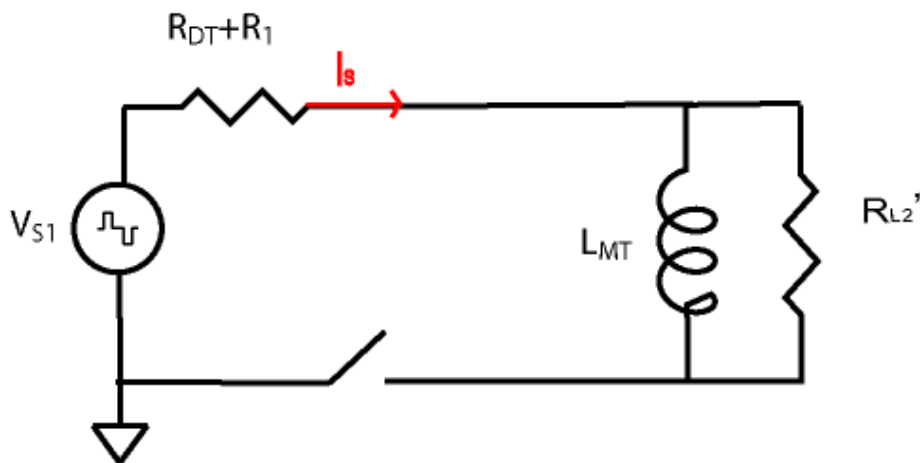


Fig. 32 Simplified equivalent circuit for the primary side.

The current i_s can be computed in time domain as

$$i_s(t) \approx \begin{cases} \frac{\Delta V}{R'_{L2}} + \frac{\Delta V}{L_{MT}}(t-t_1) & t_1 < t < t_2 \\ 0 & t_2 < t < \frac{T}{2} \end{cases} \quad (2.12)$$

being t_1-t_2 the interval during which the voltage source is positive in the semi-period $T/2$. The current waveform is periodic and alternative in the period T .

This time domain model is very simple and it can not take into account the real rise and fall time. In real life circuits the presence of turn-on, turn off and over-voltage snubbers are used to protect the transistors by improving the switching characteristic and they are not considered in this model. They can heavily affect the rise and fall time of the waveform modifying the spectrum envelope especially as regard to the upper harmonics. The current spectrum envelope when estimating primary current for EMC calculations is

$$|I(f)| = \frac{|V_s(f)| |j\omega L_{MT} + R'_{L2}|}{|j\omega L_{MT} R'_{L2}|} \quad (2.13)$$

being

$$|V_s(f)| = \begin{cases} \frac{2\Delta V\tau}{T}, & f < \frac{1}{\pi\tau} \\ \frac{2}{T} \frac{\Delta V}{\pi f}, & \frac{1}{\pi\tau} \leq f \leq \frac{1}{\pi t_r} \\ \frac{2}{T} \frac{\Delta V}{(\pi f)^2 t_r}, & f > \frac{1}{\pi t_r} \end{cases} \quad (2.14)$$

The comparison between the current spectrum computed using SPICE and the envelope model (1.13), (1.14) for different case is presented in Figs.8-10.

Voltage source	Case 1	Case 2	Case 3
Vcc [V]	155	155	155
T [μ s]	31.40	31.40	31.40
T [μ s]	7.5	7.5	7.5
t_r [ns]	300	300	300

L_{MT} [mH]	2	20	0.020
$R_{L2'}$ [Ω]	200	200	200

Tab. 3 Different case tested for the envelope model and spice simulations.

Fig.11 shows the measured time domain waveform of the current at the primary side and the predicted one using (1.12). Fig.12 shows the measured current spectrum compared with the envelope model. Fig.13 shows the current spectrum computed using spice simulator compared with the envelope model. The spike in the measured current waveform is shown in details in Fig.14, and it can not be predicted by the envelope model. This spike effect the current spectrum in the 1-3 MHz range and in the upper harmonics.

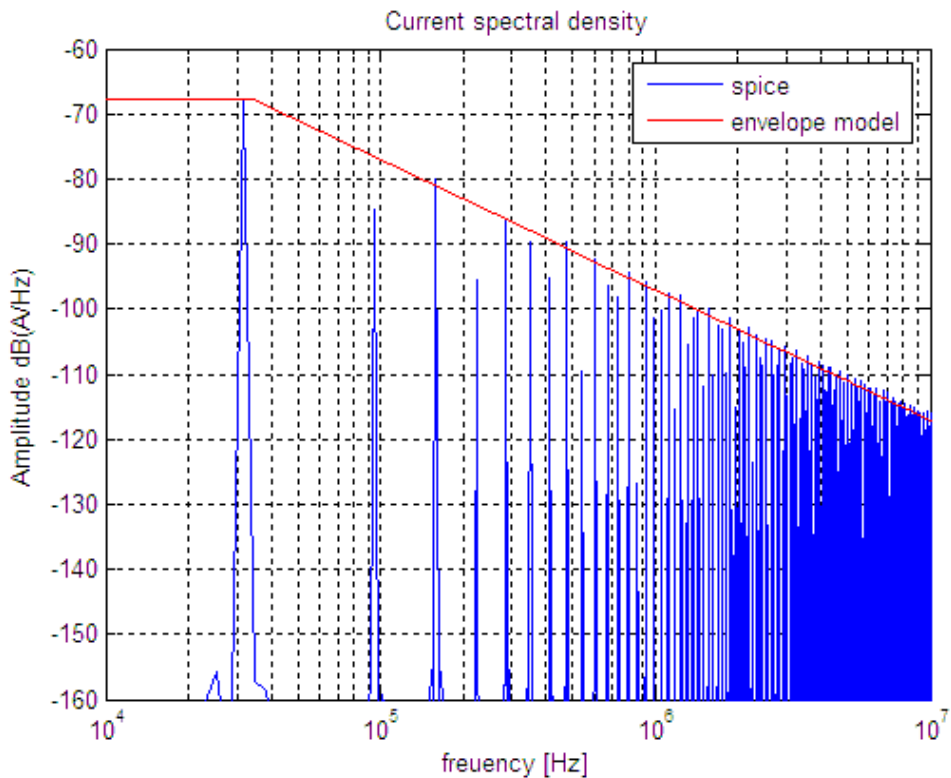


Fig. 33 Comparison between SPICE simulation and the envelope model (case 1).

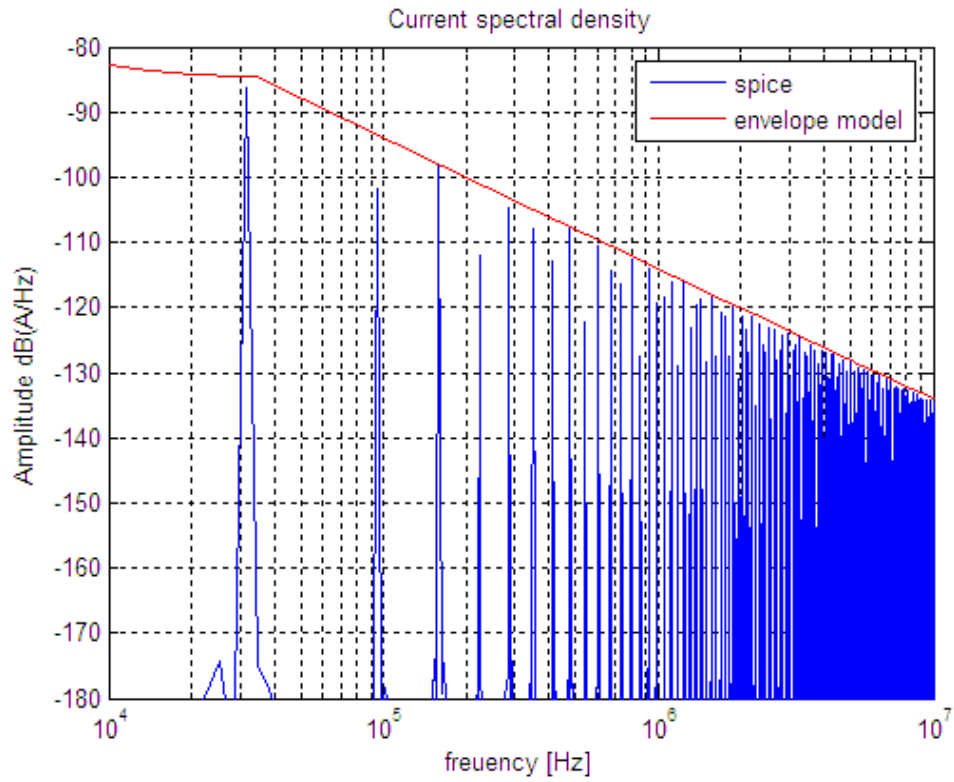


Fig. 34 Comparison between SPICE simulation and the envelope model (case 2).

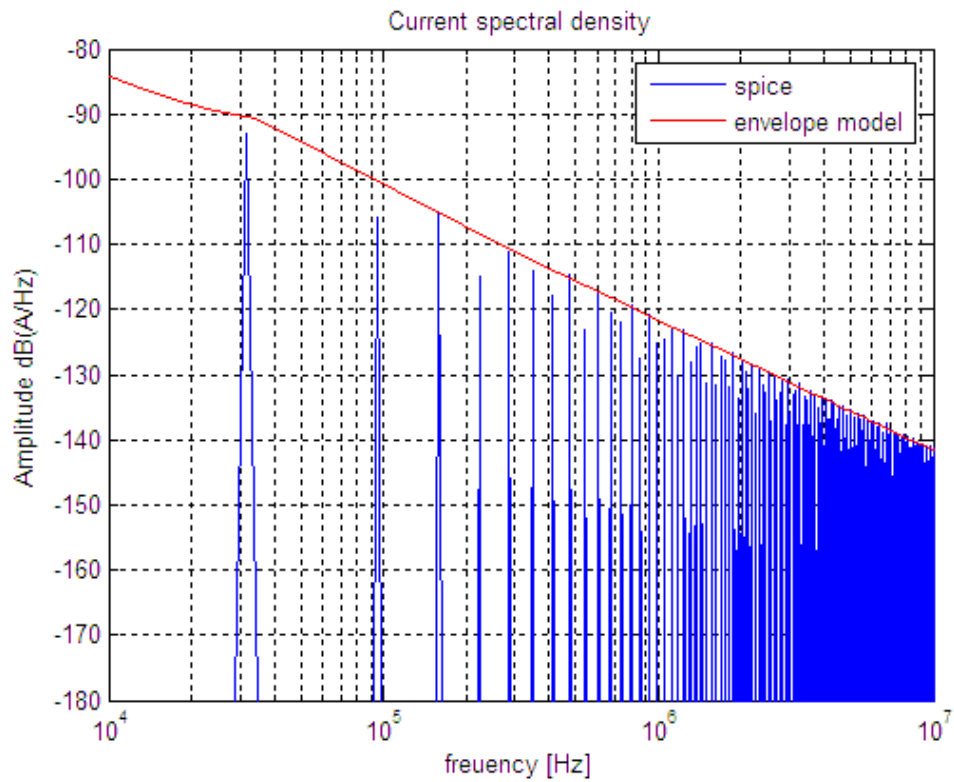


Fig. 35 Comparison between SPICE simulation and the envelope model (case 3).

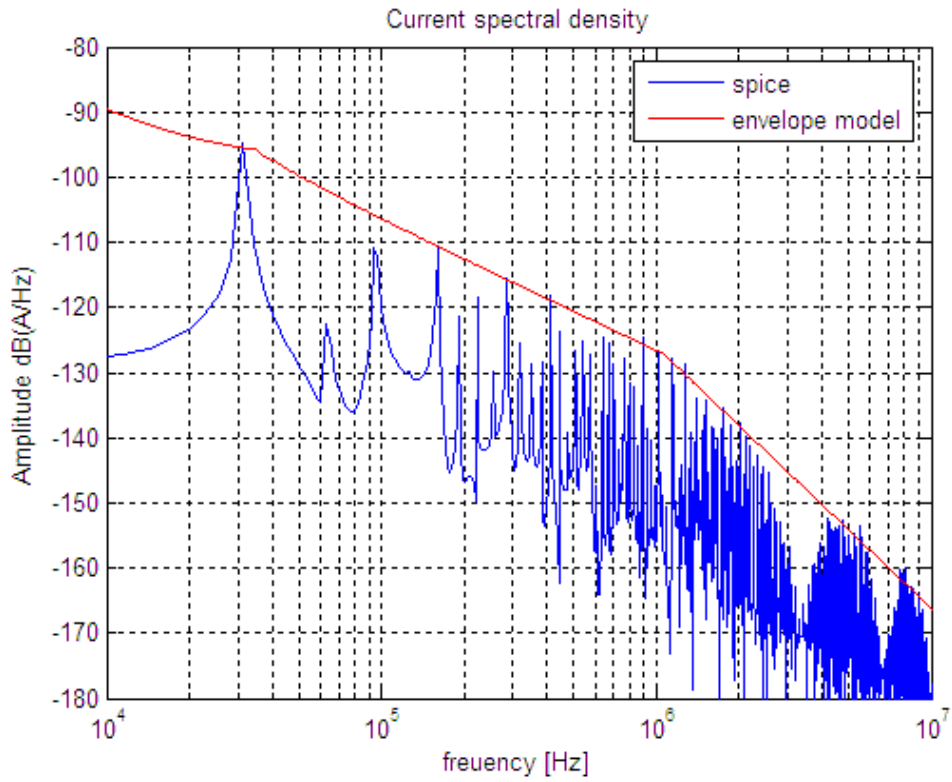


Fig. 38 Current spectral density computer using Spice simulator and envelope model.

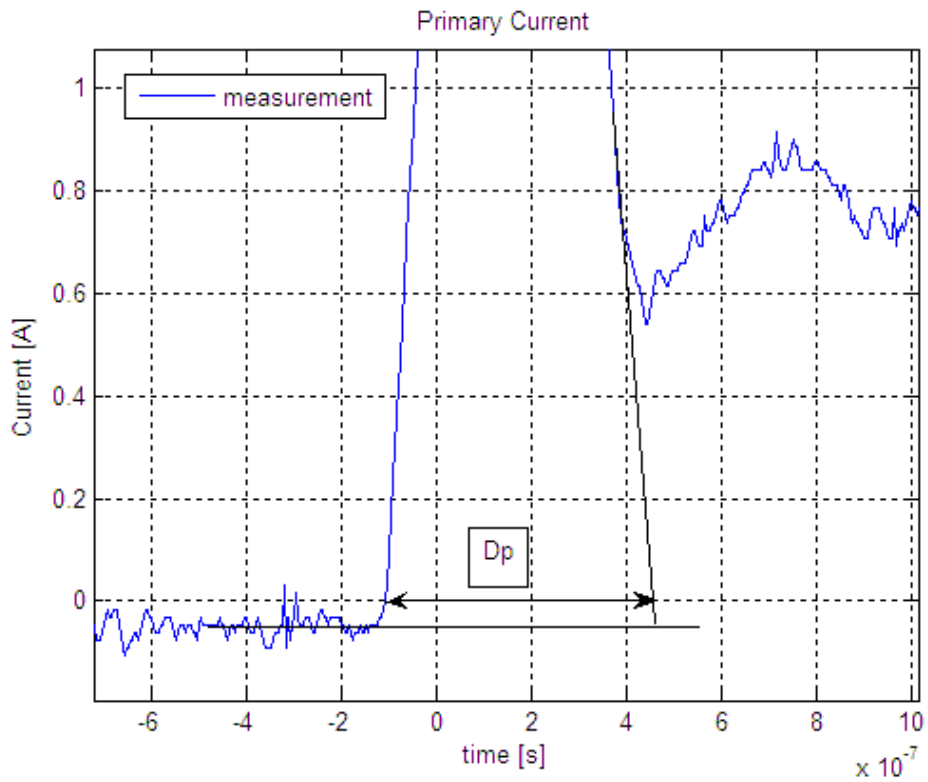


Fig. 39 Spike in time domain waveform that effect the frequency behavior in 1-3 MHz range.

Secondary Current Loop

The secondary loop comprise the transformer secondary, the rectifiers, the inductor and the load. An equivalent voltage source can be replace between point P and Q in Fig.1 and the equivalent circuit is shown in Fig.15.

A DC output voltage of a rectifier should be as ripple free as possible. Therefore, a large capacitor C_2 is connected as a filter on the DC side. This capacitor is charged after a transient time and can be replaced by an ideal DC voltage source depending on the voltage DC output.

These rectifier draw highly distorted current from the utility; This current flowing in the circuit has a DC component and higher harmonics which are point of interest of EMC. Fig.4 shows the equivalent circuit at of the secondary loop.

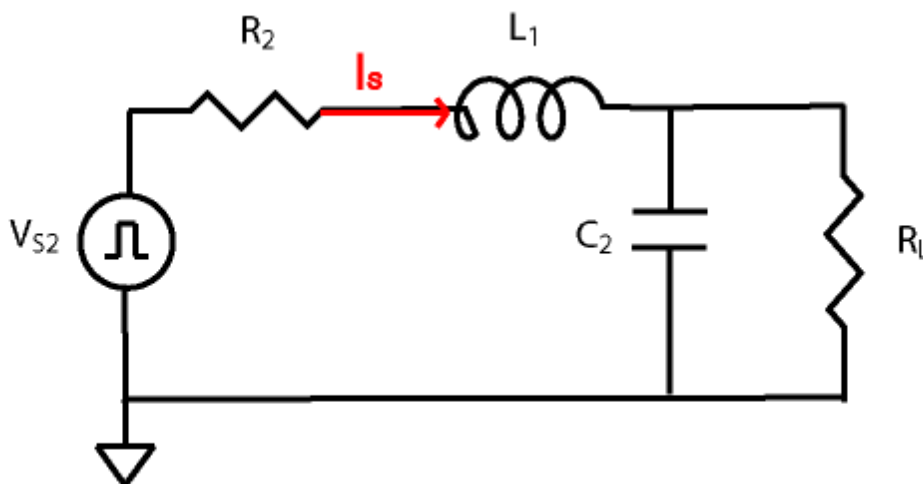


Fig. 40 Equivalent circuit of the secondary side of the transformer.

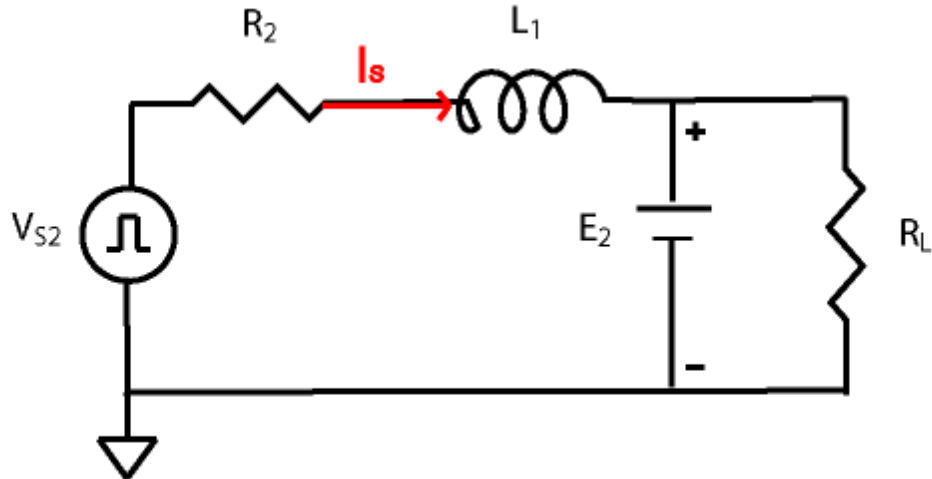


Fig. 41 Equivalent circuit of the rectifier with a load resistance after the initial transient that charge the output capacitor to voltage E_2 .

The load consist of an inductor L_1 in series with a resistor R_L and the DC voltage source E_2 . The diode begins to conduct when voltage source level exceeds the DC voltage source. This means that the DC voltage source just shifts the starting conduction point of the diodes, while it doesn't modify the current spectrum amplitude (only the phase is modified). Therefore the behavior of the noise current in the circuit is only depending on the R_2 L_1 and R_L parameters. Some different current waveforms are presented in Figs.17-22 which parameter values are summarized in tab.3.

Voltage source	Case 1	Case 2	Case 3
Vcc [V]	26	26	26
T [μ s]	15	15	15
T [μ s]	7.5	7.5	7.5
t _r [ns]	100	100	100
L_1 [μ H]	10	100	1
R_2+R_L [Ω]	10	10	10
C_2 [pF]	∞	∞	∞

Tab. 4 Different case tested for the envelope model and spice simulations.

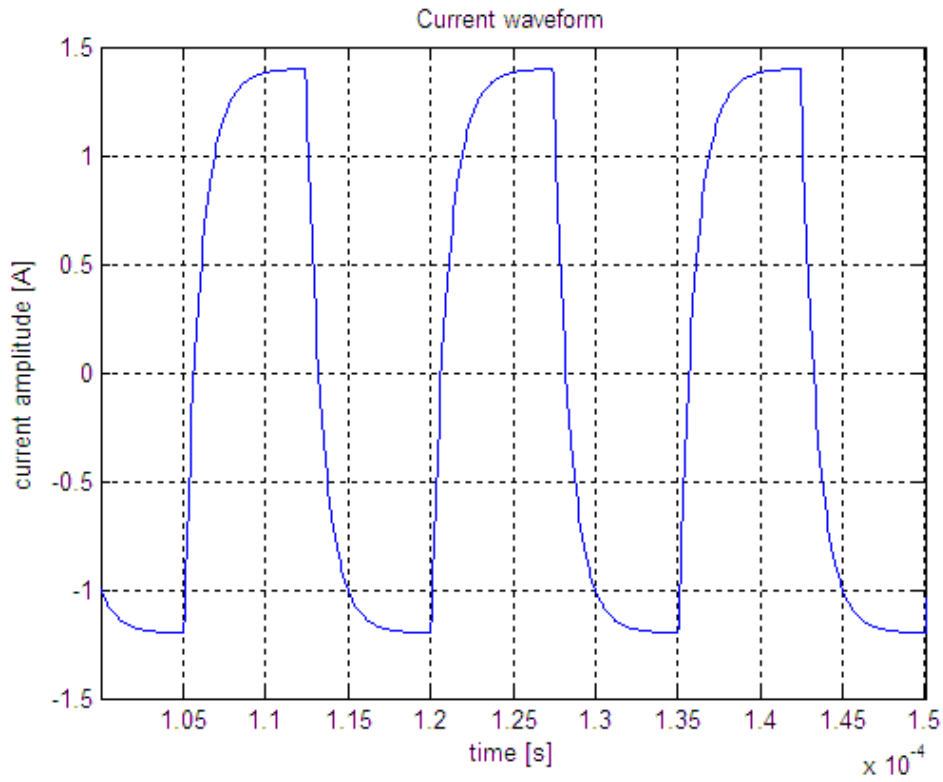


Fig. 42 Current ripple at the output voltage (case 1).

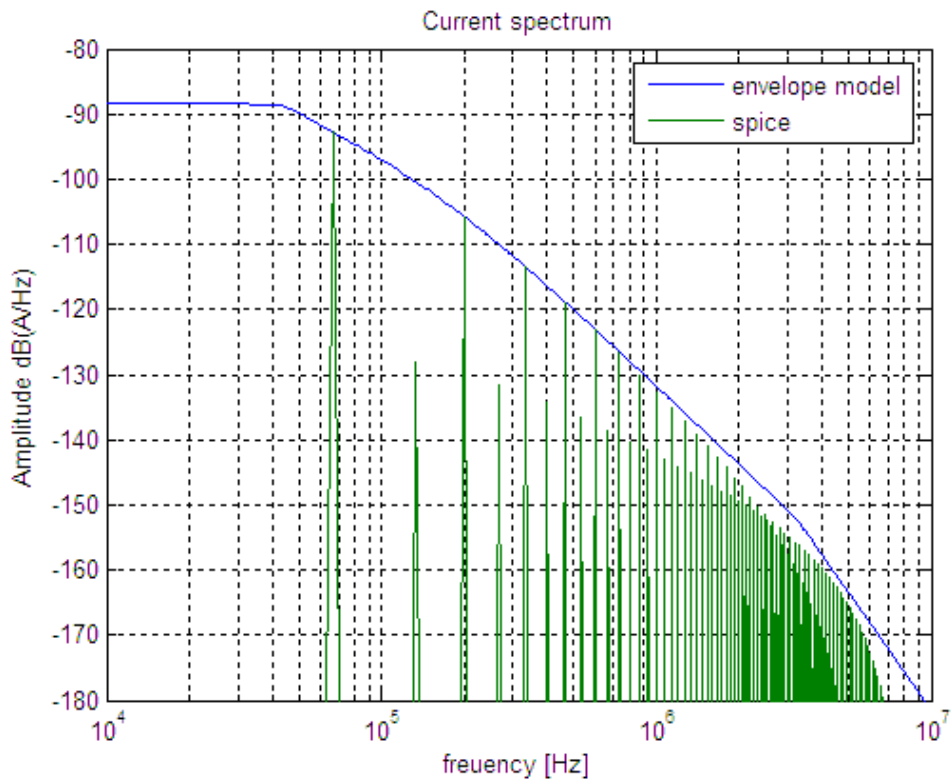


Fig. 43 Current spectral density predicted by envelope model (case 1).

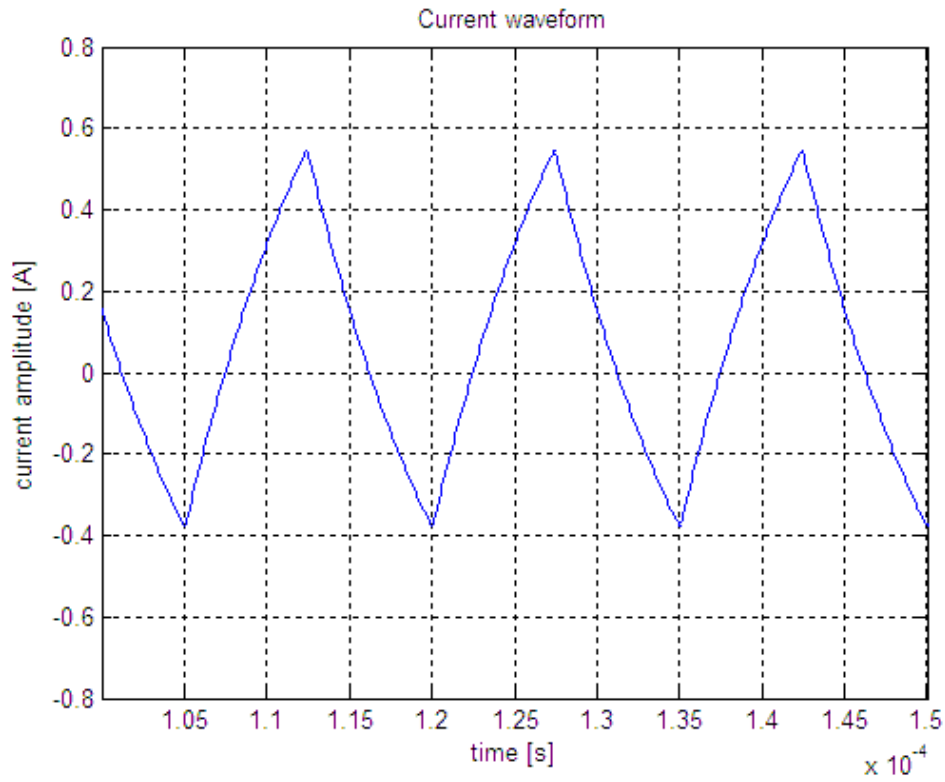


Fig. 44 Current ripple at the output voltage (case2).

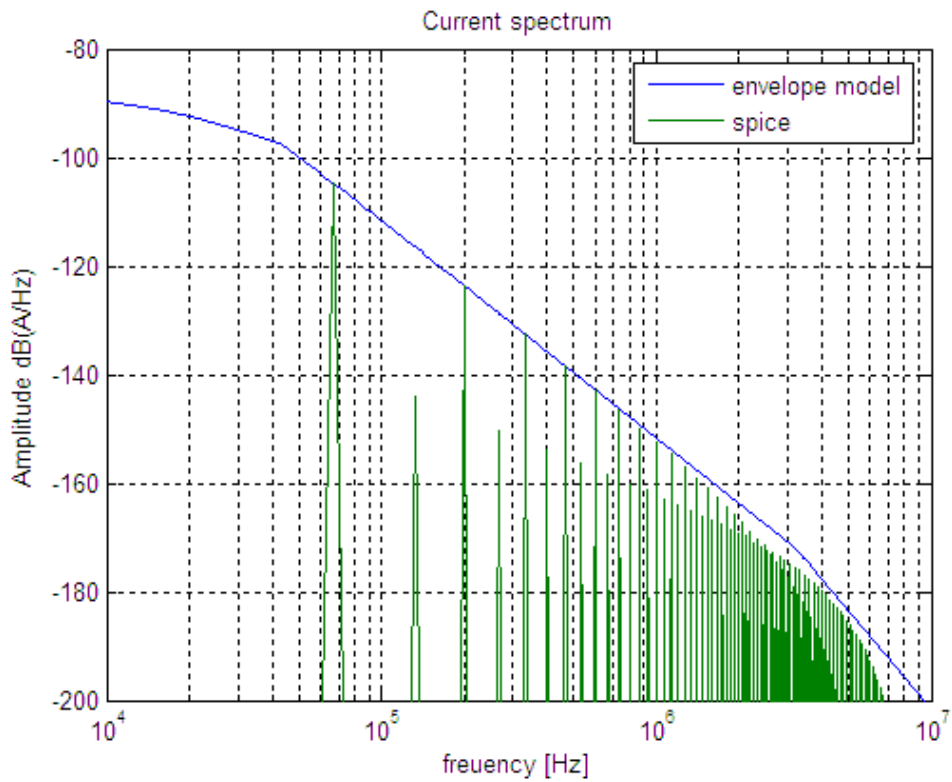


Fig. 45 Current spectral density predicted by envelope model (case 2).

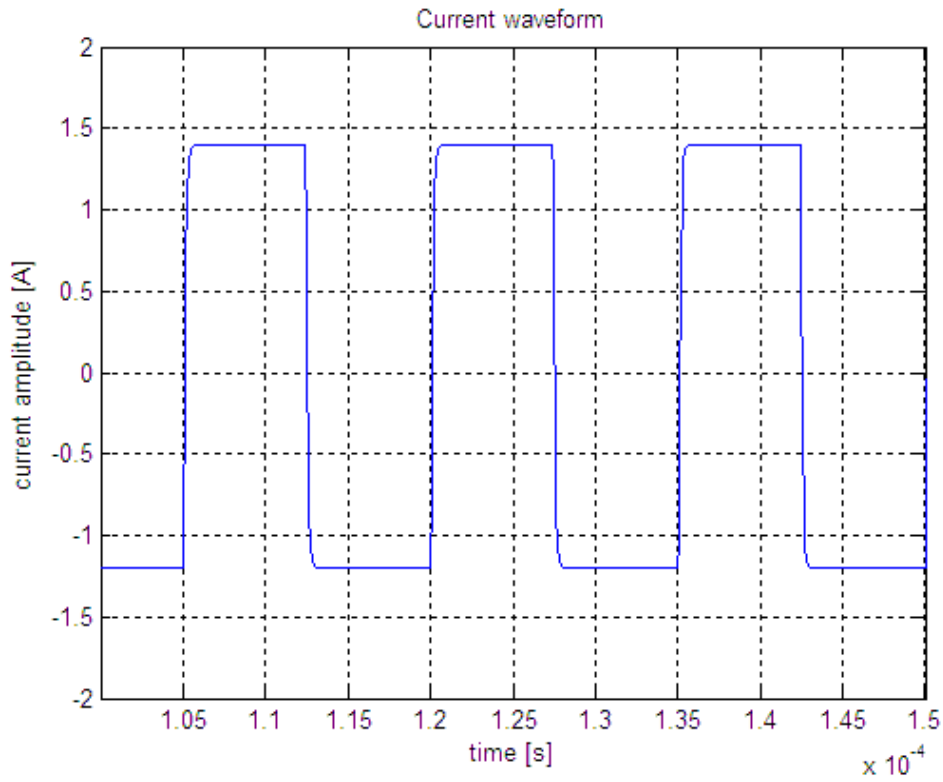


Fig. 46 Current ripple at the output voltage (case3).

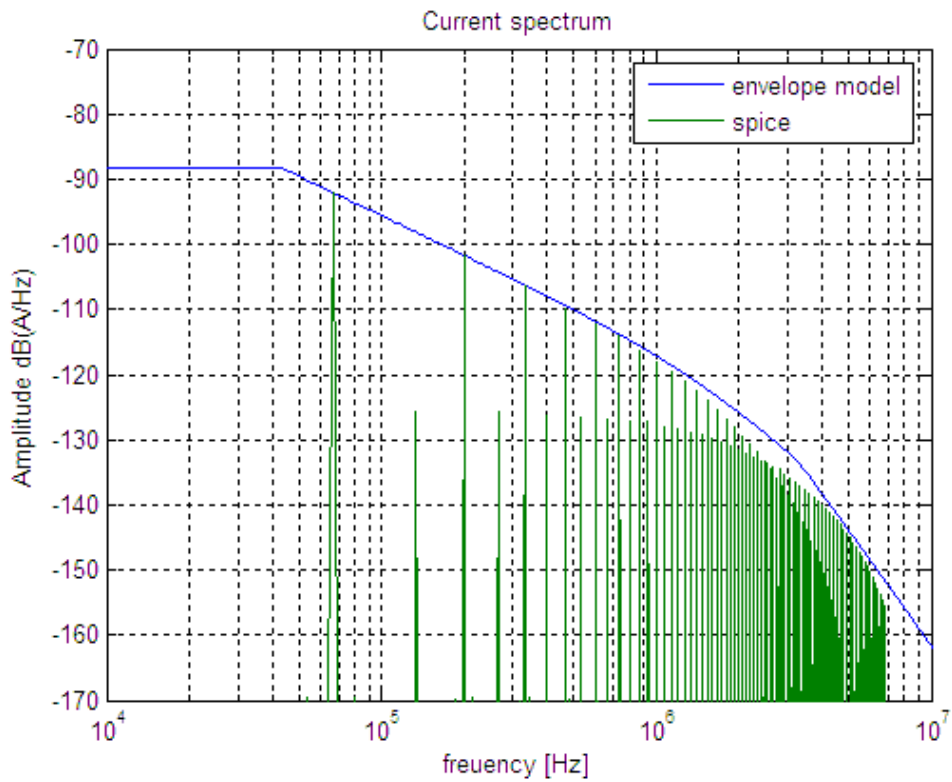


Fig. 47 Current spectral density predicted by envelope model (case 3).

According to Fig.15 the current in the secondary loop can be predicted once some parameters are computed using (1.15)-(1.20)

$$v_{s2}(t) = \frac{N_2}{N_1} \cdot \text{abs}(v_{s1}(t)) \quad (2.15)$$

$$R_2 = R_t + R_L + R_D + R_l \quad (2.16)$$

$$L_2 = L_t + L_l \quad (2.17)$$

$$L_t \approx \frac{\mu l_w}{2\pi} \left[\text{Ln}\left(\frac{2l_w}{r_w}\right) - 1 + \frac{r_w}{l_w} \right] + \frac{\mu \cdot l_w}{8\pi} \quad (2.18)$$

$$R_{t,l} = \frac{l_w}{\gamma_{cu} S_w} \quad (2.19)$$

$$R_D = \frac{V_F}{I_F} \quad (2.20)$$

being v_{s2} and v_{s1} the equivalent voltage source for the primary and secondary side of the transformer, N_1/N_2 the transformer winding turns ratio, R_t , R_l , and R_{ind} , account for the ohmic losses in traces, wires and windings between the secondary of the transformer and the load, R_D the equivalent series resistance for the diode device during t_{on} , L_2 depends on the geometry of the connection between source and load and the inductance of inductor in the secondary side. The parameter values of the equivalent circuit in Fig.15 are summarized in Tab.4

Voltage source	Parameters by datasheet	Circuit parameters	Calculated	Measured	Accuracy
A [V]	26	R_t [mΩ]	80	82	±0.15%
T [μs]	15.70	R_l [mΩ]	312	310	±0.15%
T [μs]	7.5	R_D [Ω]	1.3	/	/
t_r [ns]	100	L_l [μH]	67.6	62.8	±0.30%
t_f [ns]	300	L_t [nH]	525	510	±0.30%
N_2/N_1	6	R_L [Ω]	5.85	5.85	±0.15%

Tab. 5 Parameter values for the secondary side equivalent circuit.

The envelope model proposed for current spectrum calculations is compared with the current spectrum computed through the equivalent circuit in Fig.15 using Pspice. The result is shown in Fig.23.

The envelope model is compared with measurements and the results are shown in Figs.24-25.

The envelope current spectrum model shows a very good agreement with SPICE simulations and measurement. Some disagreement is shown with measurements at high frequency: this is probably due to the FFT algorithm that introduce not very good accuracy and the presence in the current waveform of some spikes that the model is not able to predict.

The accuracy for the measurement in frequency domain is ± 2 dB all over the frequency range.

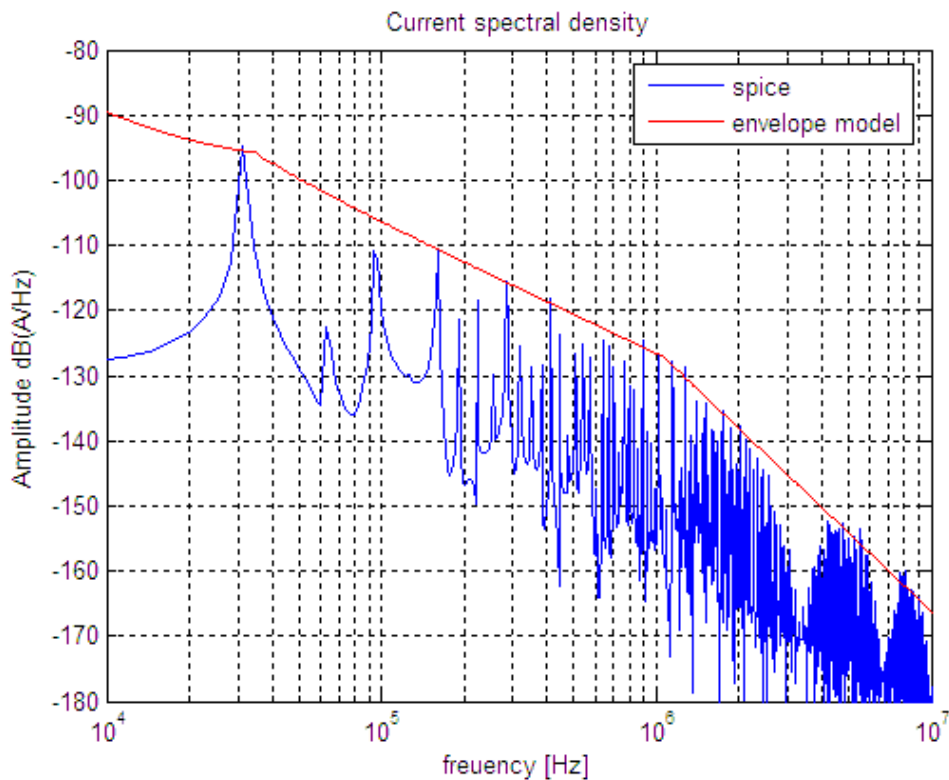


Fig. 48 Current spectrum envelope model compared with PSPICE simulations.

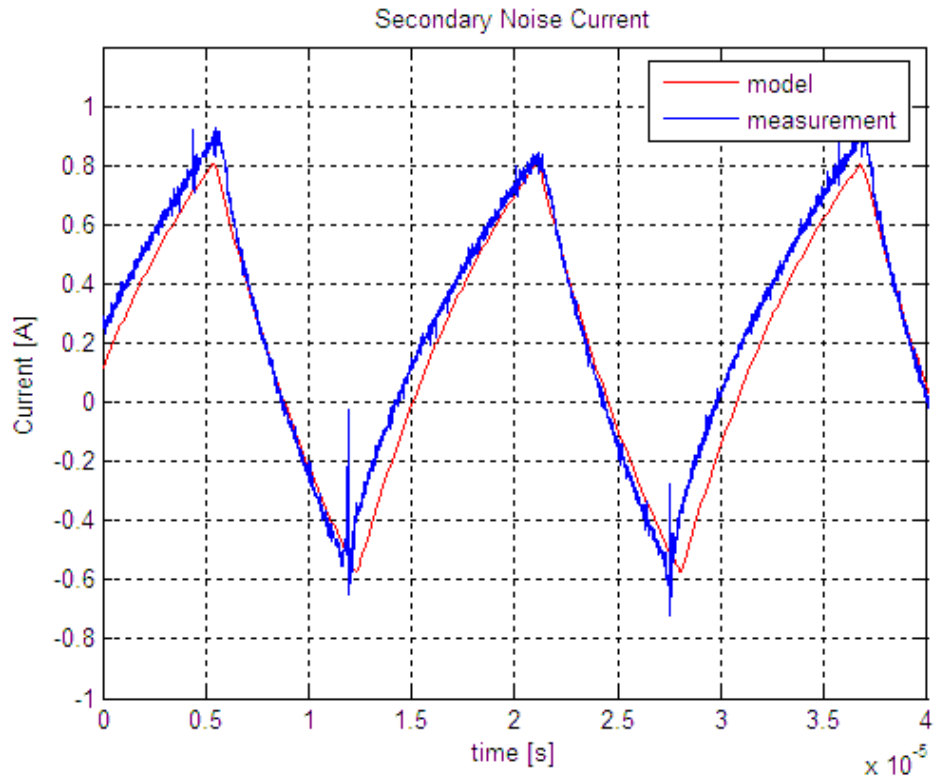


Fig. 49 Current model and measured waveform.

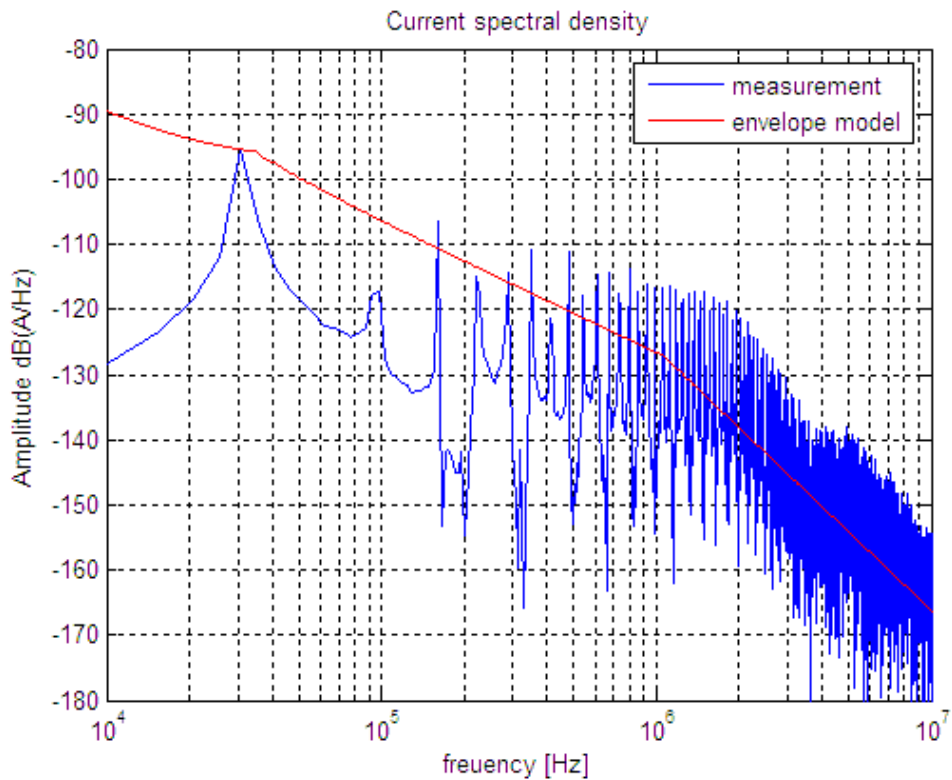


Fig. 50 Current spectrum envelope model and measured spectrum.

Equation Chapter 4 Section 3

III. Coupling mechanisms

Once the voltage and current noise sources are characterized, the coupling mechanisms need to be described.

Assuming that:

1. the current spectrum of both primary and secondary loop sources is known,
2. the voltage spectrum of the signal between the heatsinks and the ground reference of the circuit is known,
3. any susceptible circuit acting as victim can be represented by a single port equivalent circuit,
4. the receiver is in the near field region of the source ($D \ll \lambda$ D is the typical dimension of the over all source-victim ensemble and λ is the wavelength of the noise signal)
5. the source and the victim are weakly coupled (sufficiently distant so that the reaction of the victim's responses back to the source is negligible)

For the calculation of self and mutual inductance, the current flow in the loop is assumed to be a constant and independent of the loop geometry. As underlined later on, this is an intrinsic limitation of the model.

The primary and secondary loops are magnetic coupled to the victim circuit resulting in a current driven voltage source (neglecting the electric coupling between the loops and the victim) and the heatsinks are electric coupled to the victim circuit resulting in a voltage driven current source (neglecting in this case the magnetic coupling between some current flowing through the heatsink and capacitive to ground and the victim).

Due to hypothesis 4 the electric and magnetic coupling mechanisms between the source and the receiver can be modelled respectively as mutual capacitive coupling and mutual inductance coupling.

The weak coupling assumption implies that $M^2 \ll \langle L_1 L_2, C_1, C_2 \rangle \gg C_{12}$ and $1/j\omega C_{12} \gg j\omega L_1, j\omega L_2$ in the equivalent circuits Figs. 19 and 37.

Schematic views of the electric and magnetic coupling mechanisms with their sources are shown in Figs.1-3.

The EMI source supplies a time varying current in an exposed circuit loop that creates time varying a magnetic flux density which links the pick up loop in the victim circuit. A time varying magnetic flux density by Lent's law results in induced voltage within the victim's circuitry. This coupling between the source and the victim is known as *Mutual Inductive Coupling*.

At the same time, the EMC source voltage can induce a large charge densities on some exposed surface of the source. This charges creates an electric field which extends through space and a portion of this field can terminate on other charges induced in the victim circuitry. Since the electric field varies with time, the resulting time variation of the induced charge creates a current flow in the victim circuitry. This coupling between the source and the victim is known as *Mutual Capacitive Coupling*.

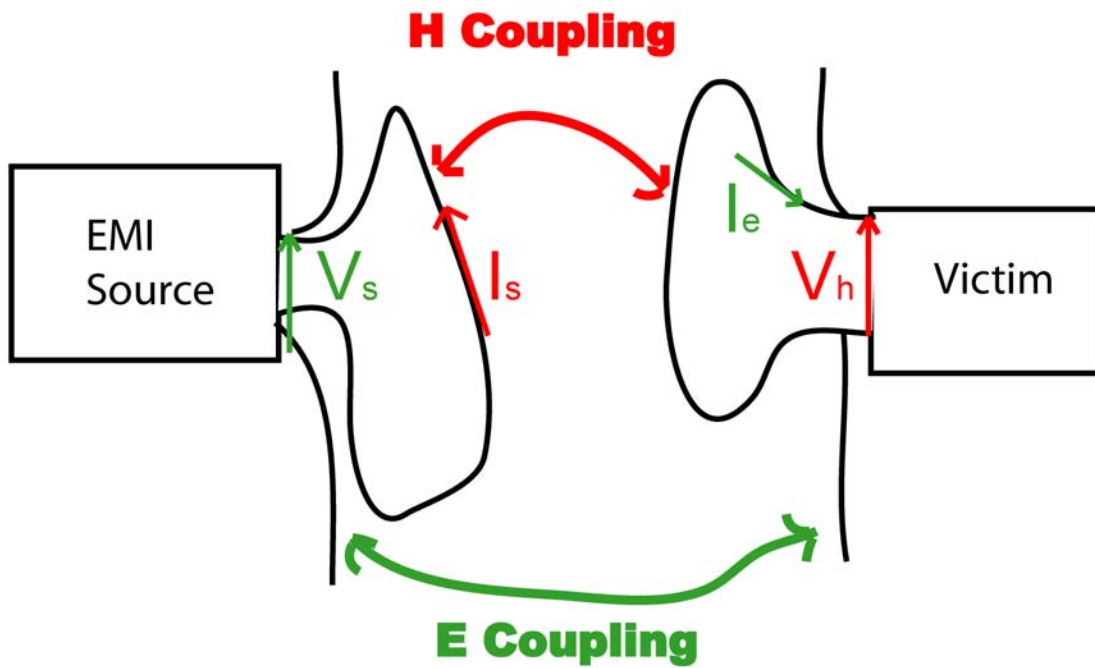


Fig. 51 Magnetic and Electric Coupling between source and victim circuits

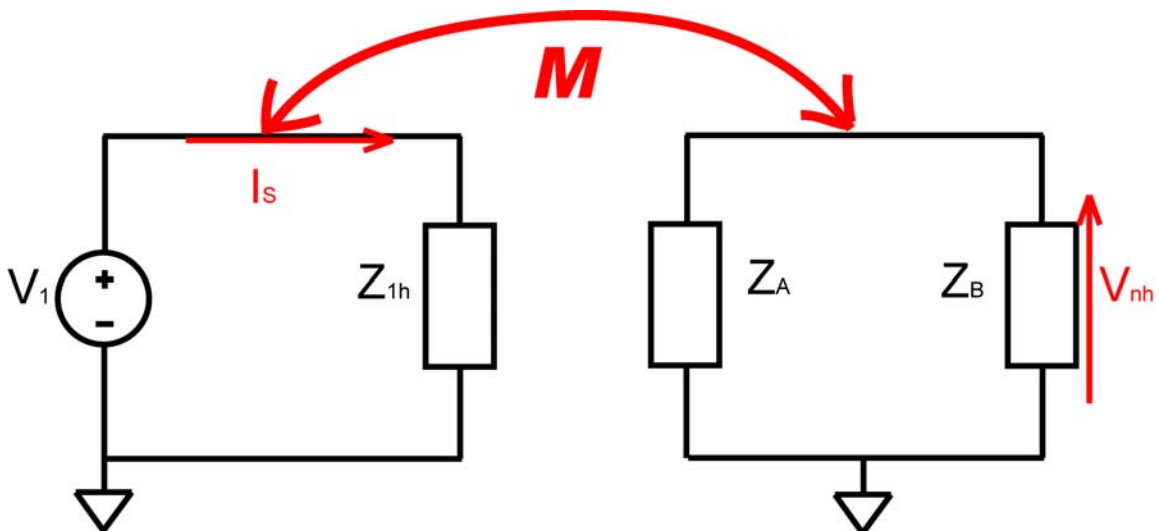


Fig. 52 Equivalent circuit for the mutual inductive coupling mechanism.

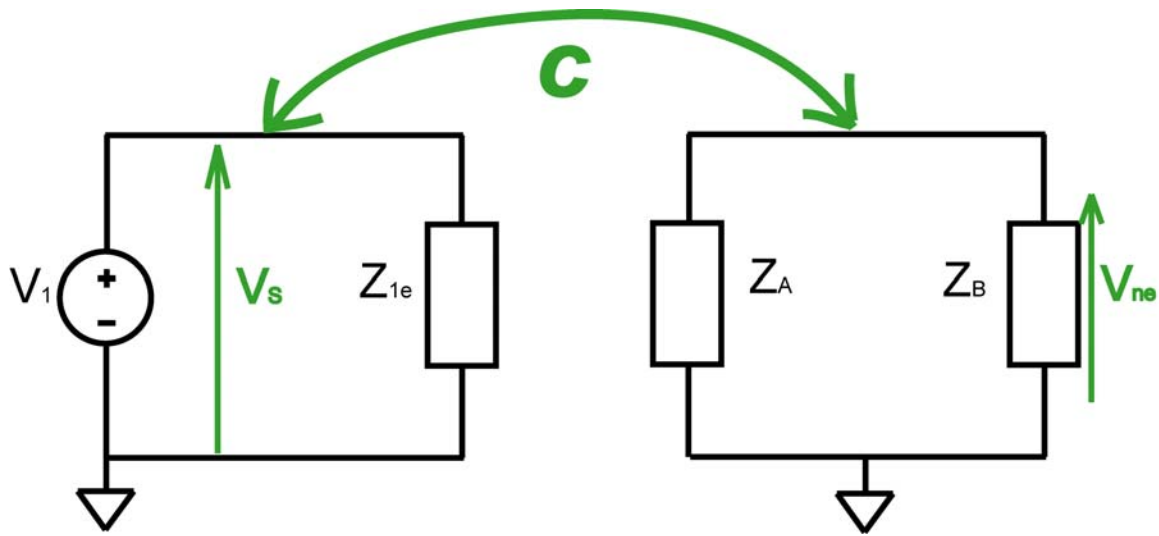


Fig. 53 Equivalent circuit for the mutual capacitive coupling mechanism.

In case of weak coupling between source and victim, the mutual inductive coupling can be represented by a current controlled voltage source as in Fig.4

$$\hat{V}_H = j\omega M \hat{I}_S \quad (3.1)$$

The mutual capacitive coupling between source and victim under the assumption of weak coupling can be represented by a voltage controlled current source as in Fig.5

$$\hat{I}_E = j\omega C \hat{V}_S \quad (3.2)$$

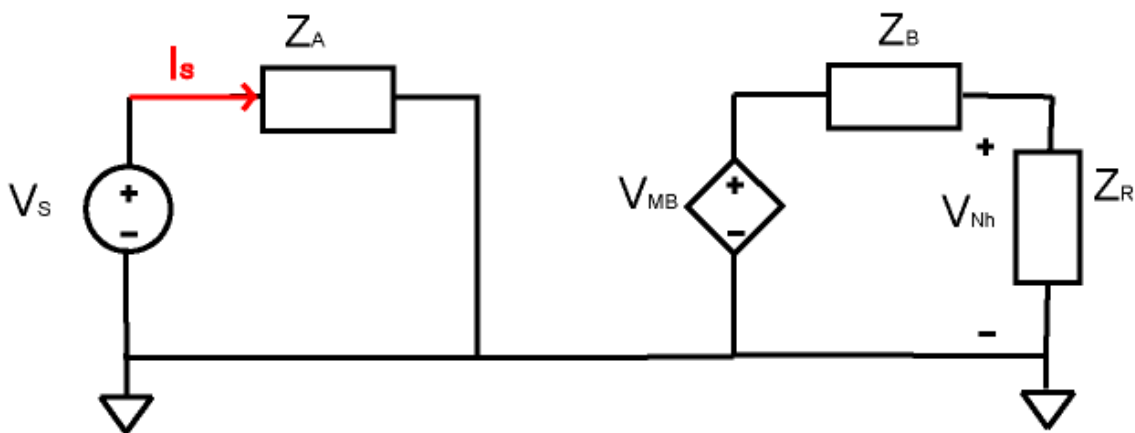


Fig. 54 Magnetic coupling equivalent circuit.

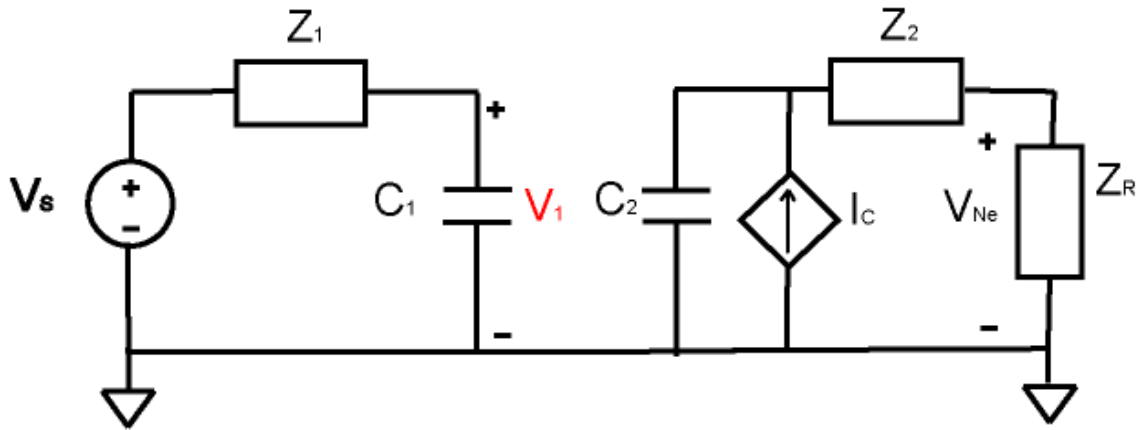


Fig. 55 Electric coupling equivalent circuit.

The noise voltage due to the magnetic coupling mechanism (Fig. 2) across the receiver can be simply modelled as

$$\hat{V}_{Nh} \approx j\omega M \hat{I}_s \cdot \left(\frac{Z_A}{Z_B + Z_A} \right) \quad (3.3)$$

while the noise voltage due to the electric coupling mechanism (Fig. 3) across the receiver is

$$\hat{V}_{Ne} = j\omega C_{12} \hat{V}_1 \frac{\frac{1}{j\omega C_2}}{\frac{1}{j\omega C_2} + \hat{Z}_2 + \hat{Z}_R} \hat{Z}_R \quad (3.4)$$

Both the mutual capacitance C and the mutual inductance M between the source and receiver depends on the geometry of the source and receiver, the medium and the distance between them.

IV. Closed formulas for mutual and self-inductance

The mutual inductance and capacitance of actual circuit configurations are usually difficult to know precisely due to the irregular geometries of the circuits, to the details of local geometries as well as to the presence of magnetic material in the surrounding environment. A lot of closed formulas can be found in literature [1-6] that can be applied in different cases, but for 3D geometry there are very few of them.

For 3D geometries, mutual inductance and capacitance can be evaluated by numerical computation using some software [7-9].

In order to validate the model, a Triple Loop Antenna (TLA) is chosen as susceptible receiver and its equivalent circuit is shown in Fig.6.

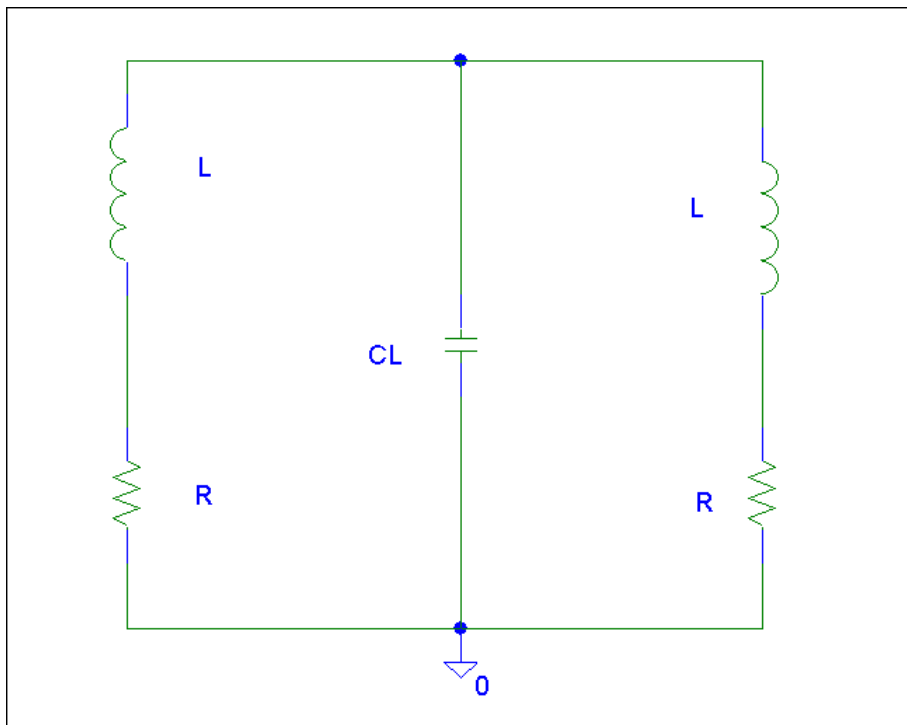


Fig. 56 Equivalent circuit of the receiving TLA.

The mutual inductance coupling is supposed to be only between the actual trace and its coplanar loop of the TLS while the mutual capacitive coupling is between an exposed metal surface and the all TLA structure.

The mutual inductance between the trace carrying the current and a loop of the TLA can be calculated with good approximation using the formula [10] of the mutual inductance between two coaxial and coplanar thin loops,

$$M = \mu \sqrt{r_{eq} \cdot r_2} \left[\left(\frac{2}{k} - k \right) \cdot I_1(k) - \frac{2}{k} \cdot I_2(k) \right] \quad (3.5)$$

$$k^2 = \frac{4r_{eq}r_2}{d^2 + (r_{eq} + r_2)^2} \quad (3.6)$$

being $I_1(k)$, $I_2(k)$ the elliptic integrals respectively of first and second kind, r_2 the radius of the TLA, μ the magnetic permeability of the medium, r_{eq} the radius of the equivalent source current loop and d the distance between the two planes containing the two loops.

The self inductance of the actual source loop can be computed using [10]

$$L = N^2 \mu r_{eq} \left[\text{Ln} \left(\frac{16r_{eq}}{d_{eq}} \right) - 2 \right] + \frac{\mu \cdot N \cdot p}{8\pi} \quad \text{for } r_{eq} > 5d_{eq} \quad (3.7)$$

Both self and mutual inductance can be calculated using (1.8) and (1.6) with two different methodologies:

- the same area criterion
- the same perimeter criterion

being r_{eq} the radius of the equivalent source current loop according to the different criteria and d_{eq} the equivalent diameter of the trace.

For the same area criterion, $r_{eq} = \sqrt{\frac{A}{\pi}}$ being A the internal area of the actual trace,

for the same perimeter criterion, $r_{eq} = \frac{p}{2\pi}$ with p the perimeter of the actual trace and $d_{eq} \approx \frac{2s}{2\pi}$ with s the width of the trace.

For the calculation of the self inductance of the actual trace the method of partial inductance is also considered [11-14].

In first instance, a test simulation (Test A) with a source loop and a coplanar coaxial receiving loop is considered. The imaginary part of the self impedance Z_{11} of the first loop and of the mutual impedance between the loop Z_{21} is computed and compared with the impedance computed using respectively (1.8) and (1.6). The results are shown in Figs. 7-8. Tab.1 summarizes the values calculated using (1.8) and (1.6) in Test A.

Test A			
Input dimension	Value [m]	Parameter output	Value [nH]
R_1	0.101	L_1	627
R_2	0.0508	L_2	2600
D_1	0.002	M_{12}	40
D_2	0.024		

Tab. 6 Test A parameter values.

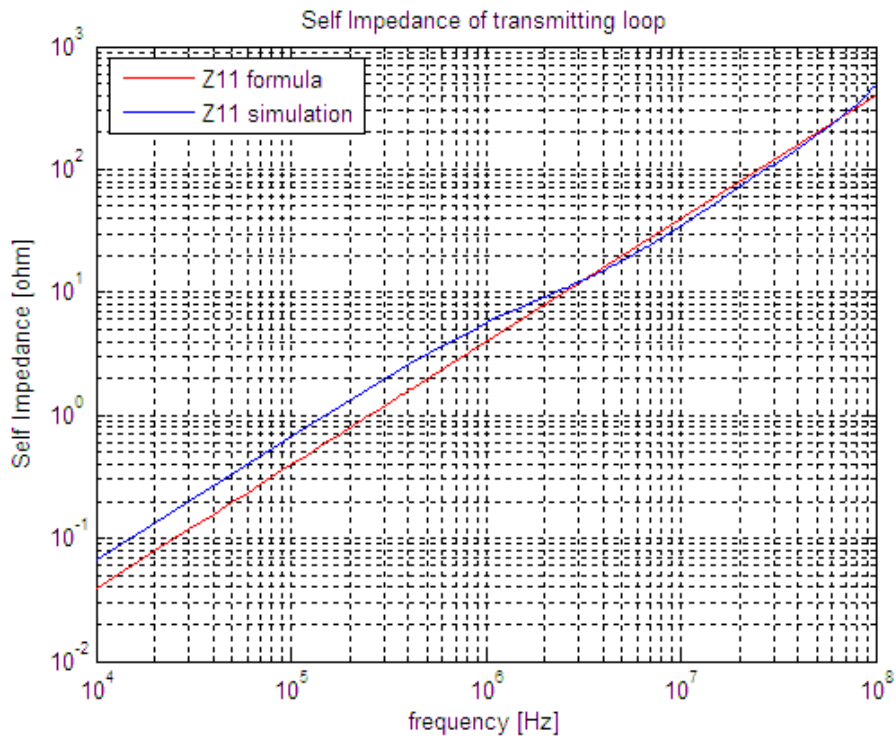


Fig. 57 Imaginary part of self impedance of the source loop Test A.

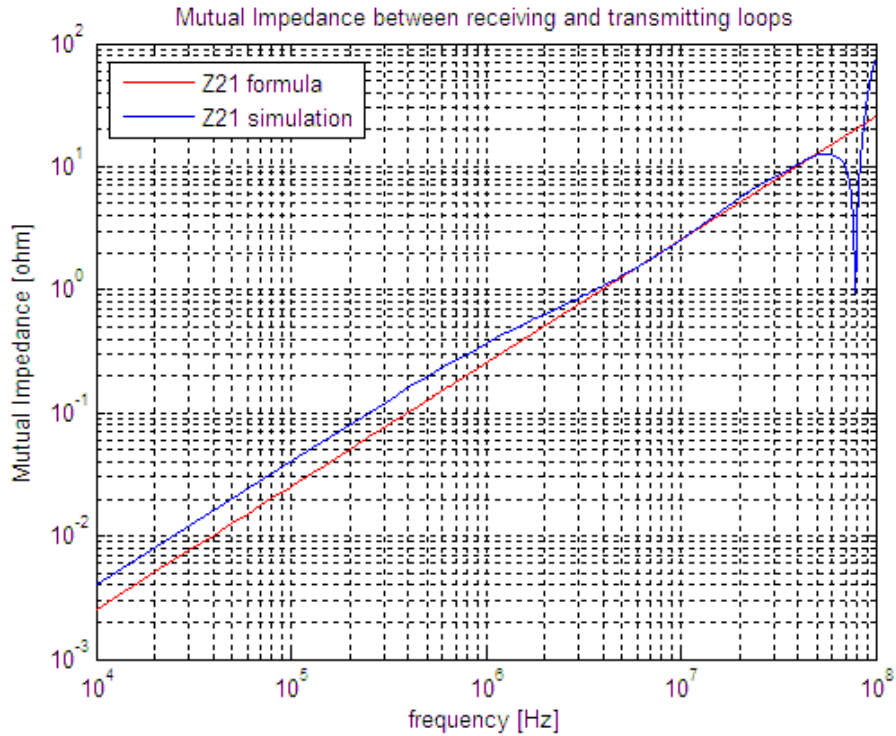


Fig. 58 Imaginary part of Mutual impedance Test A.

Different real trace geometries with 47Ω load are simulated with numerical simulator based on a FIT technique [15] and compared with the results of (1.8) and (1.6). The equivalent radius of the current loop can be calculated using the same loop area criterion or the same perimeter criterion. The self inductance of the real trace can be also calculated by the method of partial inductance [11-14]. The simulated test traces are presented in Figs.9-11.

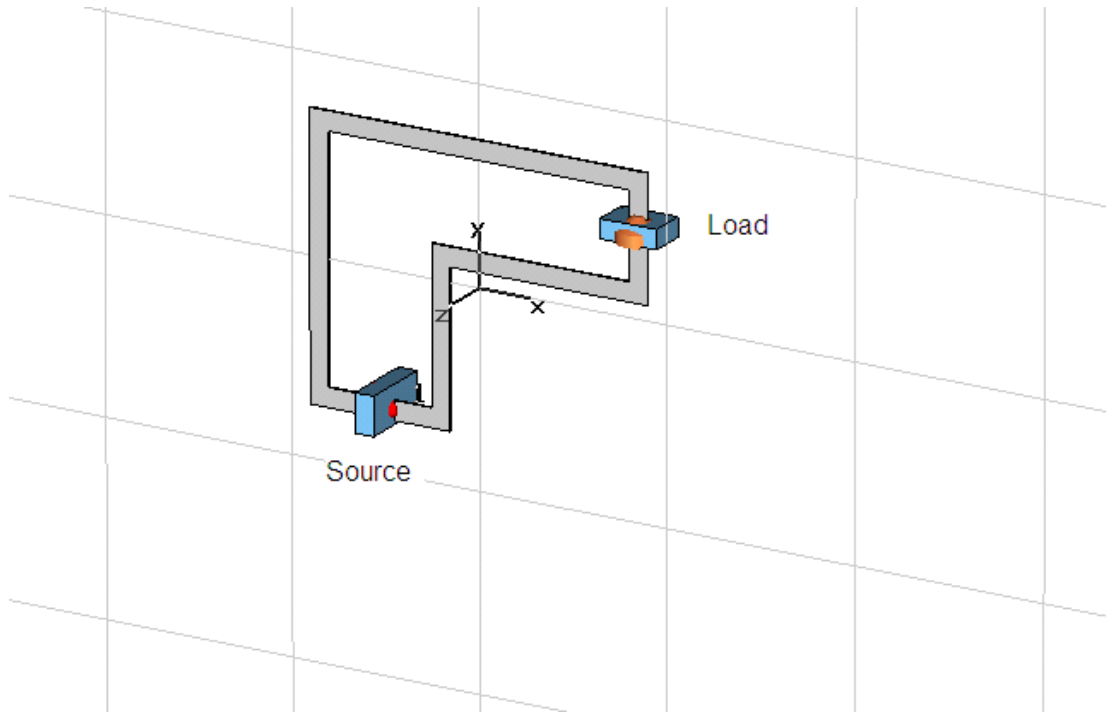


Fig.59 Test Circuit P1.

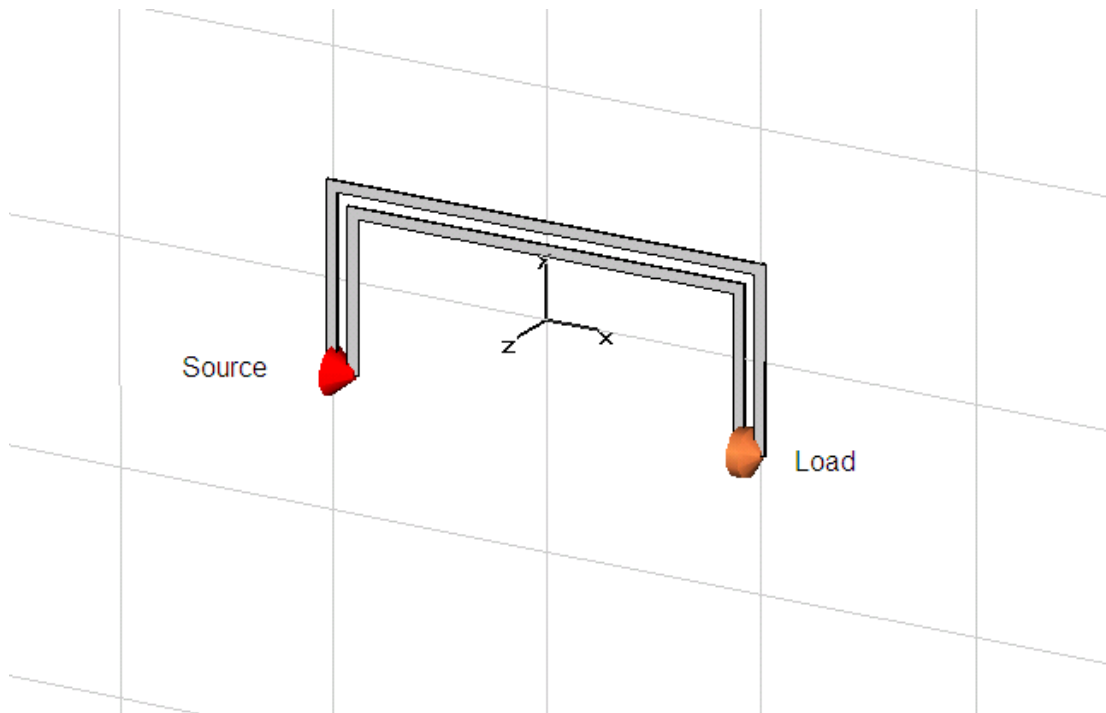


Fig.60 Test circuit P2.

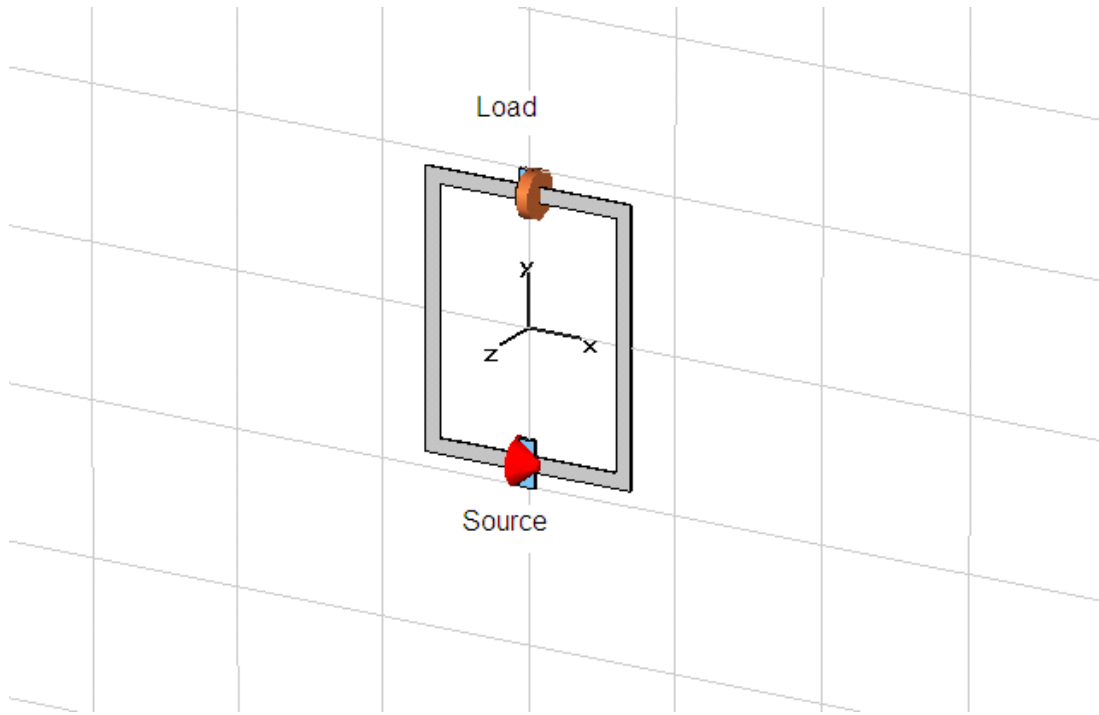


Fig.61 Test Circuit P3.

The results obtained for the mutual impedance (1.6) are shown in Figs. 12-14.

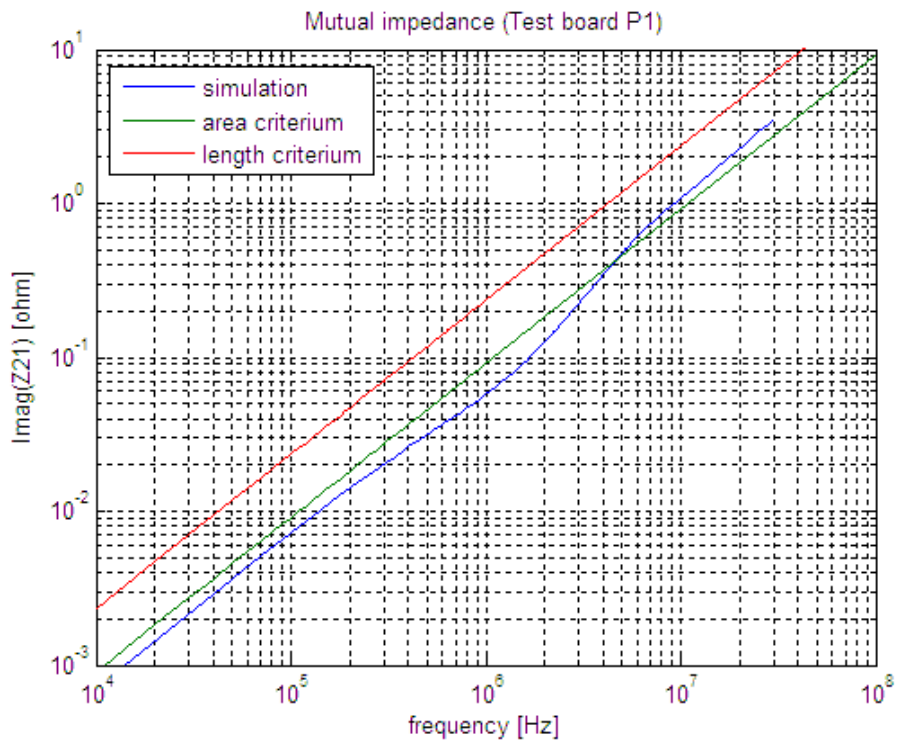


Fig. 62 Imaginary part of mutual impedance between transmitting and receiving loop (Test board P1).

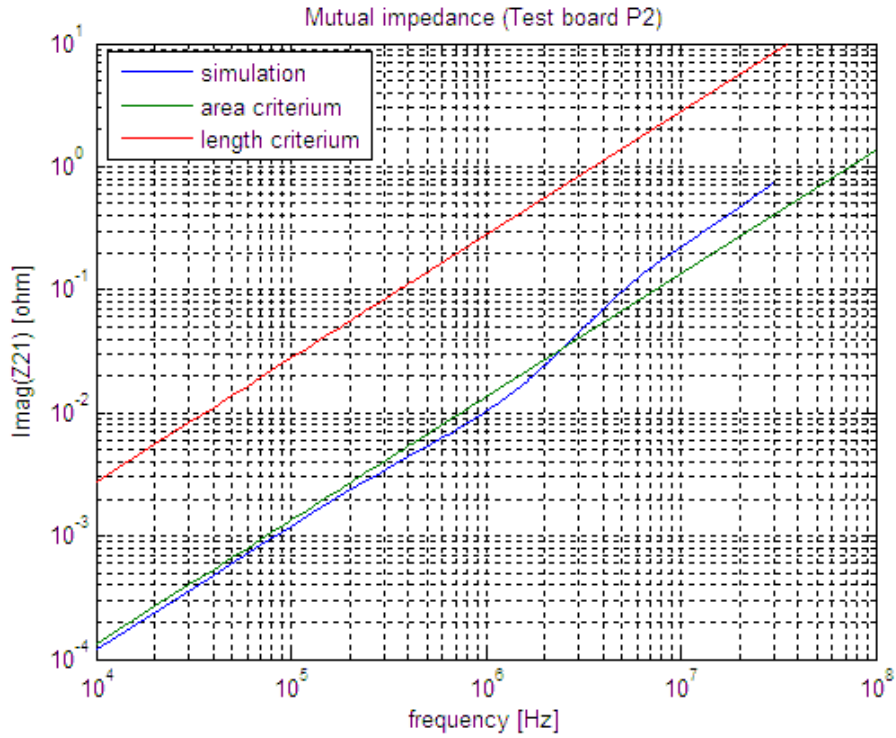


Fig. 63 Imaginary part of mutual impedance between transmitting and receiving loop (Test board P2).

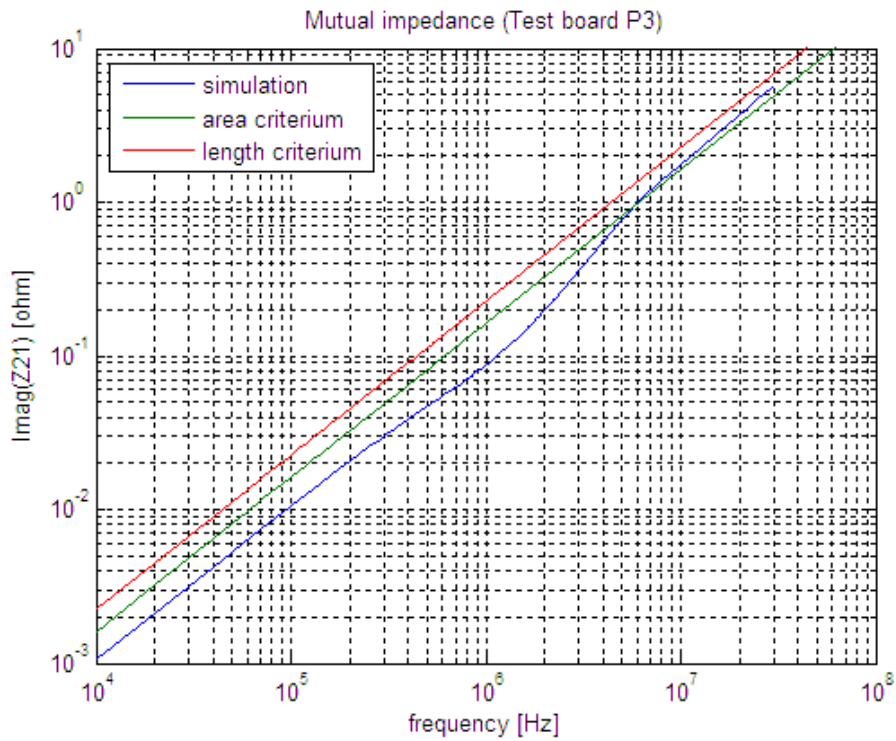


Fig. 64 Imaginary part of mutual impedance between transmitting and receiving loop (Test board P3).

Tabs.2-3 summarize the input parameter values for the test board and the computed parameters for the different test board.

Input parameter values	P1	P2	P3
Area [mq]	0.011655	0.001725	0.02065
Perimeter [m]	0.612	0.665	0.6
Width [mm]	10	5	10

Tab. 7 Input parameter values for P1, P2 and P3.

The results clearly show that the same area criterion for the equivalent radius of the source current loop gets to better agreements with simulations results in the calculation of the mutual impedance between transmitting and receiving loop. The weak coupling assumption is also verified.

Regarding to the self inductance of the Test board P1, P2, P3, the results obtained with (1.6) and using the method of partial inductance are compared with simulations and reported in Figs.15-18.

Computed parameter values	P1	P2	P3
M area criterion [nH]	14	2	26
M perimeter criterion [nH]	37	44	36
L area criterion [nH]	263	115	368
L perimeter criterion [nH]	459	602	448
L partial inductance [nH]	382	336	443
L closed formula [nH]	/		351

Tab. 8 Output parameter values for P1, P2 and P3.

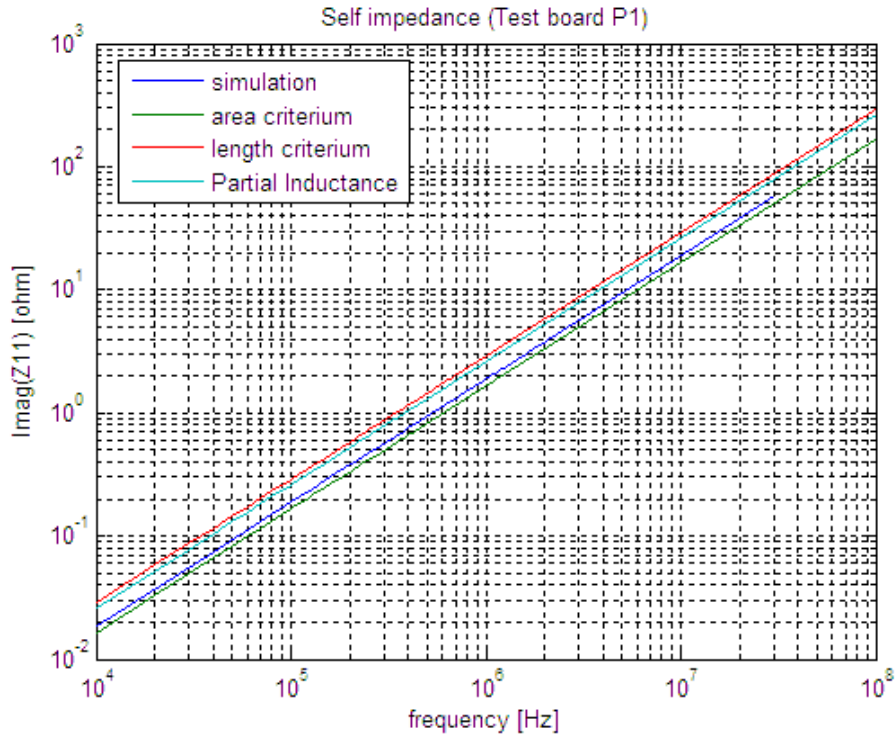


Fig. 65 Imaginary part of self impedance of Test board P1

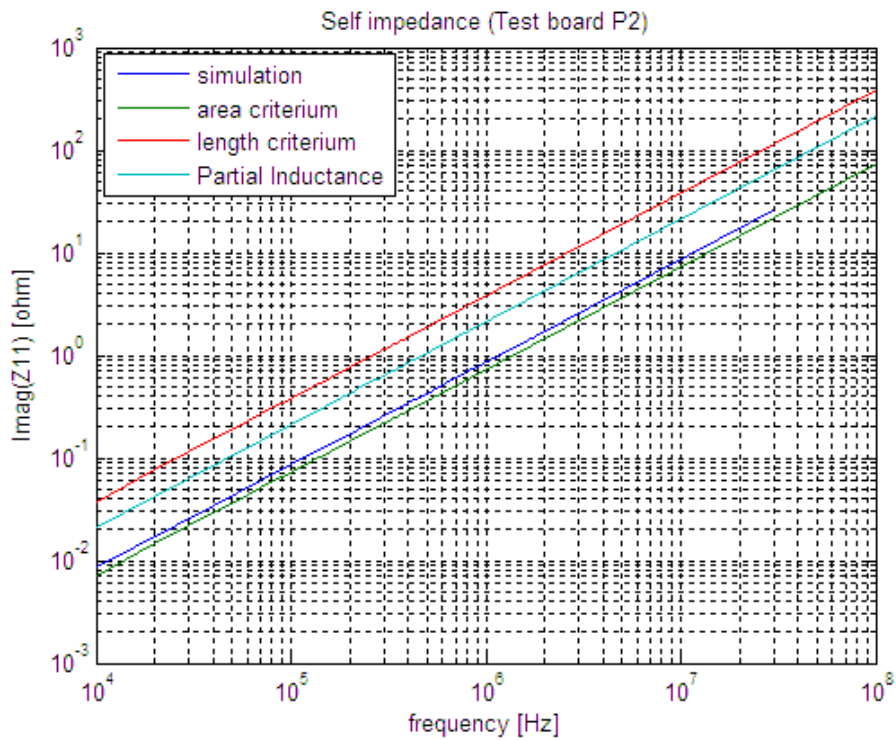


Fig. 66 Imaginary part of self impedance of Test board P2

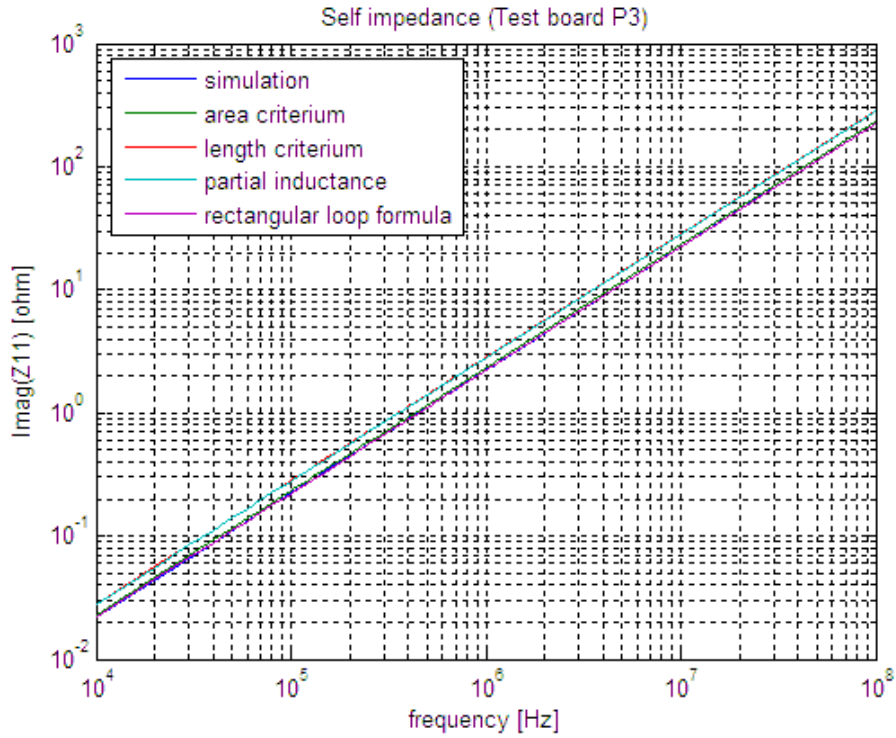


Fig. 67 Imaginary part of self impedance of Test board P3

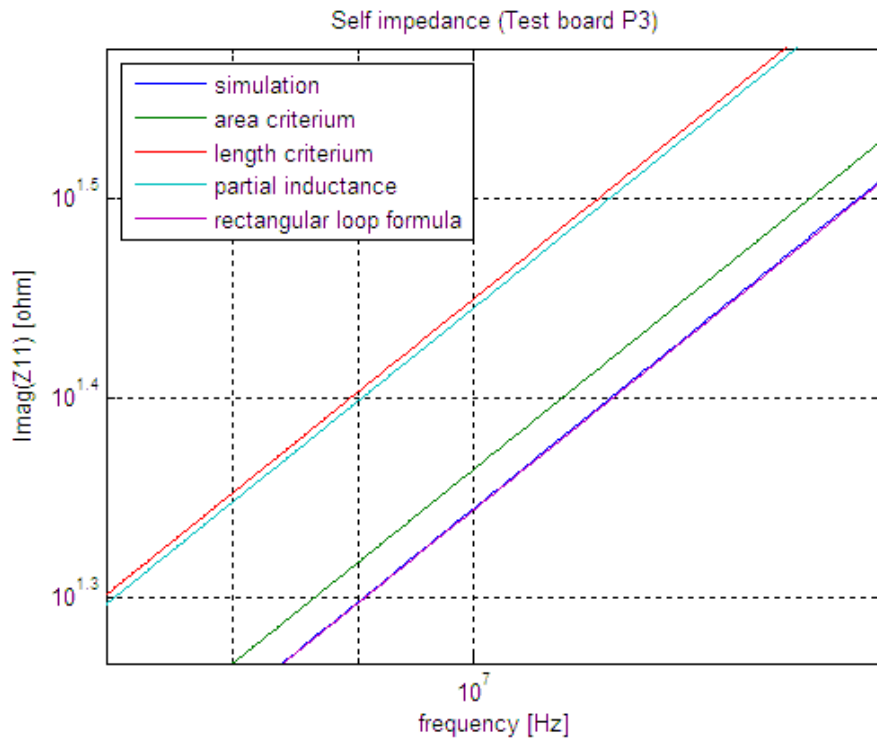


Fig. 68 A zoom view of the imaginary part of self impedance of Test board P3

The self inductance of the last board (P3) is also computed using the formula for a rectangular loop and it is in perfect agreement with the simulated results as shown in Figs.7-8.

The results clearly show that the same area criterion for the equivalent radius of the source current loop gets to better agreements with the results of simulation.

Considering different geometry configurations for wire, ribbon cable, trace, coaxial cable and twisted pair connection the self inductance generally depends on length, transversal dimension and width of a cross section of the connection as

$$L \approx \frac{\mu \cdot l}{2\pi} \log\left(\frac{D}{d}\right) \quad (3.8)$$

When $D \gg d$, L is directly proportional to the area of the loop :

$$L \leq \frac{\mu \cdot l}{2\pi} \left(\frac{D}{d}\right) = \frac{\mu \cdot A}{2\pi d} \quad (3.9)$$

The actual value of the imaginary part of the mutual and self impedance can be considered as an apparent inductance which value depends on frequency and parasitic capacitance. At high frequency the simulated value is the actual value of inductance.

V. Experimental validation of magnetic coupling

A network analyser (NA) is used to measure the transfer function between one of the test board P1, P2, P3 and one gaped loop of the TLA. The test boards are terminated with a 47Ω resistor to minimize the reflected power at the input port of the NA. One gap of the loop is shorted with copper tape and the other is chosen as output port to the NA. The equivalent circuit of the test setup of the test boards is presented in Fig.19.

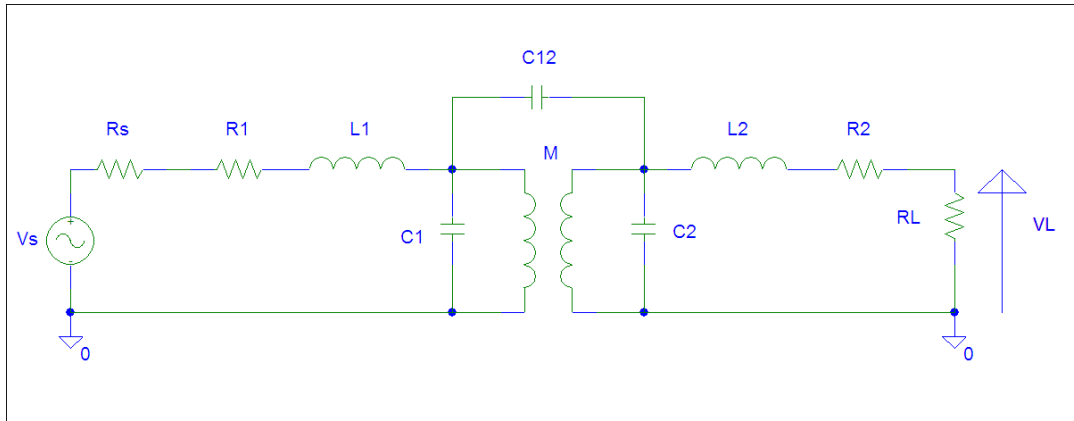


Fig. 69 Equivalent circuit for mutual inductive coupling between test boards and receiving loop.

The transfer function can be simply calculated neglecting the self capacitance C_1 of the source and receiving loop C_2 and the mutual capacitance C_{12} between them.

$$\hat{H}_M \triangleq \frac{\hat{V}_L}{\hat{V}_S} = \frac{R_L}{R_2 + j\omega L_2 + R_L} j\omega M \frac{1}{R_1 + R_S + j\omega L_1} \quad (3.10)$$

being $R_L=50 \Omega$ the input resistance of the NA, R_2 and L_2 the resistance and self inductance of the receiving loop, R_S the Thevenin equivalent resistance of the source, R_1 and L_1 the resistance and self inductance of the test boards. Tab.4 presents the parameter values of the transfer function (1.11) for different test boards.

Parameter values	P1	P2	P3
R_L [Ω]	50	50	50
R_2 [Ω]	2	2	2
L_2 [μ H]	2.60	2.60	2.60
R_1 [Ω]	1.192	1.330	1.160
R_s [Ω]	47	47	47
M area criterion [nH]	14	2	26
M perimeter criterion [nH]	37	44	36
L_1 area criterion [nH]	263	115	368
L_1 partial inductance [nH]	413	336	443
C_1 [pF]	<1	<1	<1
C_2 [pF]	2	2	2
C_{12} [pF]	~23	~25	~23

Tab. 9 Parameter's value for different test boards.

The self and mutual capacitance values are estimated using the formulas of the self capacitance of a loop (1.14) and the formula of two wire transmission line of length $2\pi\frac{r_1+r_2}{2}$ [5]. This values need only to confirm the assumption of neglecting all of them comparing with the value of inductance in the equivalent circuit in Figs.19 (weak coupling approximation).

Test board P1, P2, P3 are shown in Figs.20-22.

The magnitude and phase of the transfer function (1.11) is measured and compared with three different cases:

1. mutual and self inductance computed using the same area criterium,
2. mutual and self inductance computed using the same perimeter criterium,
3. mutual inductance computed using the same area criterium and self inductance using the method of partial inductance.

The results obtained are presented in Fig.23-28.

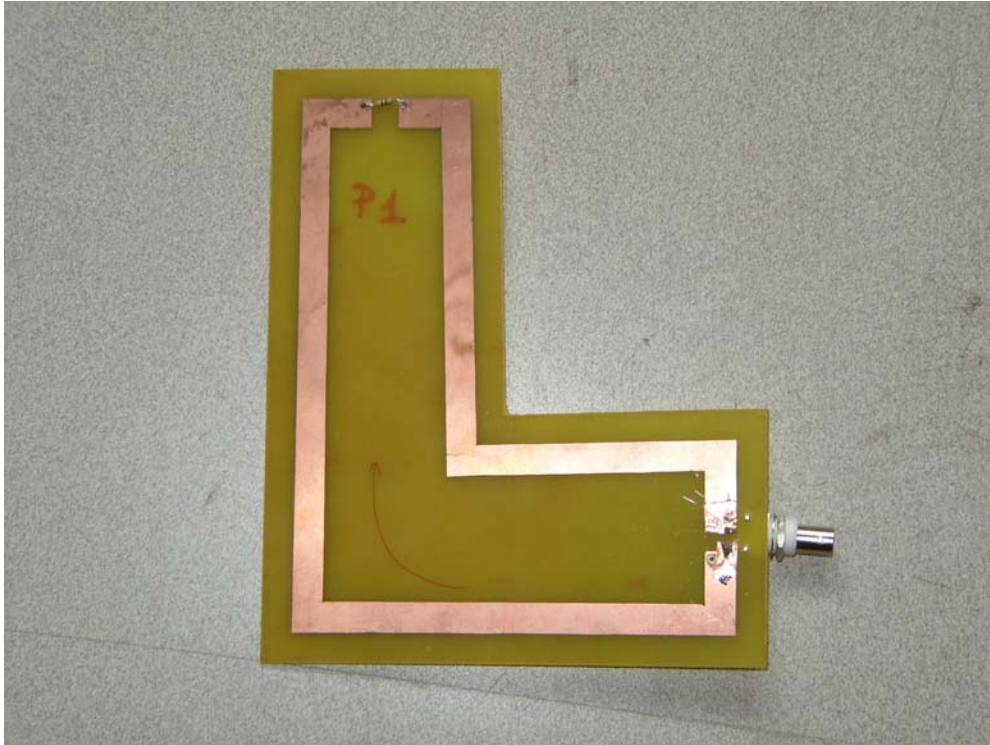


Fig. 70 Test board P1

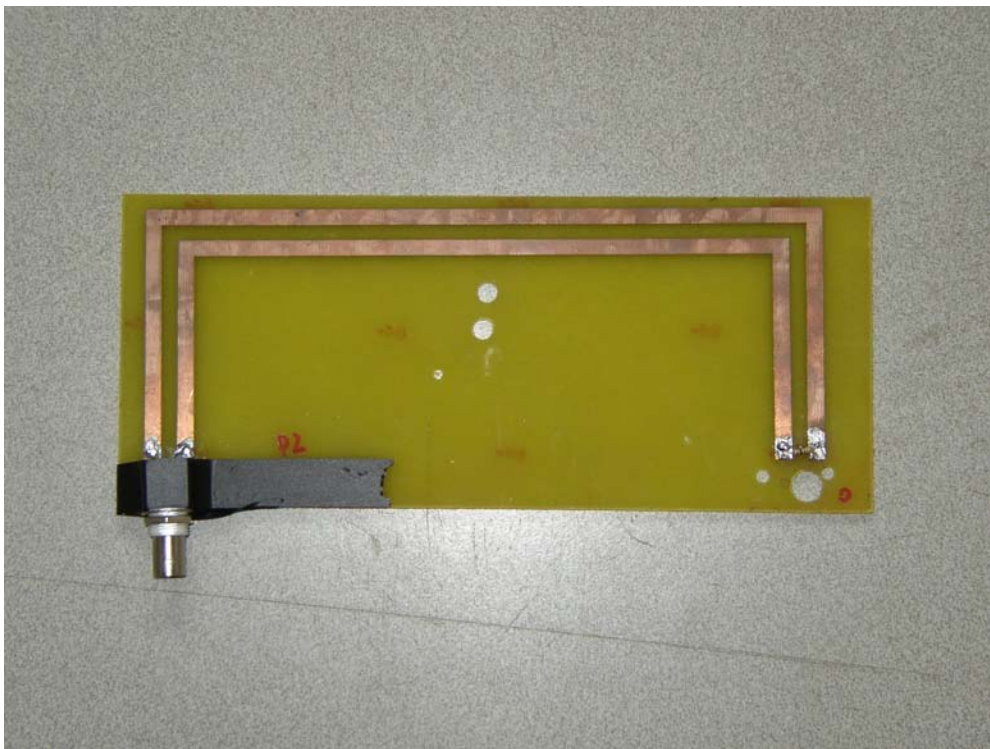


Fig. 71 Test board P2

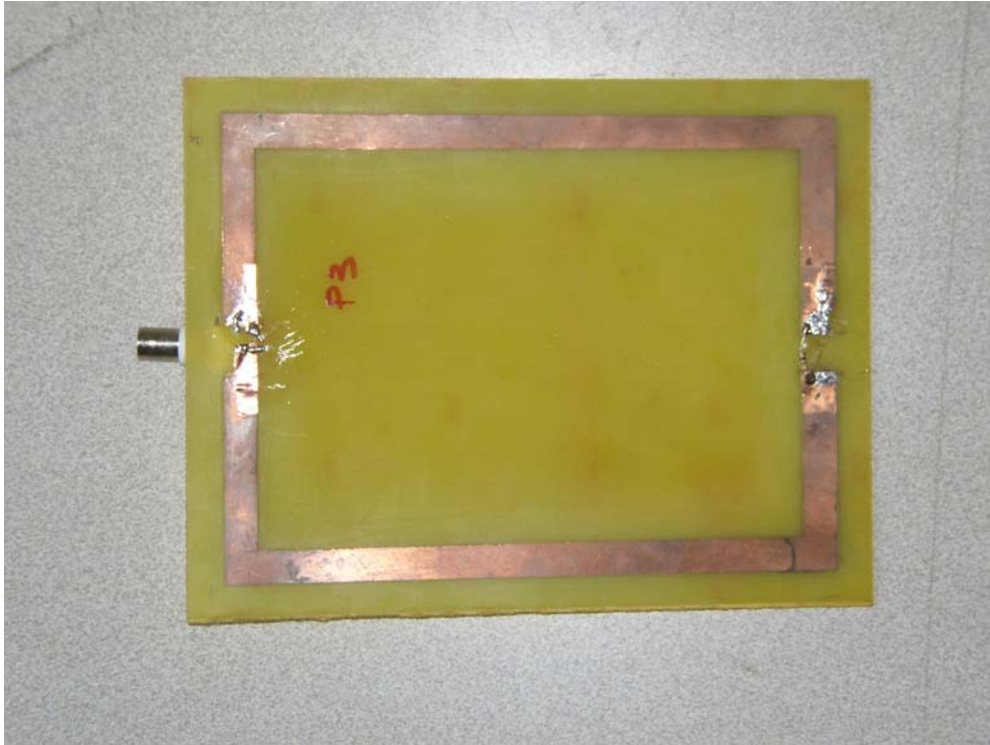


Fig. 72 Test board P3.

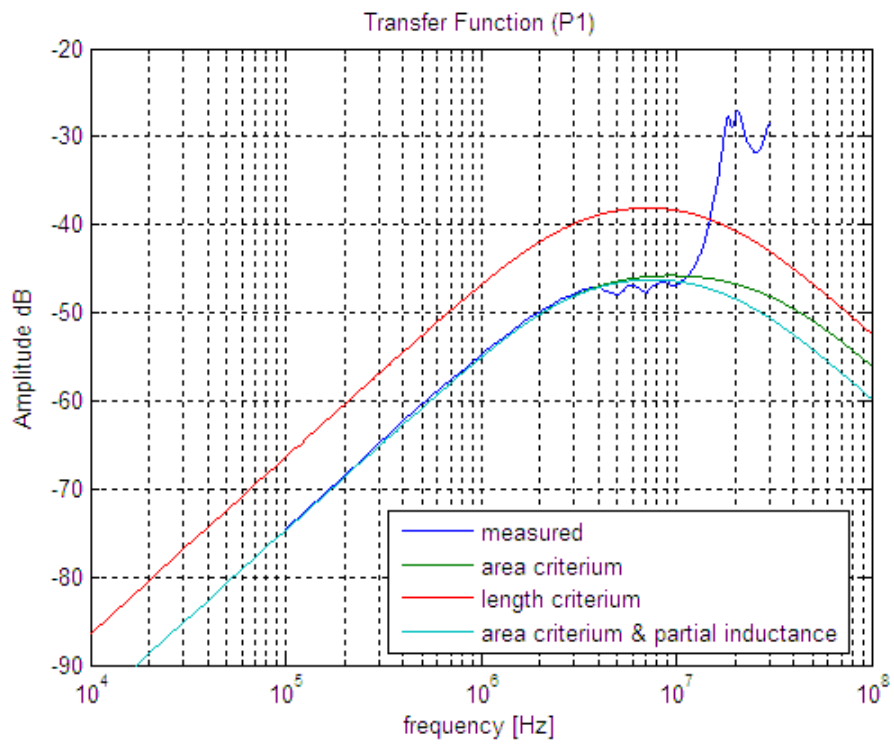


Fig. 73 Magnitude of transfer function for the test board P1.

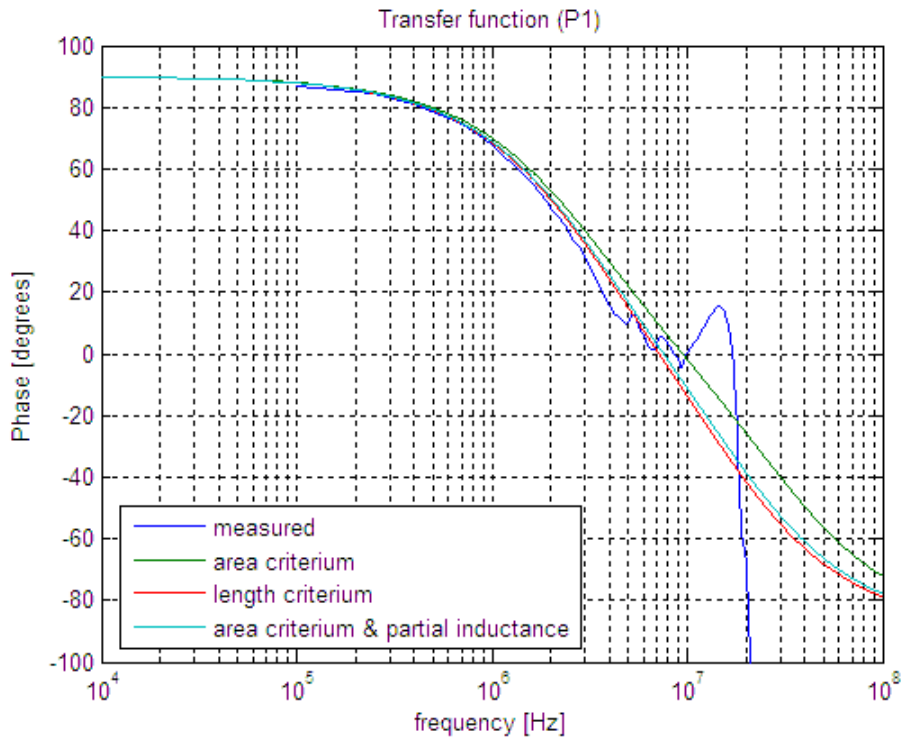


Fig. 74 Phase of transfer function for the test board P1.

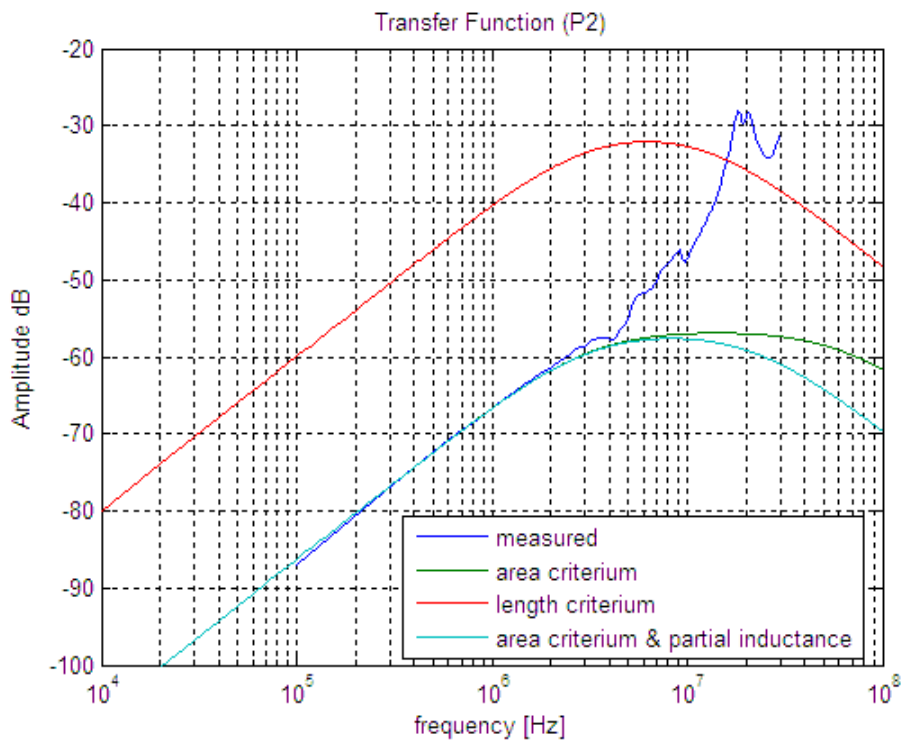


Fig. 75 Magnitude of transfer function for the test board P2.

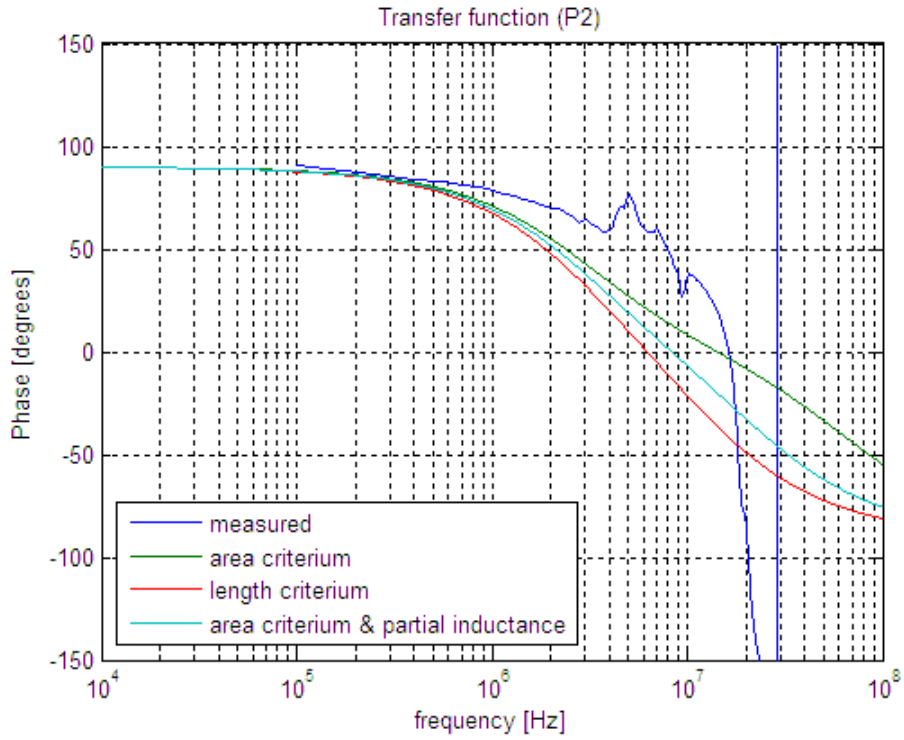


Fig. 76 Phase of transfer function for the test board P2.

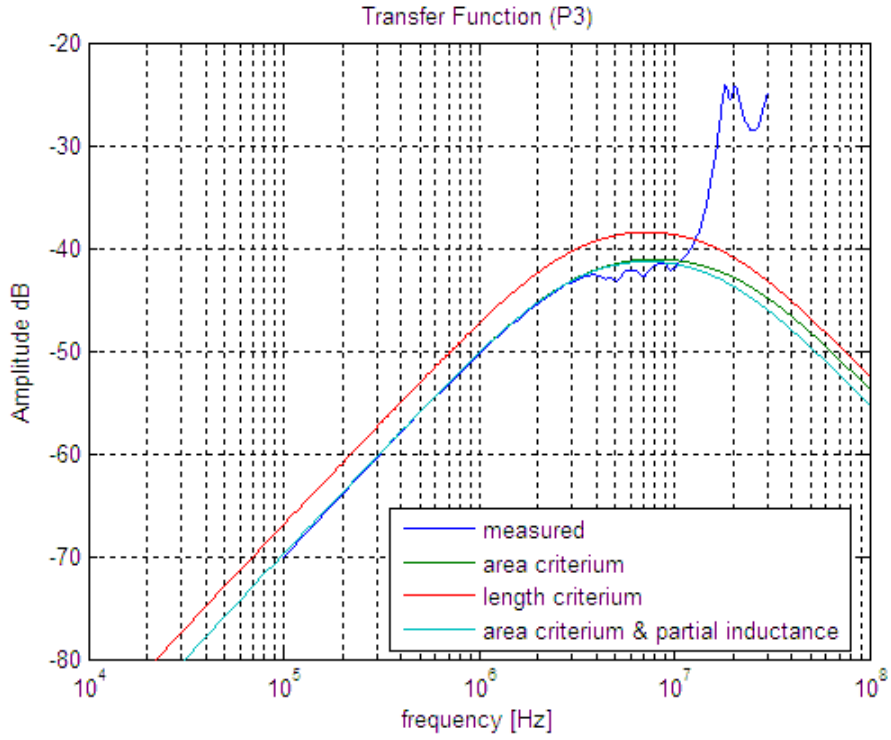


Fig. 77 Magnitude of transfer function for the test board P3.

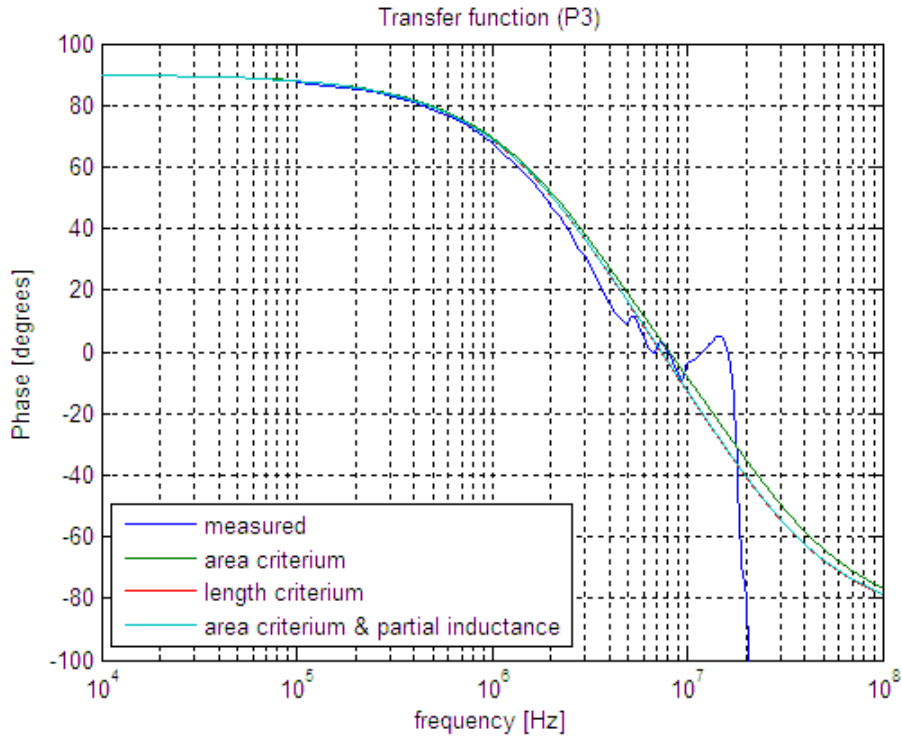


Fig. 78 Phase of transfer function for the test board P3.

The proposed model which parameters are computed using the same area criterion shows a very good agreement with experimental results for all the test boards.

For complex geometry trace, the model which parameters are calculated with the area criterium for the mutual inductance and partial inductance method for the self inductance can be either used. The model shows a very good agreement with experimental results up to 10 MHz.

For this particular configuration one point of the receiving loop is connected to ground and the loop behaves as a $\lambda/4$ resonant dipole at about 24 MHz.

Generally the loop antenna is not connected to ground and its resonance frequency ($\lambda/2$) is about 48 MHz and this allows to extend the frequency range of the model up to 30 MHz.

An intrinsic limitation to the model consists in the fact that it doesn't take into account the spatial density current and voltage distribution on the receiving loop and this doesn't allow to predict the resonant peak of the magnitude of transfer function and the shift of phase at about 20 MHz.

VI. Closed formula for mutual capacitance

The mutual capacitance between some smooth metal piece (ex: an heatsink) and the TLA can be calculated with good approximation using the formula for a spherical capacitor [10]

$$C_{12} = 4\pi\epsilon \frac{r_{eq} \cdot r_2}{r_2 - r_{eq}}, \quad (3.11)$$

being r_2 the radius of the TLA, ϵ the permeability of the medium and r_{eq} the radius of the equivalent sphere of the heatsink. Different real heatsink geometries are simulated with an electromagnetic numerical code [15] (FIT technique) and compared with the results obtained with (1.12). The self capacitance of the heatsink (source) can be computed using

$$C_1 = 4\pi\epsilon r_{eq} \quad (3.12)$$

being r_{eq} the radius of the equivalent source according to the different criteria.

Both self and mutual capacitance can be calculated using two different methodologies:

- the same surface criterion
- the same volume criterion.

For the same surface criterion, $r_{eq} = \sqrt{\frac{S}{4\pi}}$ being S the surface of the exposed metal object,

and for the same volume criterion $r_{eq} = \sqrt[3]{\frac{3V}{4\pi}}$ with V the volume of the exposed metal object.

The self capacitance of the TLA can be computed with [16]

$$C_2 = 3 \frac{2\epsilon r_2}{\left[\ln\left(\frac{16r_2}{d_2}\right) - 2 \right]} \quad (3.13)$$

being d_2 the diameter of the wire section of the loop.

Firstly, two test simulations are considered:

Test A is a single sphere in free space which self capacitance is calculated by (1.13)

Test B is a sphere inside a TLA; a voltage source is connected between sphere and TLA and the equivalent capacitance from the voltage source is calculated as

$$C_{eq} = C_{12} + \frac{C_1 \cdot C_2}{C_1 + C_2} \quad (3.14)$$

The imaginary part of the self admittance of the sphere and the equivalent admittance between the sphere and the TLA is computed and compared with the admittance computed using (1.13) and (1.15).

Tab.5 summarizes the values calculated using (1.15),(1.14),(1.13) in Test A and Test B.

Test A / Test B			
Input dimension	Value [m]	Parameter output	Value [pF]
R_1	0.1000	C_1	11
R_2	0.0508	C_2	7
D_2	0.0240	C_{12}	14

Tab. 10 Test A and B parameter values.

The results are shown in Figs. 29-30.

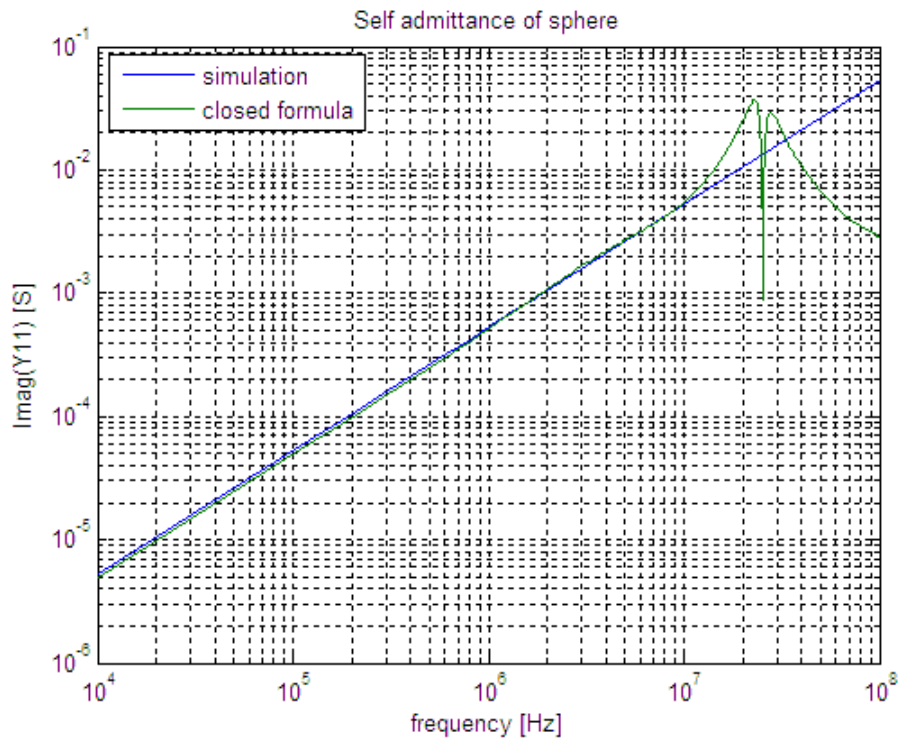


Fig. 79 Imaginary part of self admittance of the sphere in Test A

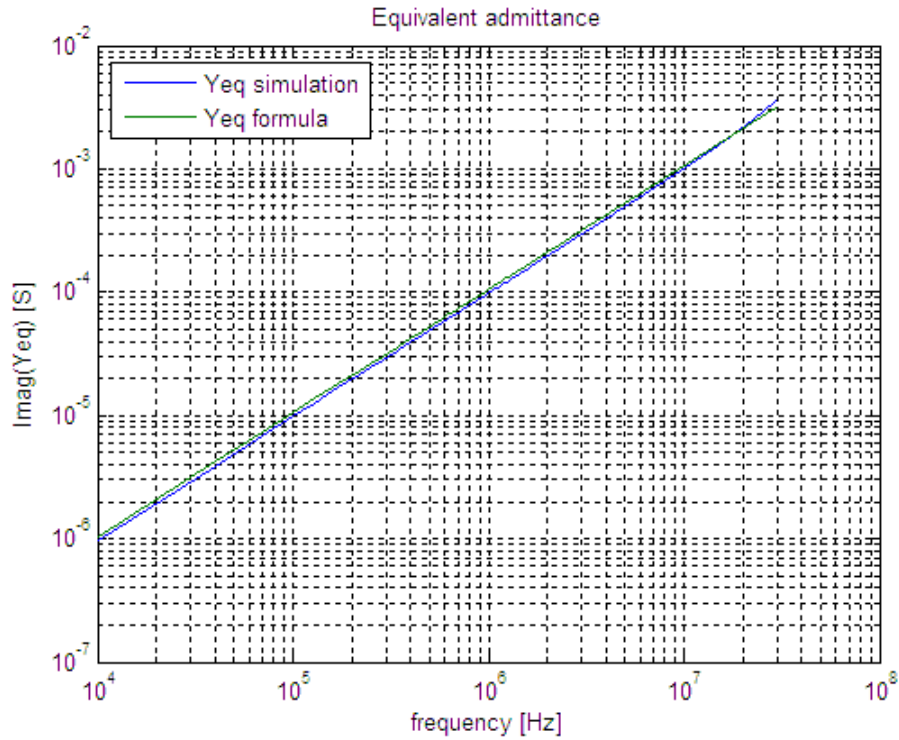


Fig. 80 Imaginary part of equivalent admittance in Test B

Different real heatsinks are simulated with numerical simulator based on a FIT technique [15]. Each of them are set in the TLA and the equivalent capacitance from the source is computed and compared with the results of (1.15).

The equivalent radius of the heatsink can be calculated using the same surface criterion or the same volume criterion as already mentioned. The simulated test heatsinks are presented in in Figs.31-33.

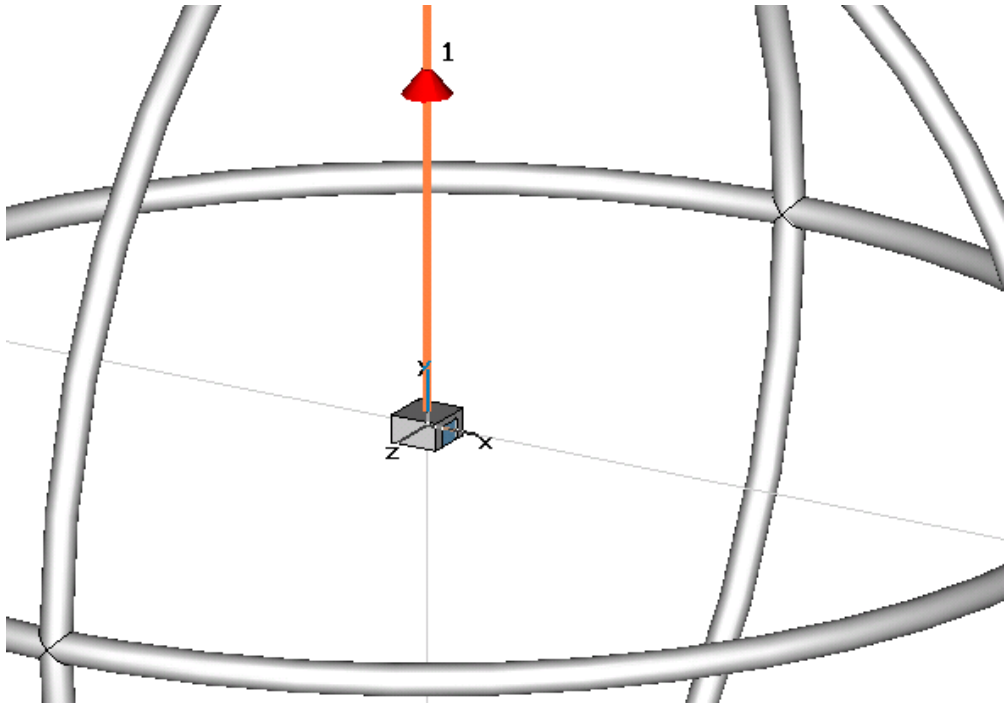


Fig.81 Test heatsink Q1

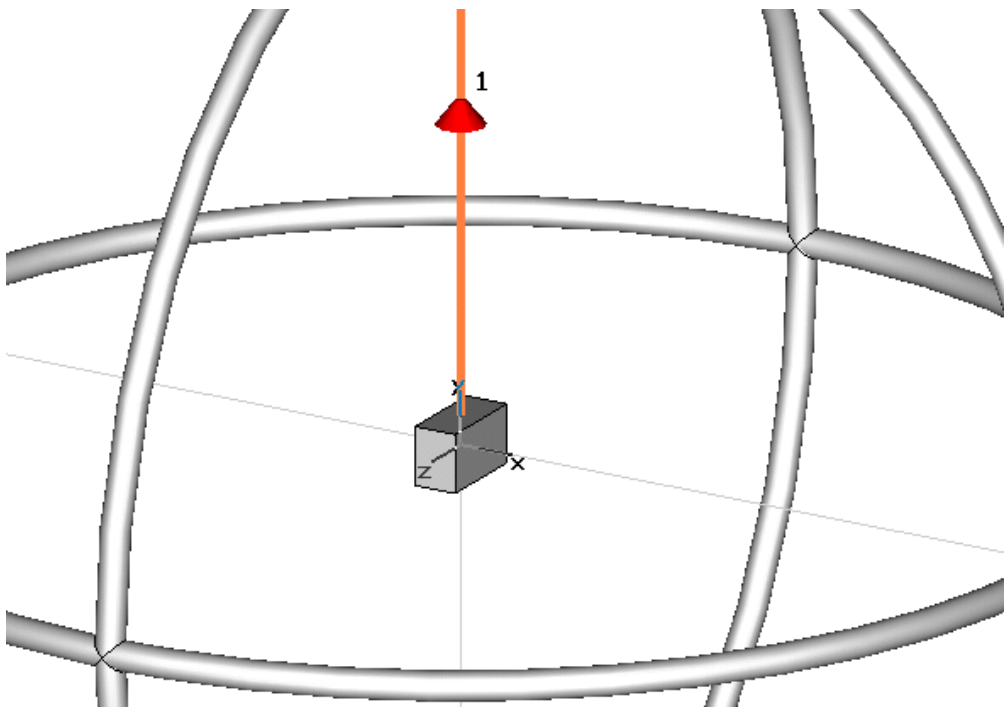


Fig.82 Test heatsink Q2

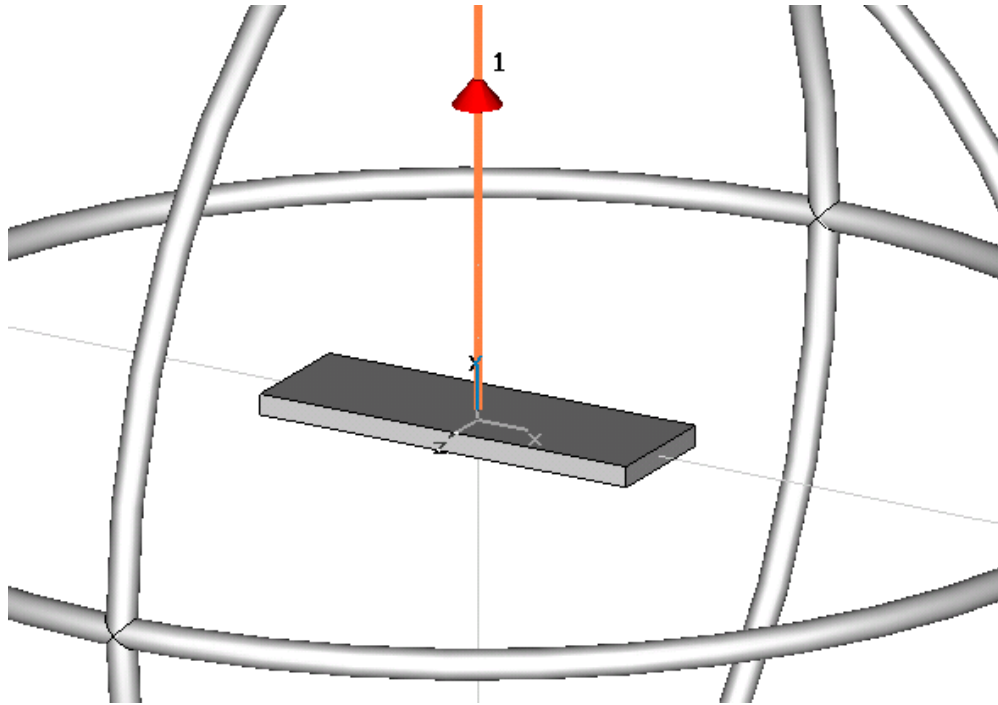


Fig.83 Test heatsink P3

The results obtained for the equivalent admittance $\hat{Y}_{eq} = j\omega C_{eq}$ are shown in Figs. 34-36.

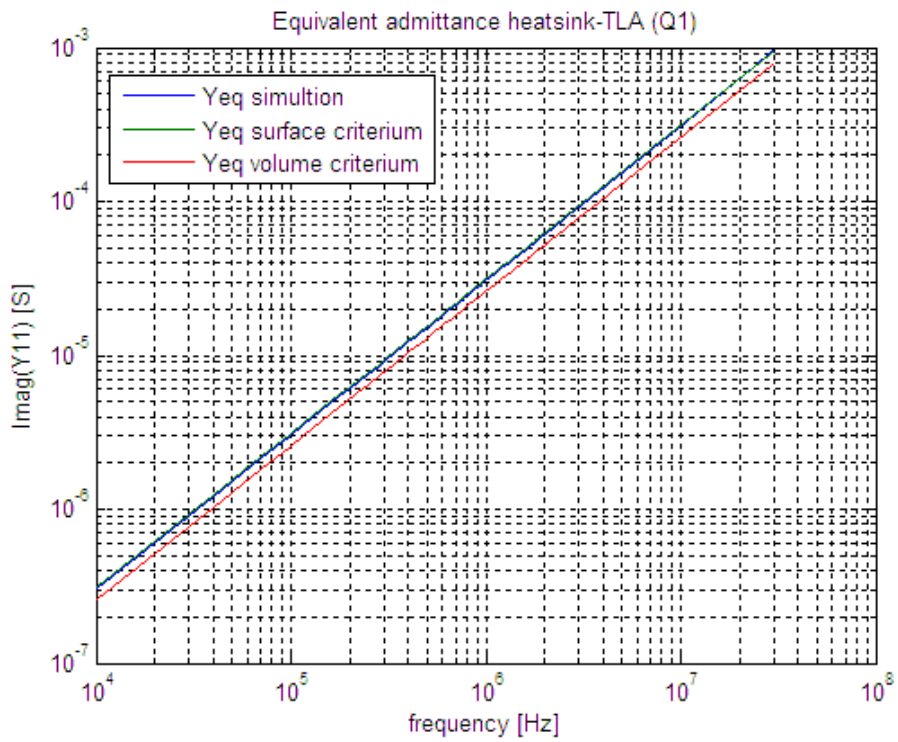


Fig. 84 Imaginary part of equivalent admittance of heatsink-TLA (Test board Q1)

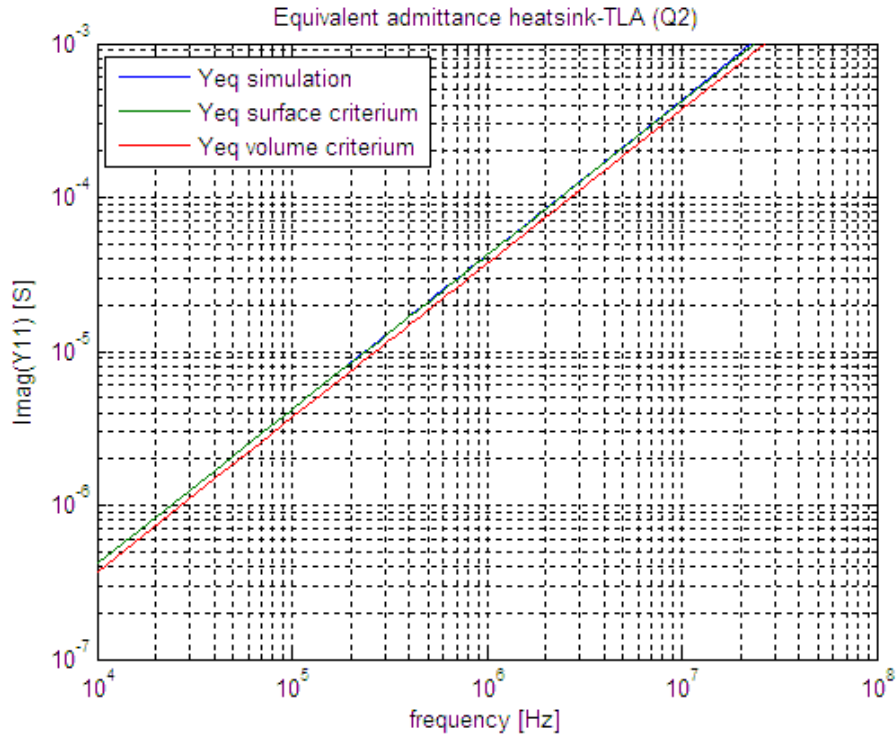


Fig. 85 Imaginary part of equivalent admittance heatsink-TLA (Test board Q2)

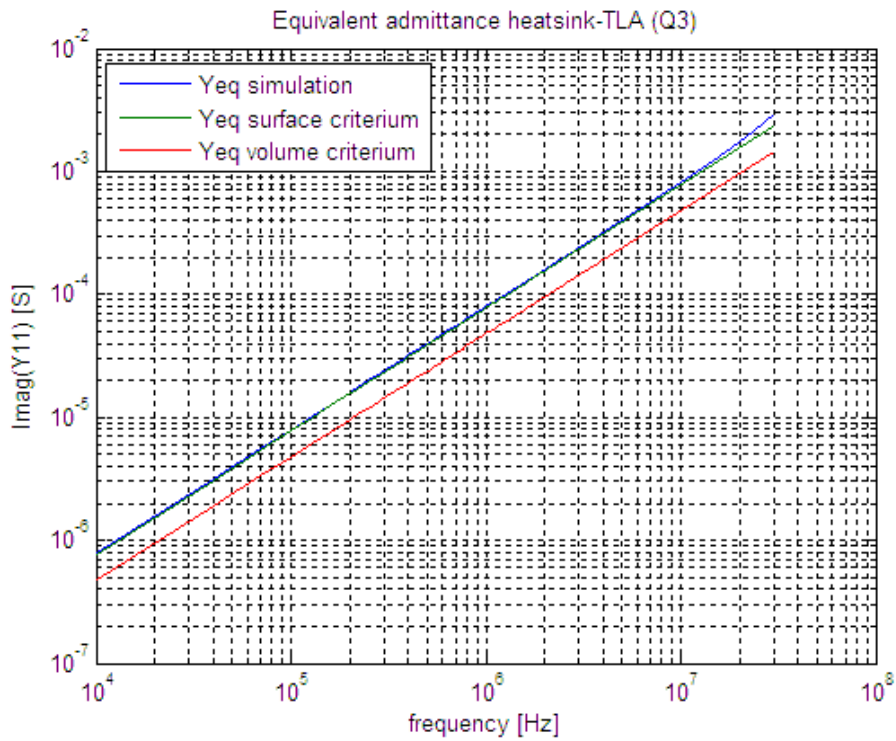


Fig. 86 Imaginary part of equivalent admittance heatsink-TLA (Test board Q3)

Tabs.6-7 summarize the input parameter values and the computed parameters for the different test heatsinks.

Input parameter values	Q1	Q2	Q3
Surface [mq]	0.004608	0.015220	0.087184
Volume [mc]	0.00001656	0.000118864	0.0004896

Tab. 11 Input parameter values for the test heatsink.

Computed parameter values	Q1	Q2	Q3
Mutual C area criterion [pF]	3	4	11
Mutual C volume criterion [pF]	2	3	6
Self C area criterion [pF]	3	4	9
Self C volume criterion [pF]	2	3	5
Self TLA C [pF]	7	7	7

Tab. 12 Computed parameter values for the test heatsink.

The results clearly show that the same surface criterion for calculation of mutual capacitance between the heatsink and the TLA get to better agreements with simulation results.

The actual values of the imaginary part of the mutual and self impedance can be considered as an apparent inductance which value depends on frequency and parasitic inductance.

VII. Experimental validation of electric coupling

A network analyser (NA) is used to measure the transfer function between one of the test heatsink Q1, Q2, Q3 and one gaped loop of the TLA. The NA RF source is terminated with a 47 Ω resistor, to minimize the reflected power at the input port; one of the resistor's termination is connected to a copper plane strictly bound to the heatsink. One gap of the loop is shorted with copper tape and the other is chosen as output port to the NA. The equivalent circuit of the test setup is presented in Fig.37.

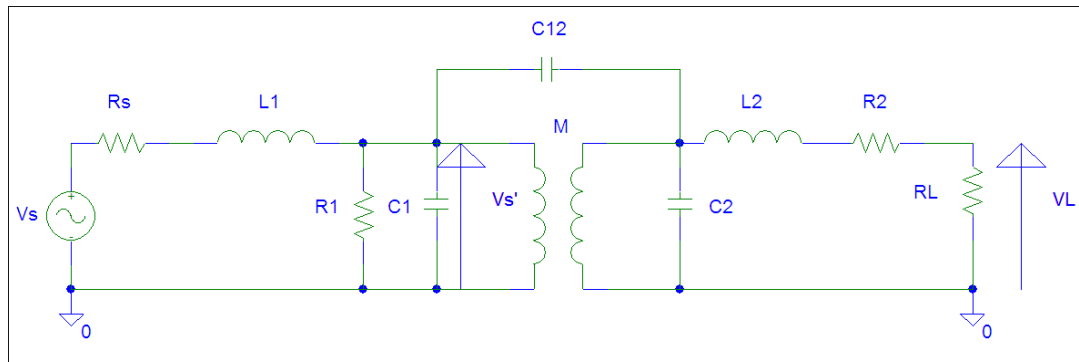


Fig. 87 Equivalent circuit for mutual capacitive coupling between test heatsink and receiving loop.

The transfer function can be simply calculated neglecting the self capacitance and self inductance of the source and the mutual inductance between heatsink and the receiving loop.

Under these assumptions $\hat{V}_S^i \approx \frac{\hat{V}_S}{2}$ and

$$\hat{H}_E = \frac{R_L}{1 + j\omega C_2(R_2 + j\omega L_2 + R_L)} j\omega C_{12} \frac{\hat{V}_S^i}{1 + j\omega C_{12} \frac{(R_2 + R_L + j\omega L_2)}{1 + j\omega C_2(R_2 + R_L + j\omega L_2)}} \quad (3.15)$$

being $R_L=50 \Omega$ the input resistance of the NA, R_2 and L_2 the resistance and self inductance of the receiving loop, R_S the Thevenin equivalent resistance of the source, R_1 and L_1 the resistance and self inductance of the test boards bound to the heatsink.

Tab.8 presents the parameter's values of the transfer function for the different test heatsinks.

Parameter values	Q1	Q2	Q3
R_L [Ω]	50	50	50

R_2 [Ω]	2	2	2
L_2 [μ H]	2.60	2.60	2.60
R_1 [Ω]	47	47	47
R_s [Ω]	50	50	50
L_1 [nH]	5	5	5
M [nH]	<5	<5	<5
C_{12} area criterion [pF]	3	4	11
C_{12} volume criterion [pF]	2	3	6
C_1 area criterion [pF]	3	4	9
C_1 volume criterion [pF]	2	3	5
C_2 [pF]	7	7	7

Tab. 13 Parameter values for the test heatsink.

The values of the self inductance in Tab.8 are computed using formula of the rectangular loop [5] and the values of the mutual inductance can be supposed to be always less than the self inductance values. Those parameters show that they can be neglected compared to the value of self and mutual capacitance in the equivalent circuit in Fig.37.

Test heatsinks Q1, Q2, Q3 are shown in Figs.38-40.

The magnitude and phase of the transfer function (1.16) are measured and compared with those computed with:

1. mutual and self capacitance computed using the same surface criterium,
2. mutual and self capacitance computed using the same volume criterium.

The results obtained are presented in Fig.41-46.



Fig. 88 Test heatsink Q1



Fig. 89 Test heatsink Q2



Fig. 90 Test heatsink Q3

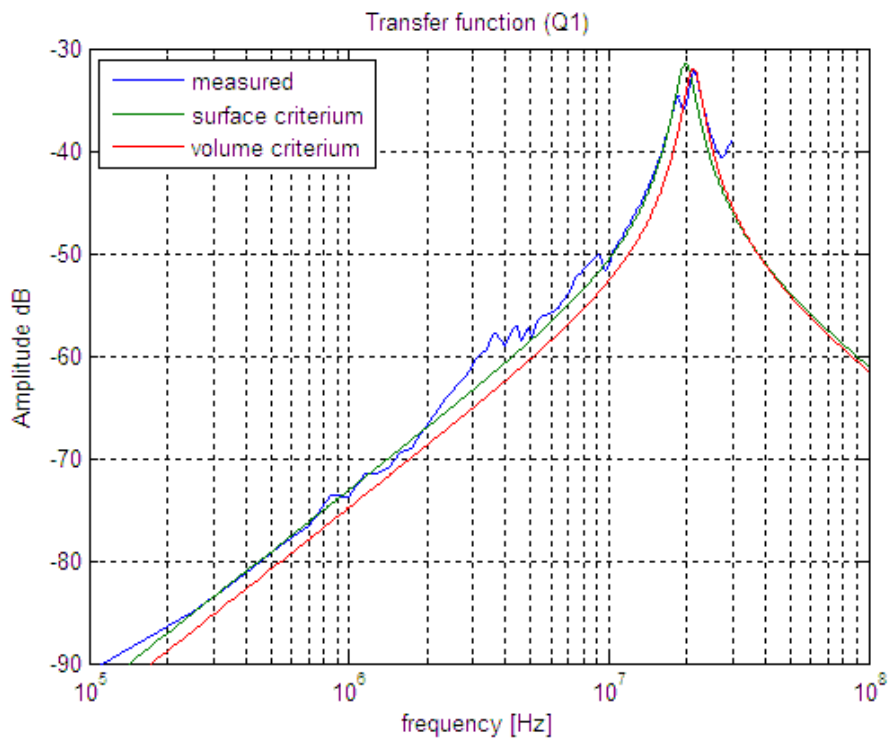


Fig. 91 Magnitude of transfer function for the test heatsink Q1.

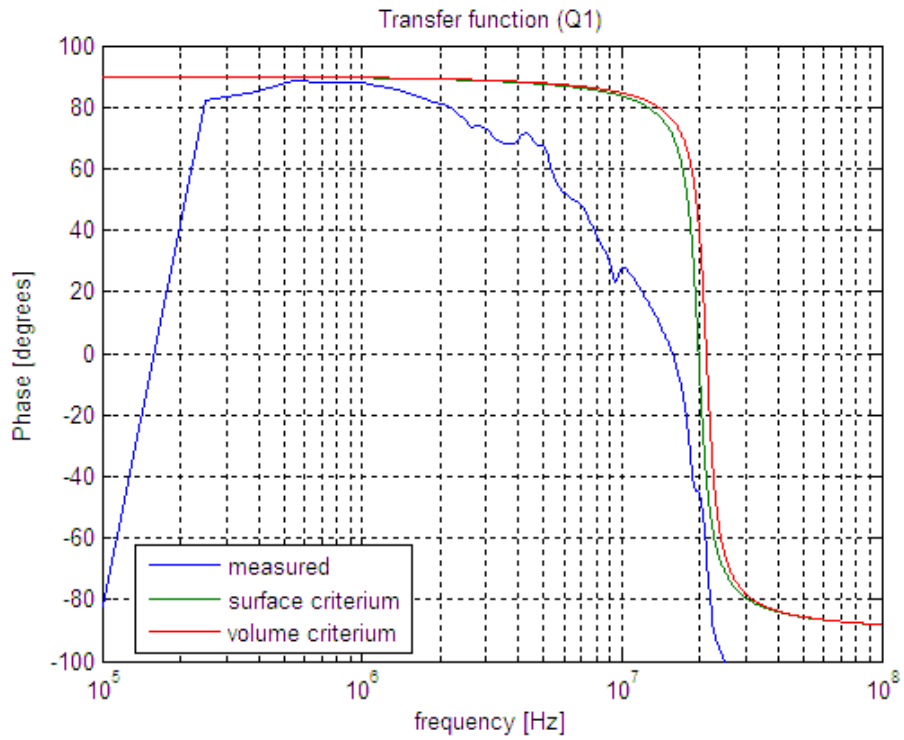


Fig. 92 Phase of transfer function for the test heatsink Q1.

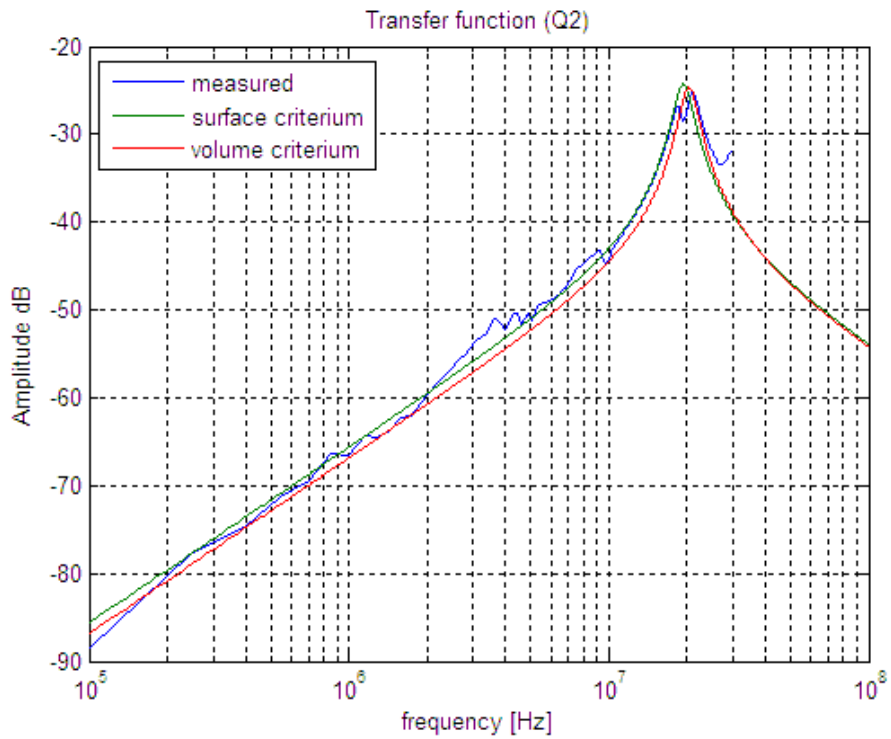


Fig. 93 Magnitude of transfer function for the test heatsink Q2.

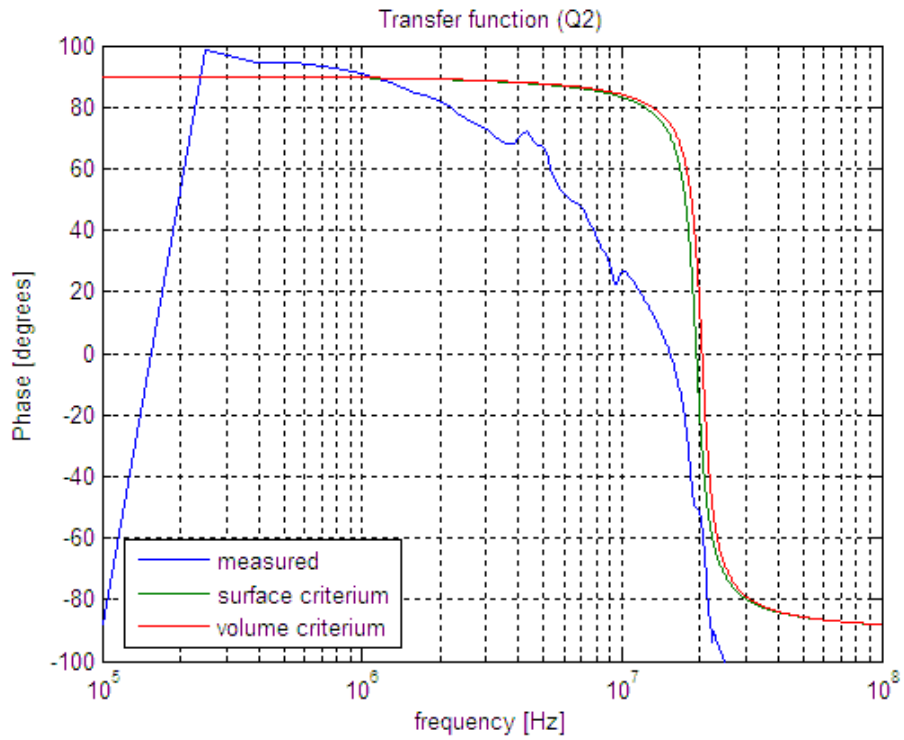


Fig. 94 Phase of transfer function for the test heatsink Q2.

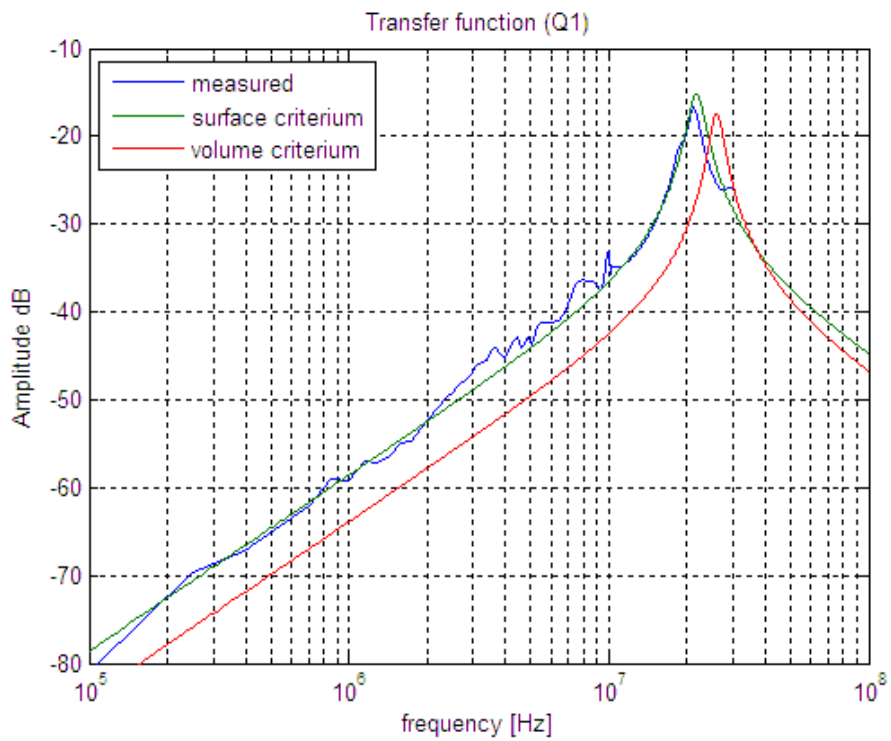


Fig. 95 Magnitude of transfer function for the test heatsink Q3.

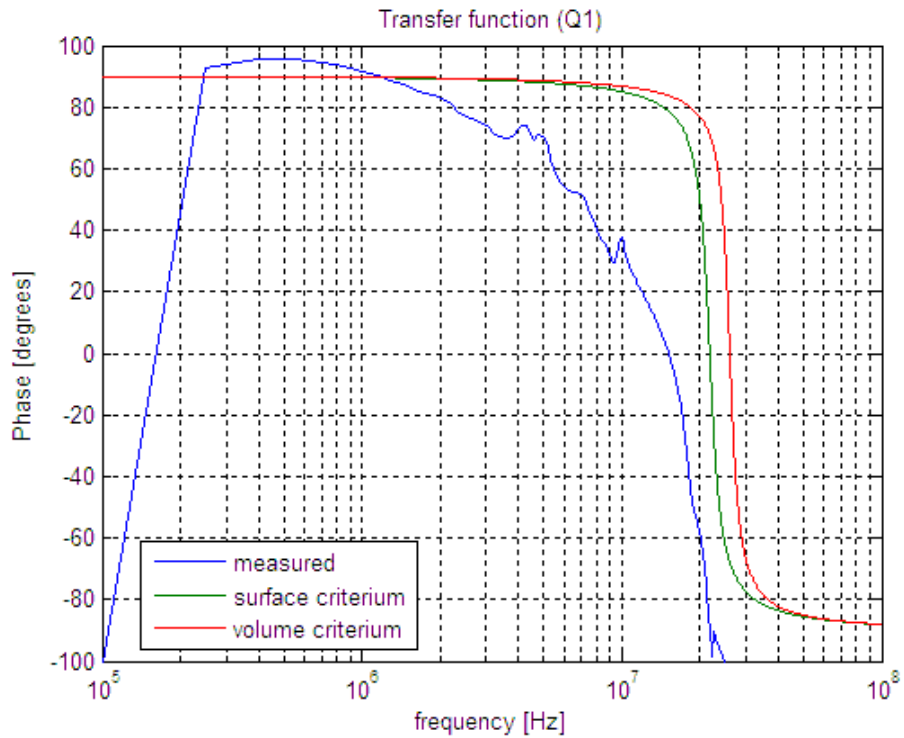


Fig. 96 Phase of transfer function for the test heatsink Q3.

The proposed model (1.16) which parameters are computed using the same surface criterion shows a good agreement with experimental results for all the test heatsinks.

Some more investigation in the phase plots differences would be necessary but so far it is possible to underline that the general behaviour of the transfer function is well represented by the proposed model.

The accuracy when measuring the amplitude and phase transfer function in is ± 1 dB and ± 6 degrees.

Equation Chapter 4 Section 3

III. Coupling mechanisms

Once the voltage and current noise sources are characterized, the coupling mechanisms need to be described.

Assuming that:

6. the current spectrum of both primary and secondary loop sources is known,
7. the voltage spectrum of the signal between the heatsinks and the ground reference of the circuit is known,
8. any susceptible circuit acting as victim can be represented by a single port equivalent circuit,
9. the receiver is in the near field region of the source ($D \ll \lambda$ D is the typical dimension of the over all source-victim ensemble and λ is the wavelength of the noise signal)
10. the source and the victim are weakly coupled (sufficiently distant so that the reaction of the victim's responses back to the source is negligible)

For the calculation of self and mutual inductance, the current flow in the loop is assumed to be a constant and independent of the loop geometry. As underlined later on, this is an intrinsic limitation of the model.

The primary and secondary loops are magnetic coupled to the victim circuit resulting in a current driven voltage source (neglecting the electric coupling between the loops and the victim) and the heatsinks are electric coupled to the victim circuit resulting in a voltage driven current source (neglecting in this case the magnetic coupling between some current flowing through the heatsink and capacitive to ground and the victim).

Due to hypothesis 4 the electric and magnetic coupling mechanisms between the source and the receiver can be modelled respectively as mutual capacitive coupling and mutual inductance coupling.

The weak coupling assumption implies that $M^2 \ll \langle L_1 L_2, C_1, C_2 \rangle \gg C_{12}$ and $1/j\omega C_{12} \gg j\omega L_1, j\omega L_2$ in the equivalent circuits Figs. 19 and 37.

Schematic views of the electric and magnetic coupling mechanisms with their sources are shown in Figs.1-3.

The EMI source supplies a time varying current in an exposed circuit loop that creates time varying a magnetic flux density which links the pick up loop in the victim circuit. A time varying magnetic flux

density by Lent's law results in induced voltage within the victim's circuitry. This coupling between the source and the victim is known as *Mutual Inductive Coupling*.

At the same time, the EMC source voltage can induce a large charge densities on some exposed surface of the source. This charges creates an electric field which extends through space and a portion of this field can terminate on other charges induced in the victim circuitry. Since the electric field varies with time, the resulting time variation of the induced charge creates a current flow in the victim circuitry. This coupling between the source and the victim is known as *Mutual Capacitive Coupling*.

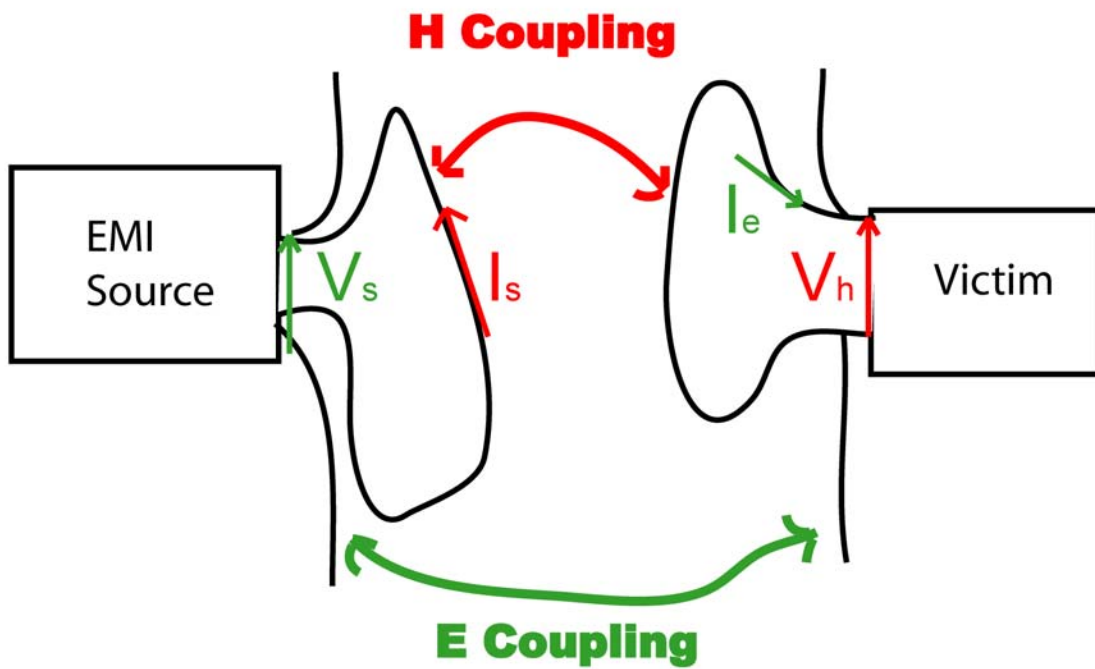


Fig. 97 Magnetic and Electric Coupling between source and victim circuits

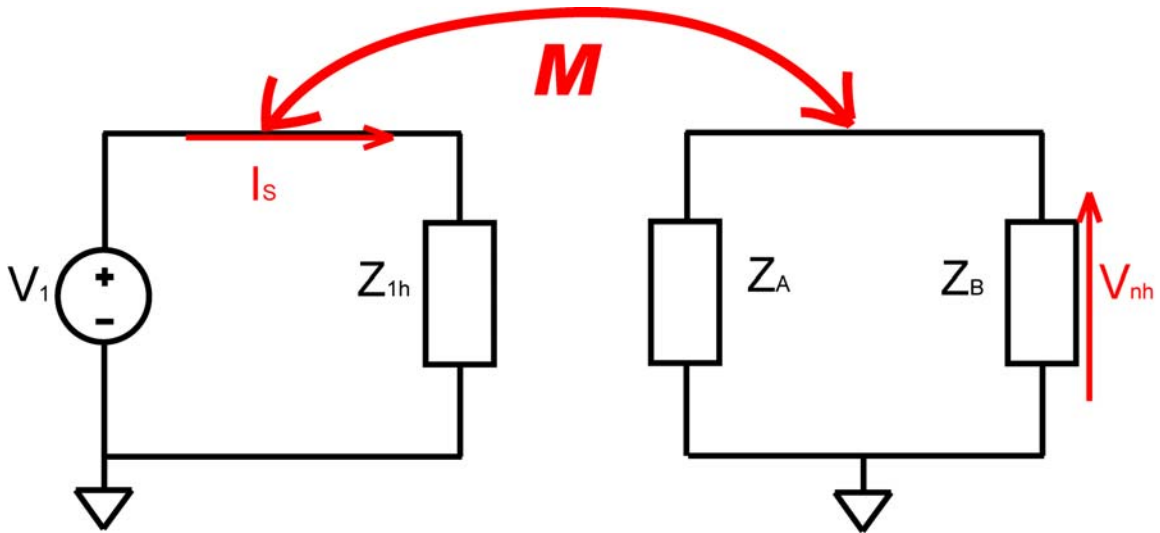


Fig. 98 Equivalent circuit for the mutual inductive coupling mechanism.

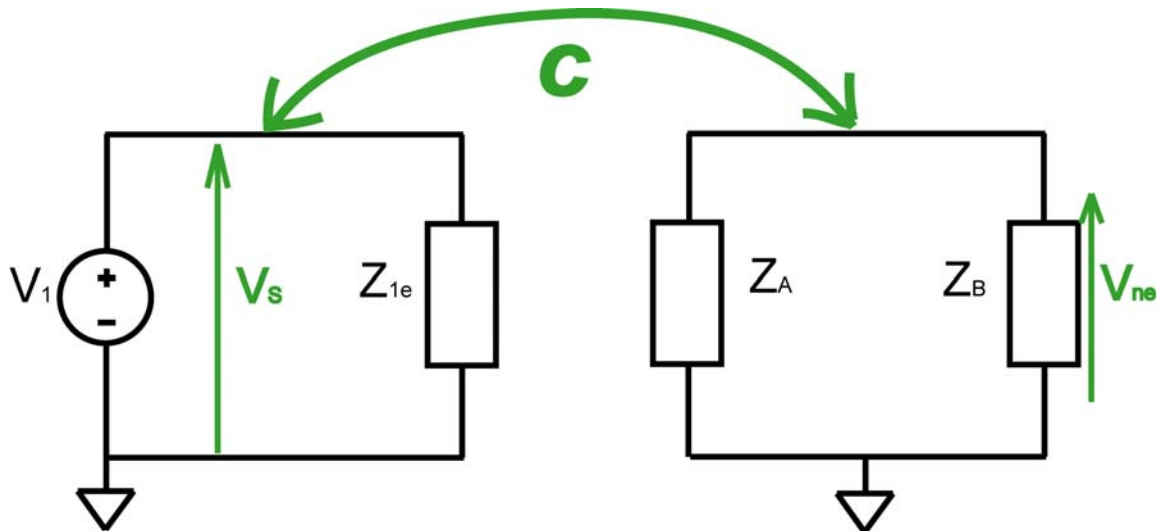


Fig. 99 Equivalent circuit for the mutual capacitive coupling mechanism.

In case of weak coupling between source and victim, the mutual inductive coupling can be represented by a current controlled voltage source as in Fig.4

$$\hat{V}_H = j\omega M \hat{I}_S \quad (3.1)$$

The mutual capacitive coupling between source and victim under the assumption of weak coupling can be represented by a voltage controlled current source as in Fig.5

$$\hat{I}_E = j\omega C \hat{V}_S \quad (3.2)$$

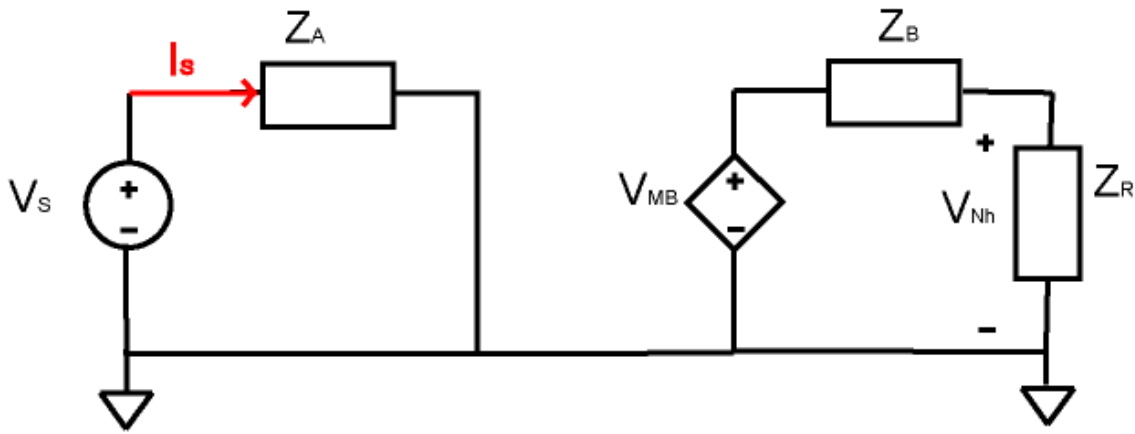


Fig. 100 Magnetic coupling equivalent circuit.

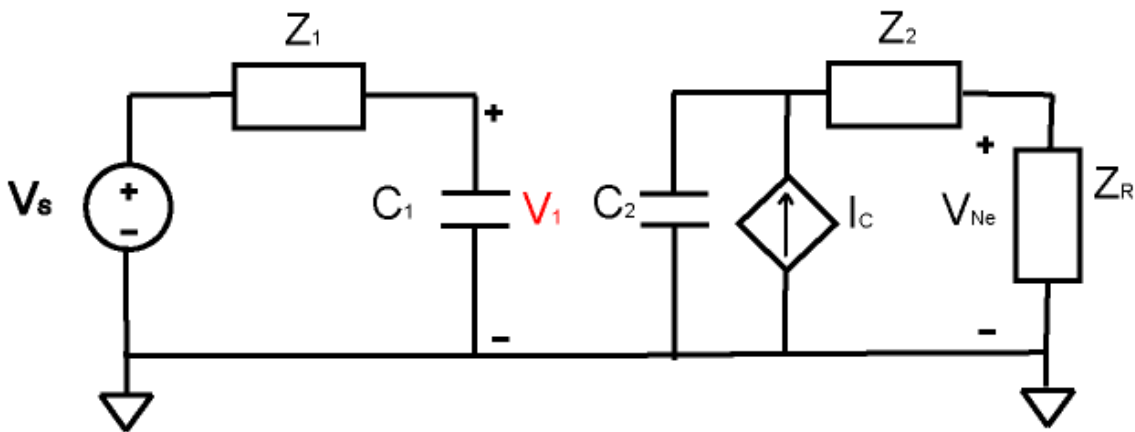


Fig. 101 Electric coupling equivalent circuit.

The noise voltage due to the magnetic coupling mechanism (Fig. 2) across the receiver can be simply modelled as

$$\hat{V}_{Nh} \approx j\omega M \hat{I}_s \cdot \left(\frac{Z_A}{Z_B + Z_A} \right) \quad (3.3)$$

while the noise voltage due to the electric coupling mechanism (Fig. 3) across the receiver is

$$\hat{V}_{Ne} = j\omega C_{12} \hat{V}_1 \frac{1}{\frac{1}{j\omega C_2} + \hat{Z}_2 + \hat{Z}_R} \hat{Z}_R \quad (3.4)$$

Both the mutual capacitance C and the mutual inductance M between the source and receiver depends on the geometry of the source and receiver, the medium and the distance between them.

IV. Closed formulas for mutual and self-inductance

The mutual inductance and capacitance of actual circuit configurations are usually difficult to know precisely due to the irregular geometries of the circuits, to the details of local geometries as well as to the presence of magnetic material in the surrounding environment. A lot of closed formulas can be found in literature [1-6] that can be applied in different cases, but for 3D geometry there are very few of them.

For 3D geometries, mutual inductance and capacitance can be evaluated by numerical computation using some software [7-9].

In order to validate the model, a Triple Loop Antenna (TLA) is chosen as susceptible receiver and its equivalent circuit is shown in Fig.6.

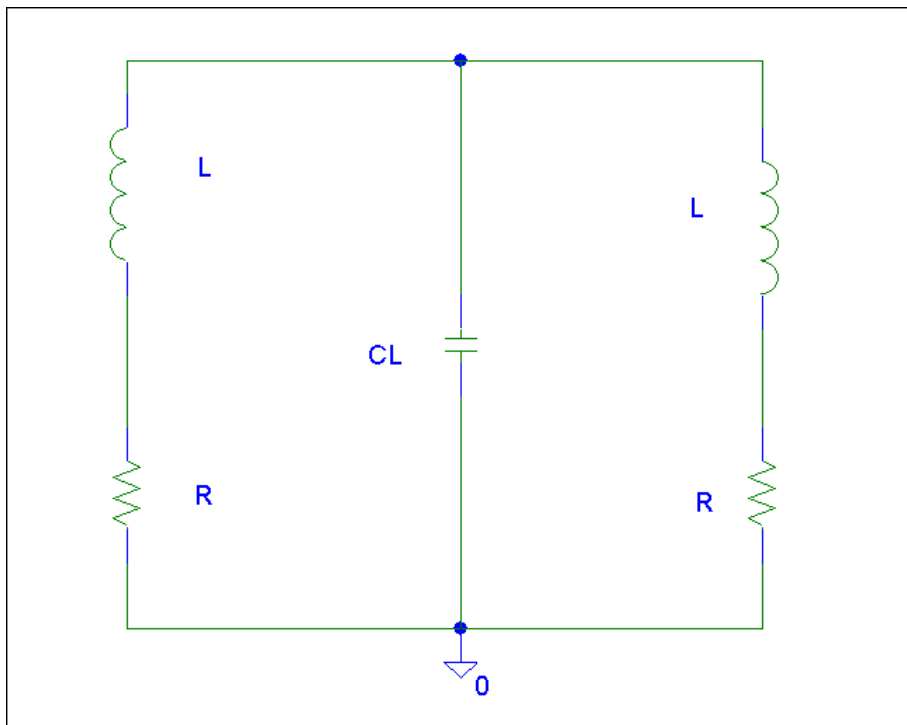


Fig. 102 Equivalent circuit of the receiving TLA.

The mutual inductance coupling is supposed to be only between the actual trace and its coplanar loop of the TLS while the mutual capacitive coupling is between an exposed metal surface and the all TLA structure.

The mutual inductance between the trace carrying the current and a loop of the TLA can be calculated with good approximation using the formula [10] of the mutual inductance between two coaxial and coplanar thin loops,

$$M = \mu \sqrt{r_{eq} \cdot r_2} \left[\left(\frac{2}{k} - k \right) \cdot I_1(k) - \frac{2}{k} \cdot I_2(k) \right] \quad (3.5)$$

$$k^2 = \frac{4r_{eq}r_2}{d^2 + (r_{eq} + r_2)^2} \quad (3.6)$$

being $I_1(k)$, $I_2(k)$ the elliptic integrals respectively of first and second kind, r_2 the radius of the TLA, μ the magnetic permeability of the medium, r_{eq} the radius of the equivalent source current loop and d the distance between the two planes containing the two loops.

The self inductance of the actual source loop can be computed using [10]

$$L = N^2 \mu r_{eq} \left[\text{Ln} \left(\frac{16r_{eq}}{d_{eq}} \right) - 2 \right] + \frac{\mu \cdot N \cdot p}{8\pi} \quad \text{for } r_{eq} > 5d_{eq} \quad (3.7)$$

Both self and mutual inductance can be calculated using (1.8) and (1.6) with two different methodologies:

- the same area criterion
- the same perimeter criterion

being r_{eq} the radius of the equivalent source current loop according to the different criteria and d_{eq} the equivalent diameter of the trace.

For the same area criterion, $r_{eq} = \sqrt{\frac{A}{\pi}}$ being A the internal area of the actual trace,

for the same perimeter criterion, $r_{eq} = \frac{p}{2\pi}$ with p the perimeter of the actual trace and $d_{eq} \approx \frac{2s}{2\pi}$ with s the width of the trace.

For the calculation of the self inductance of the actual trace the method of partial inductance is also considered [11-14].

In first instance, a test simulation (Test A) with a source loop and a coplanar coaxial receiving loop is considered. The imaginary part of the self impedance Z_{11} of the first loop and of the mutual impedance between the loop Z_{21} is computed and compared with the impedance computed using respectively (1.8) and (1.6). The results are shown in Figs. 7-8. Tab.1 summarizes the values calculated using (1.8) and (1.6) in Test A.

Test A			
Input dimension	Value [m]	Parameter output	Value [nH]
R_1	0.101	L_1	627
R_2	0.0508	L_2	2600
D_1	0.002	M_{12}	40
D_2	0.024		

Tab. 14 Test A parameter values.

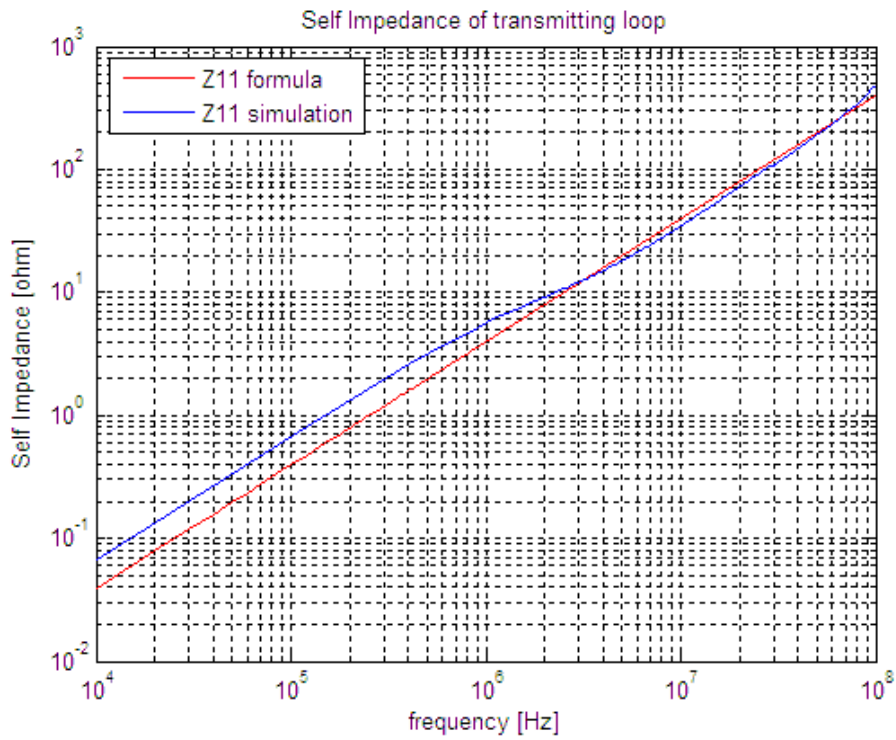


Fig. 103 Imaginary part of self impedance of the source loop Test A.

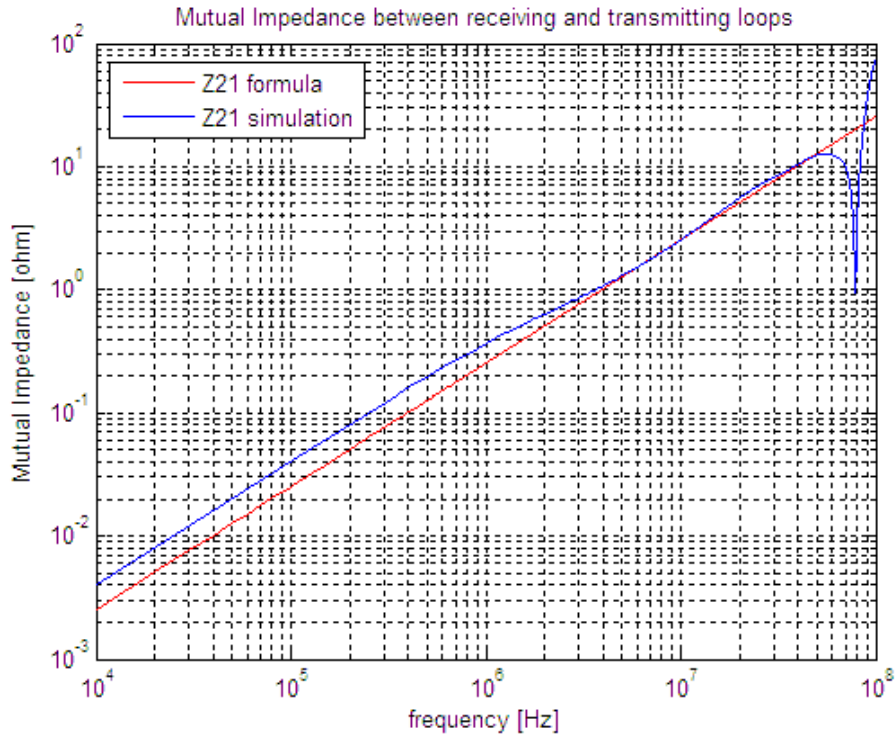


Fig. 104 Imaginary part of Mutual impedance Test A.

Different real trace geometries with 47Ω load are simulated with numerical simulator based on a FIT technique [15] and compared with the results of (1.8) and (1.6). The equivalent radius of the current loop can be calculated using the same loop area criterion or the same perimeter criterion. The self inductance of the real trace can be also calculated by the method of partial inductance [11-14]. The simulated test traces are presented in Figs.9-11.

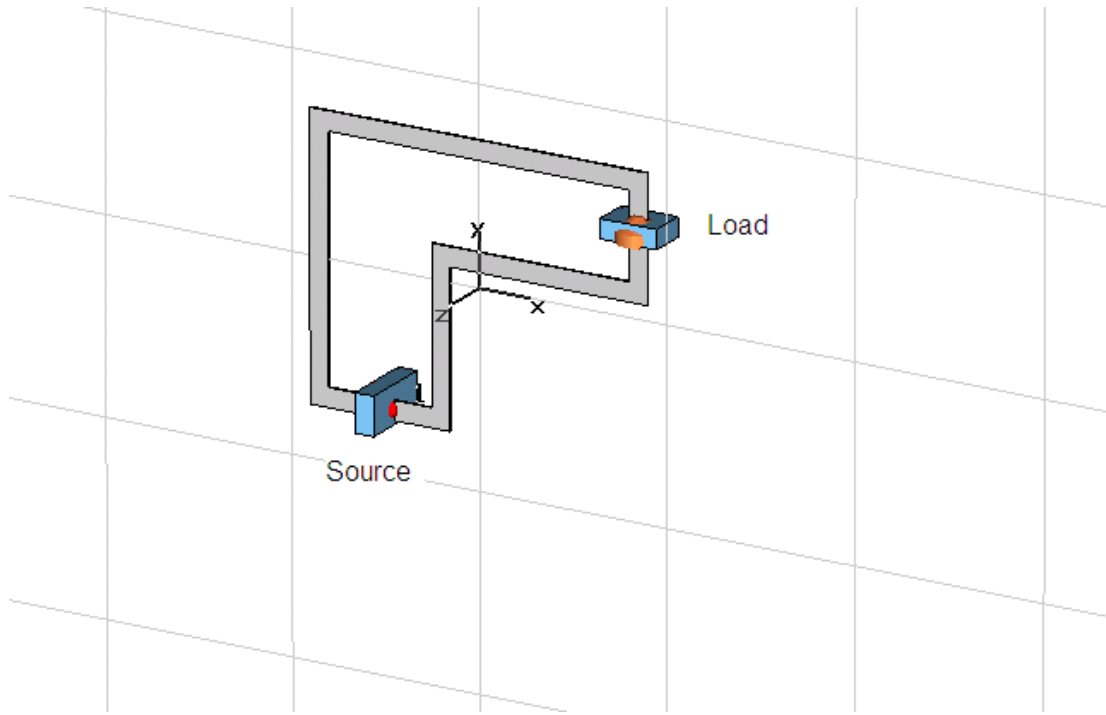


Fig.105 Test Circuit P1.

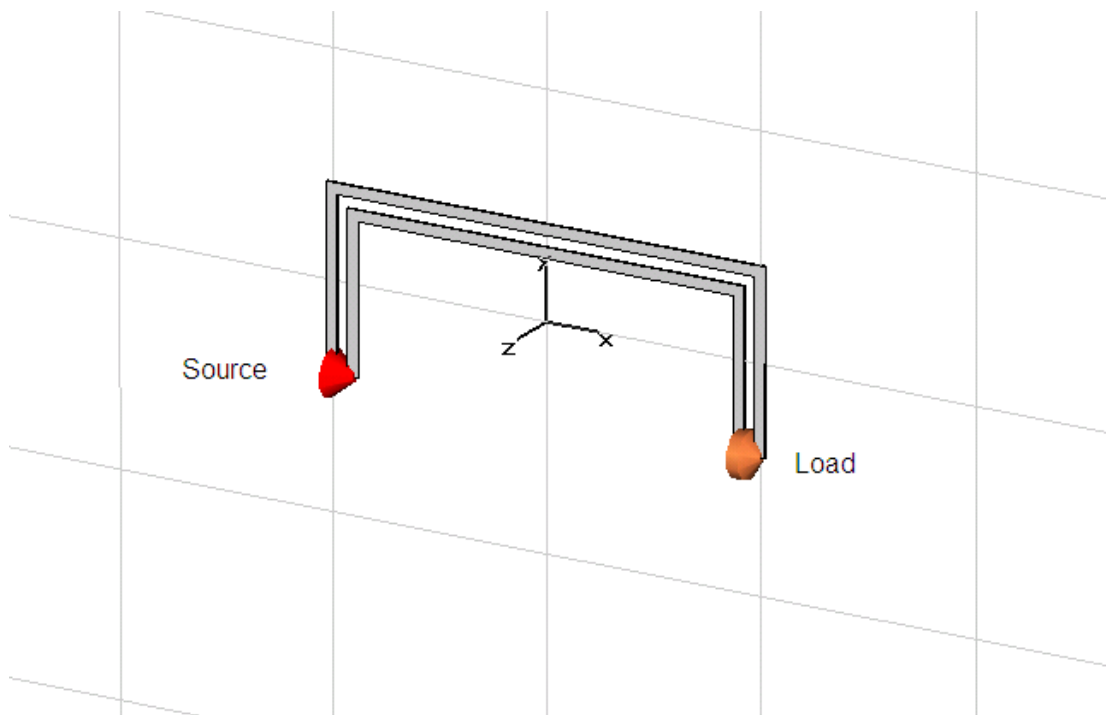


Fig.106 Test circuit P2.

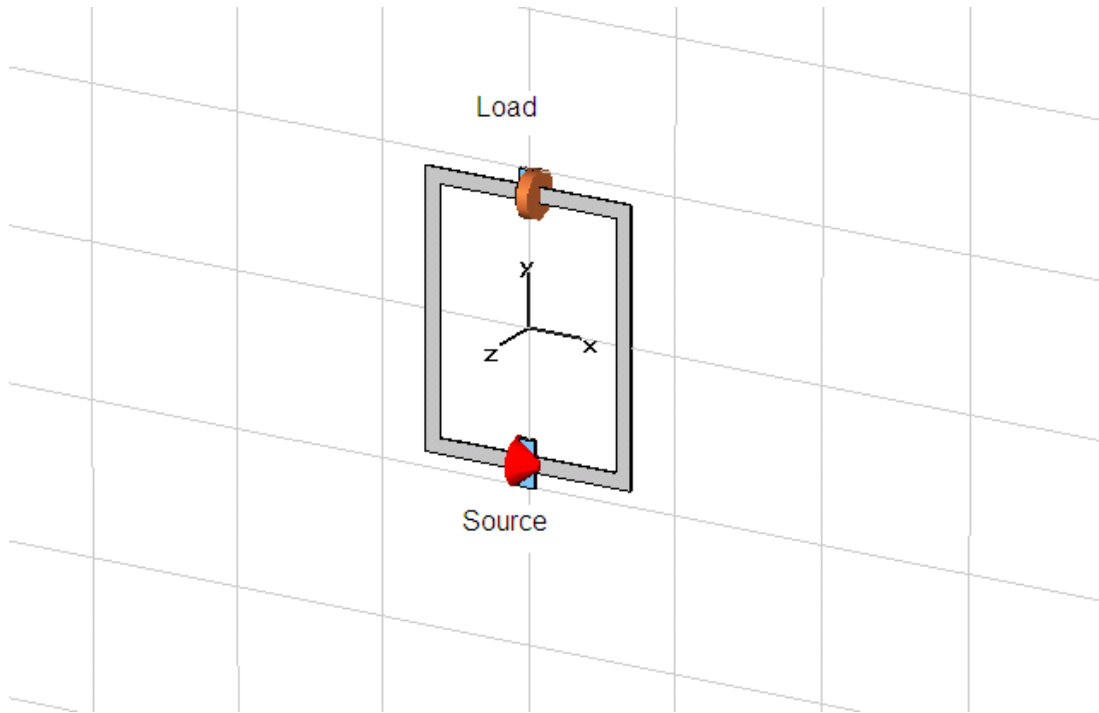


Fig.107 Test Circuit P3.

The results obtained for the mutual impedance (1.6) are shown in Figs. 12-14.

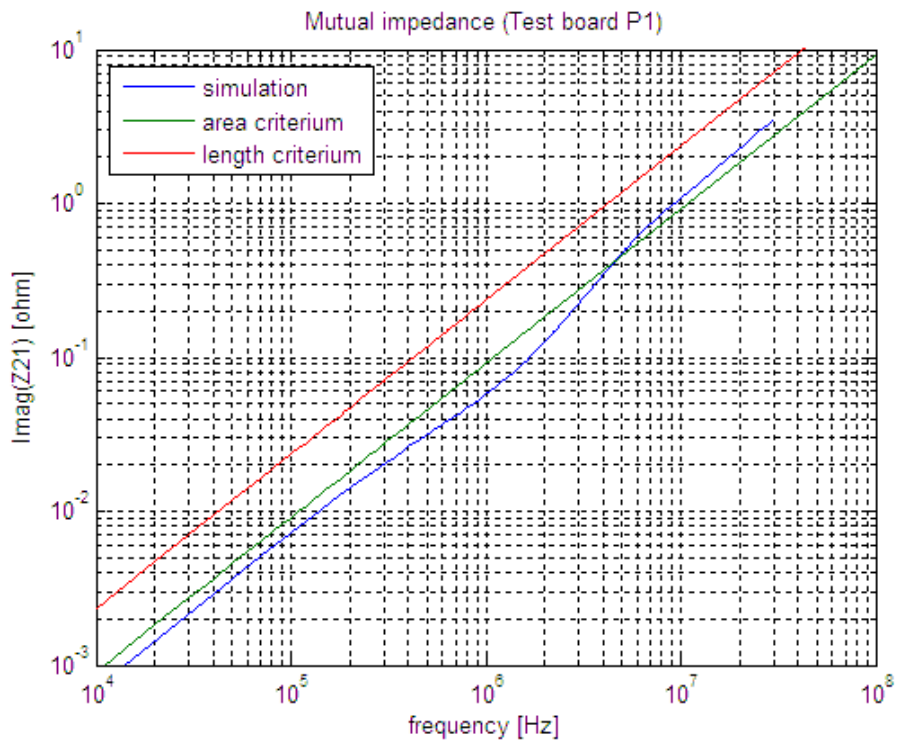


Fig. 108 Imaginary part of mutual impedance between transmitting and receiving loop (Test board P1).

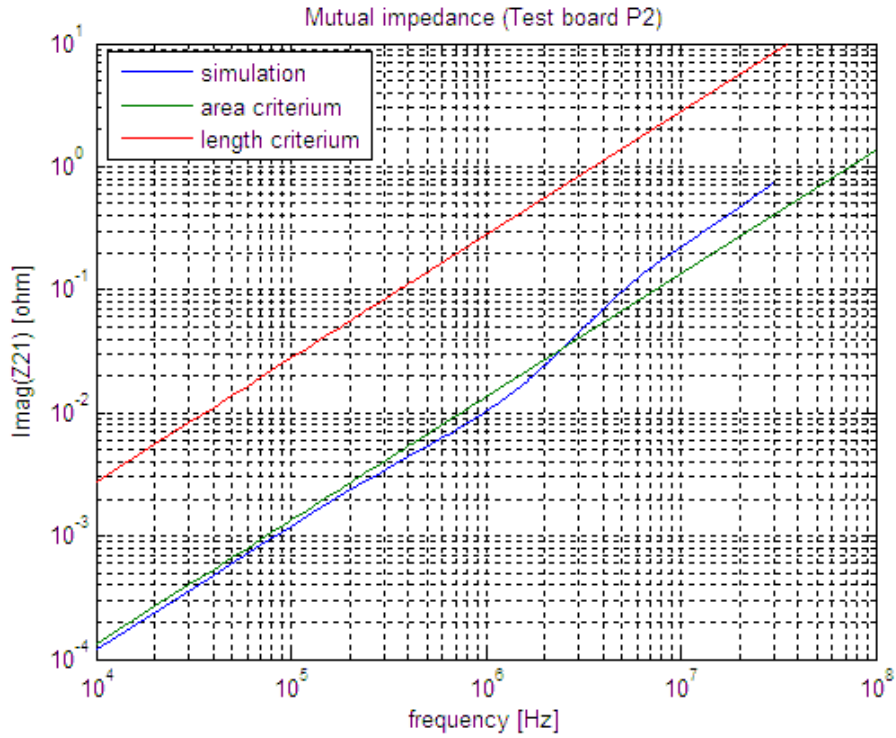


Fig. 109 Imaginary part of mutual impedance between transmitting and receiving loop (Test board P2).

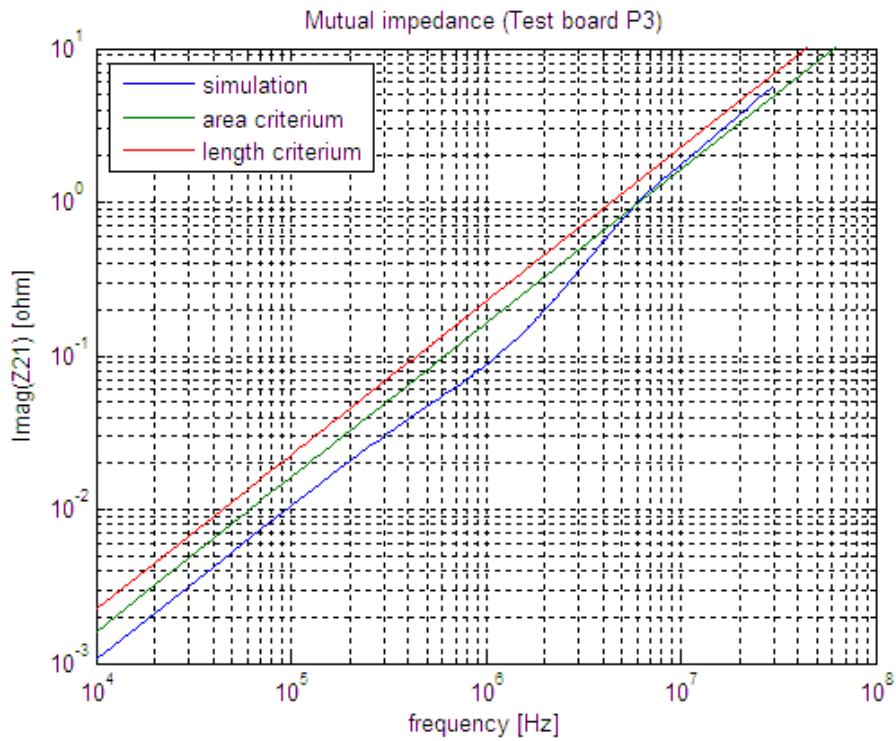


Fig. 110 Imaginary part of mutual impedance between transmitting and receiving loop (Test board P3).

Tabs.2-3 summarize the input parameter values for the test board and the computed parameters for the different test board.

Input parameter values	P1	P2	P3
Area [mq]	0.011655	0.001725	0.02065
Perimeter [m]	0.612	0.665	0.6
Width [mm]	10	5	10

Tab. 15 Input parameter values for P1, P2 and P3.

The results clearly show that the same area criterion for the equivalent radius of the source current loop gets to better agreements with simulations results in the calculation of the mutual impedance between transmitting and receiving loop. The weak coupling assumption is also verified.

Regarding to the self inductance of the Test board P1, P2, P3, the results obtained with (1.6) and using the method of partial inductance are compared with simulations and reported in Figs.15-18.

Computed parameter values	P1	P2	P3
M area criterion [nH]	14	2	26
M perimeter criterion [nH]	37	44	36
L area criterion [nH]	263	115	368
L perimeter criterion [nH]	459	602	448
L partial inductance [nH]	382	336	443
L closed formula [nH]	/		351

Tab. 16 Output parameter values for P1, P2 and P3.

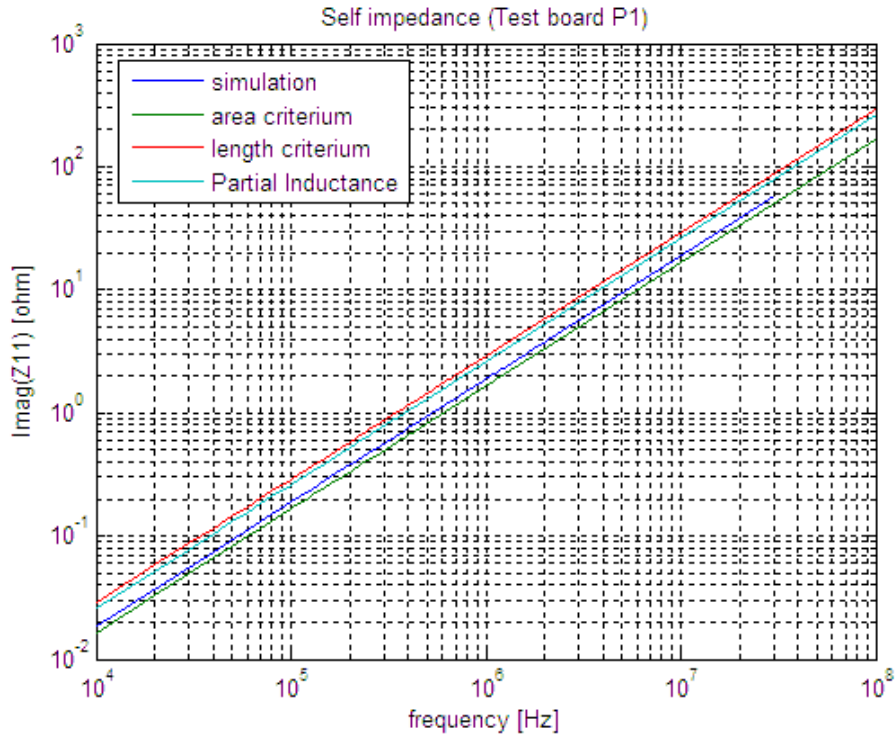


Fig. 111 Imaginary part of self impedance of Test board P1

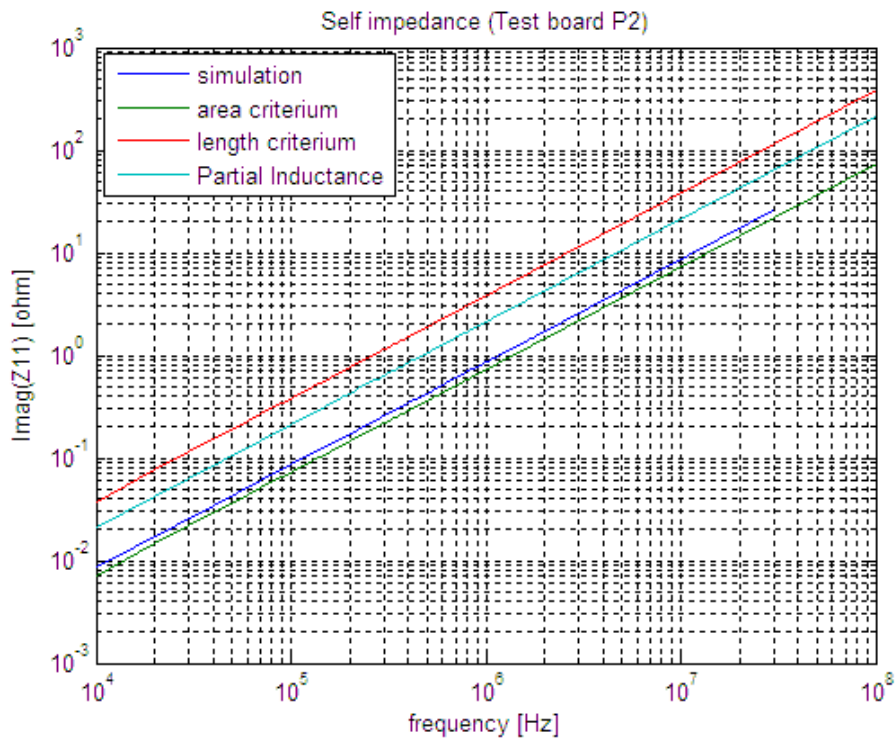


Fig. 112 Imaginary part of self impedance of Test board P2

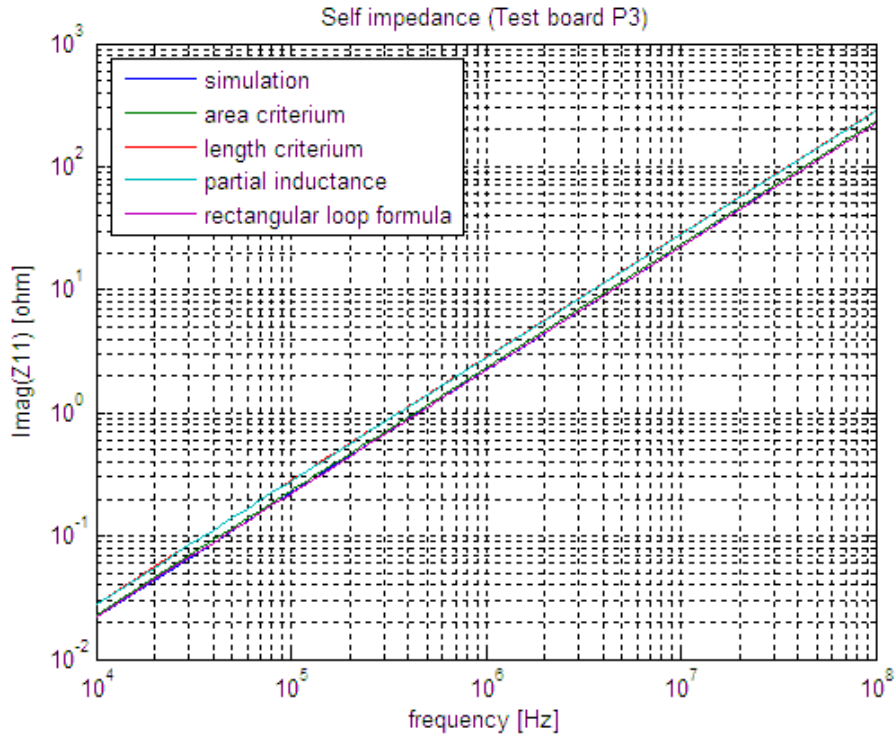


Fig. 113 Imaginary part of self impedance of Test board P3

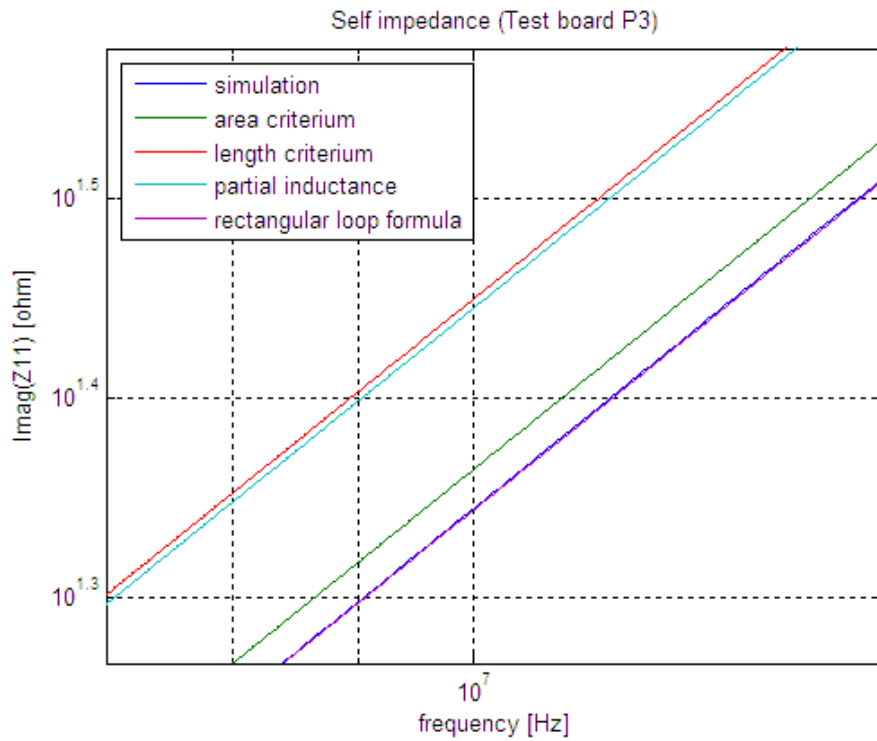


Fig. 114 A zoom view of the imaginary part of self impedance of Test board P3

The self inductance of the last board (P3) is also computed using the formula for a rectangular loop and it is in perfect agreement with the simulated results as shown in Figs.7-8.

The results clearly show that the same area criterion for the equivalent radius of the source current loop gets to better agreements with the results of simulation.

Considering different geometry configurations for wire, ribbon cable, trace, coaxial cable and twisted pair connection the self inductance generally depends on length, transversal dimension and width of a cross section of the connection as

$$L \approx \frac{\mu \cdot l}{2\pi} \log\left(\frac{D}{d}\right) \quad (3.8)$$

When $D \gg d$, L is directly proportional to the area of the loop :

$$L \leq \frac{\mu \cdot l}{2\pi} \left(\frac{D}{d}\right) = \frac{\mu \cdot A}{2\pi d} \quad (3.9)$$

The actual value of the imaginary part of the mutual and self impedance can be considered as an apparent inductance which value depends on frequency and parasitic capacitance. At high frequency the simulated value is the actual value of inductance.

V. Experimental validation of magnetic coupling

A network analyser (NA) is used to measure the transfer function between one of the test board P1, P2, P3 and one gaped loop of the TLA. The test boards are terminated with a 47Ω resistor to minimize the reflected power at the input port of the NA. One gap of the loop is shorted with copper tape and the other is chosen as output port to the NA. The equivalent circuit of the test setup of the test boards is presented in Fig.19.

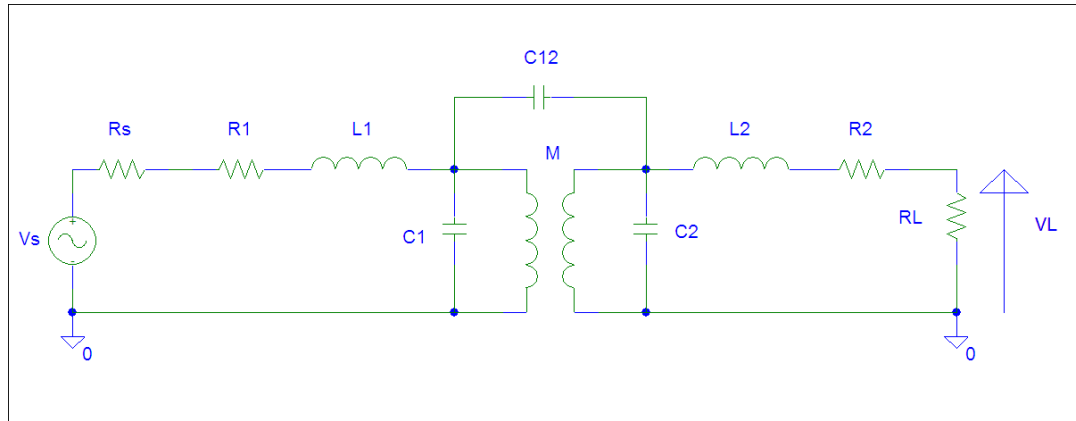


Fig. 115 Equivalent circuit for mutual inductive coupling between test boards and receiving loop.

The transfer function can be simply calculated neglecting the self capacitance C_1 of the source and receiving loop C_2 and the mutual capacitance C_{12} between them.

$$\hat{H}_M \triangleq \frac{\hat{V}_L}{\hat{V}_S} = \frac{R_L}{R_2 + j\omega L_2 + R_L} j\omega M \frac{1}{R_1 + R_S + j\omega L_1} \quad (3.10)$$

being $R_L=50 \Omega$ the input resistance of the NA, R_2 and L_2 the resistance and self inductance of the receiving loop, R_S the Thevenin equivalent resistance of the source, R_1 and L_1 the resistance and self inductance of the test boards. Tab.4 presents the parameter values of the transfer function (1.11) for different test boards.

Parameter values	P1	P2	P3
R_L [Ω]	50	50	50
R_2 [Ω]	2	2	2
L_2 [μ H]	2.60	2.60	2.60
R_1 [Ω]	1.192	1.330	1.160
R_s [Ω]	47	47	47
M area criterion [nH]	14	2	26
M perimeter criterion [nH]	37	44	36
L_1 area criterion [nH]	263	115	368
L_1 partial inductance [nH]	413	336	443
C_1 [pF]	<1	<1	<1
C_2 [pF]	2	2	2
C_{12} [pF]	~23	~25	~23

Tab. 17 Parameter's value for different test boards.

The self and mutual capacitance values are estimated using the formulas of the self capacitance of a loop (1.14) and the formula of two wire transmission line of length $2\pi\frac{r_1+r_2}{2}$ [5]. This values need only to confirm the assumption of neglecting all of them comparing with the value of inductance in the equivalent circuit in Figs.19 (weak coupling approximation).

Test board P1, P2, P3 are shown in Figs.20-22.

The magnitude and phase of the transfer function (1.11) is measured and compared with three different cases:

4. mutual and self inductance computed using the same area criterium,
5. mutual and self inductance computed using the same perimeter criterium,
6. mutual inductance computed using the same area criterium and self inductance using the method of partial inductance.

The results obtained are presented in Fig.23-28.

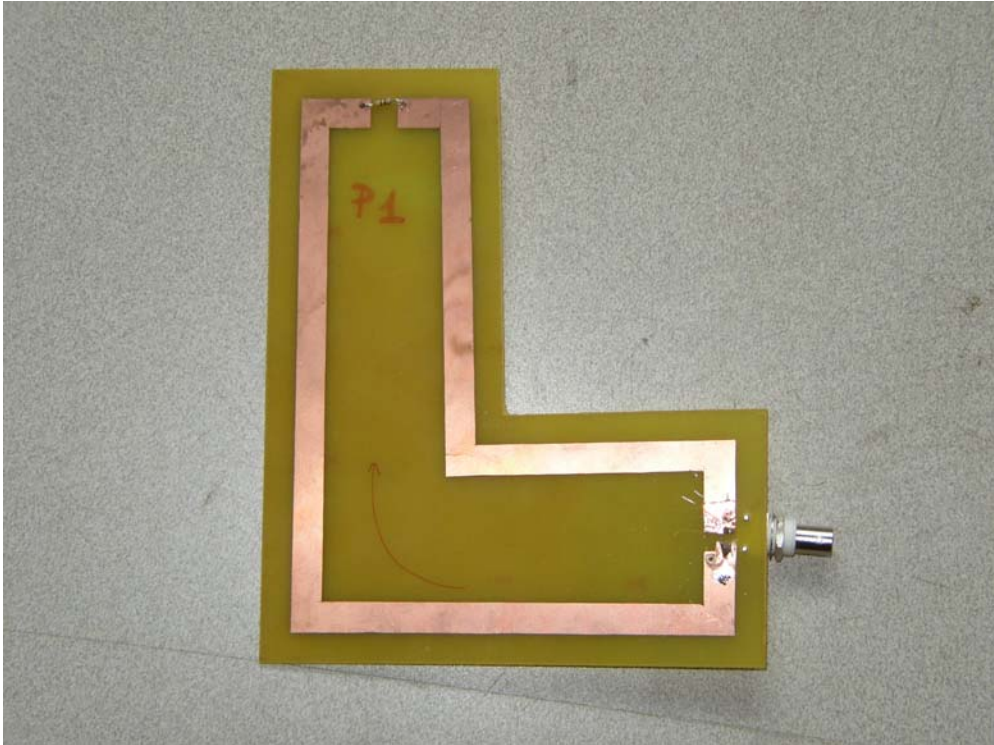


Fig. 116 Test board P1

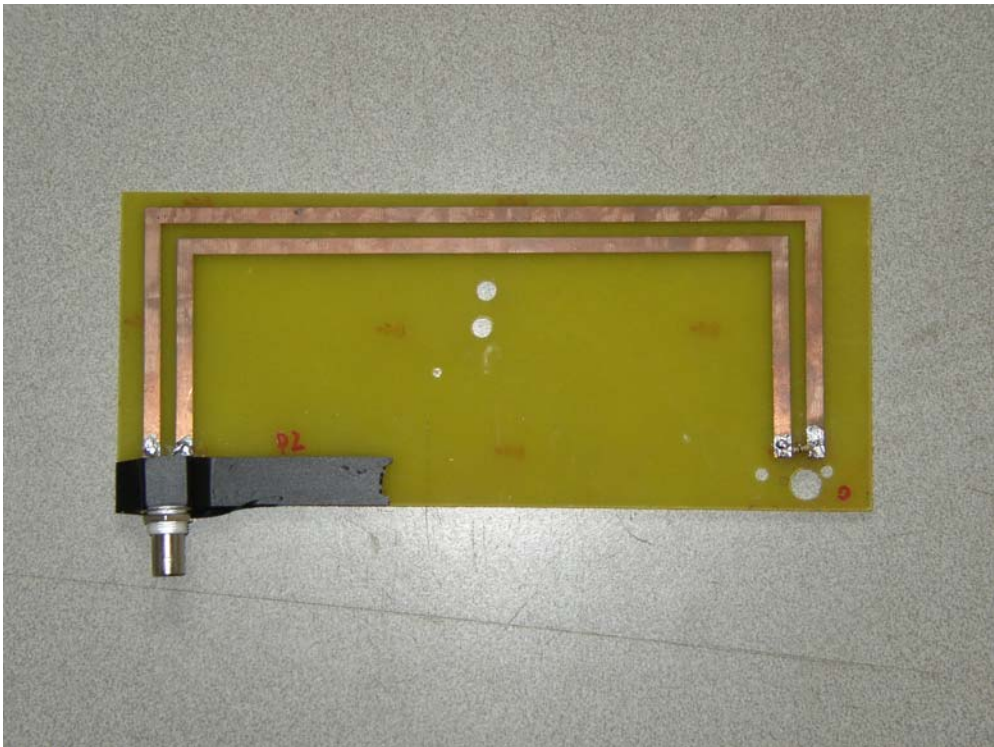


Fig. 117 Test board P2

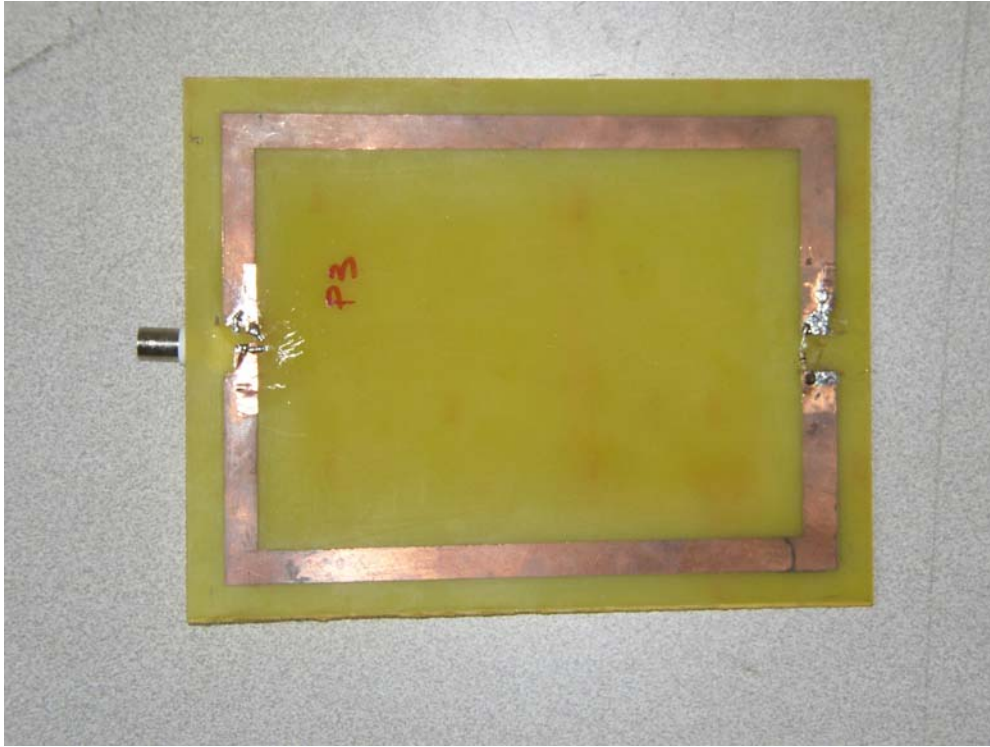


Fig. 118 Test board P3.

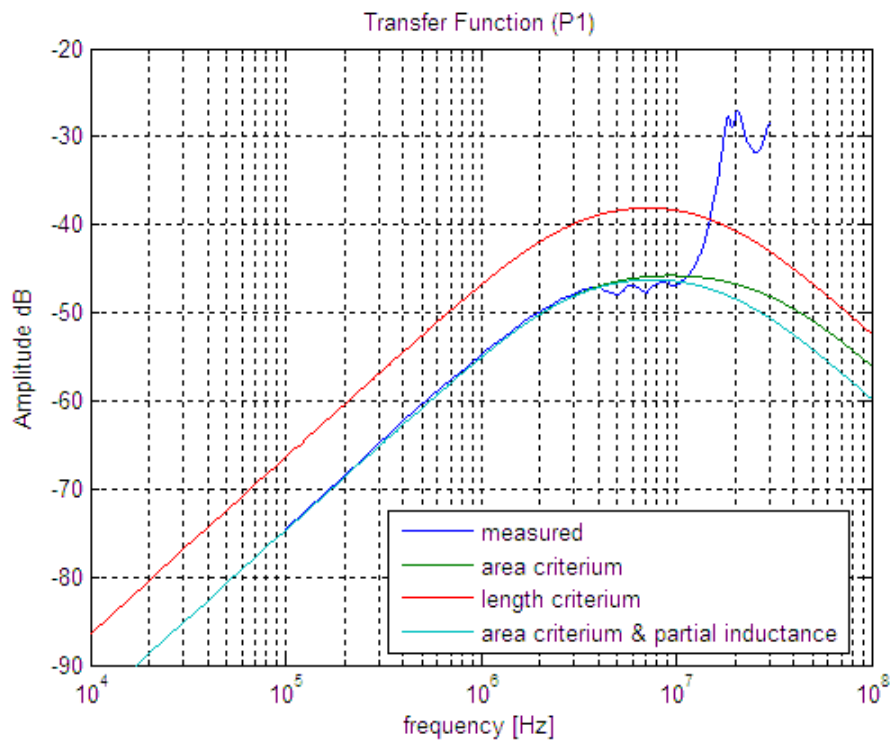


Fig. 119 Magnitude of transfer function for the test board P1.

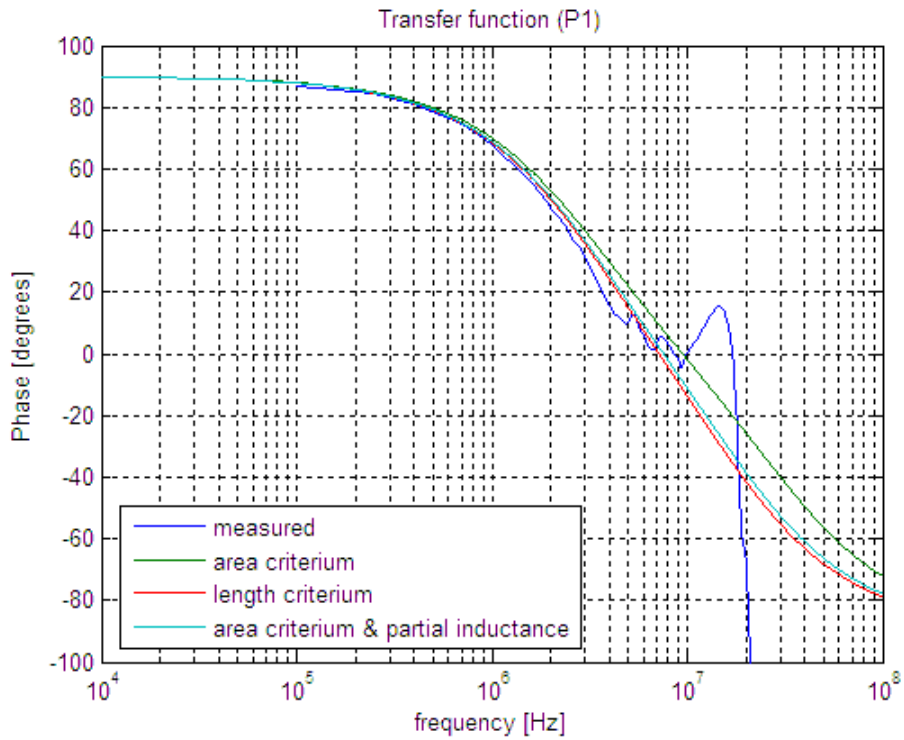


Fig. 120 Phase of transfer function for the test board P1.

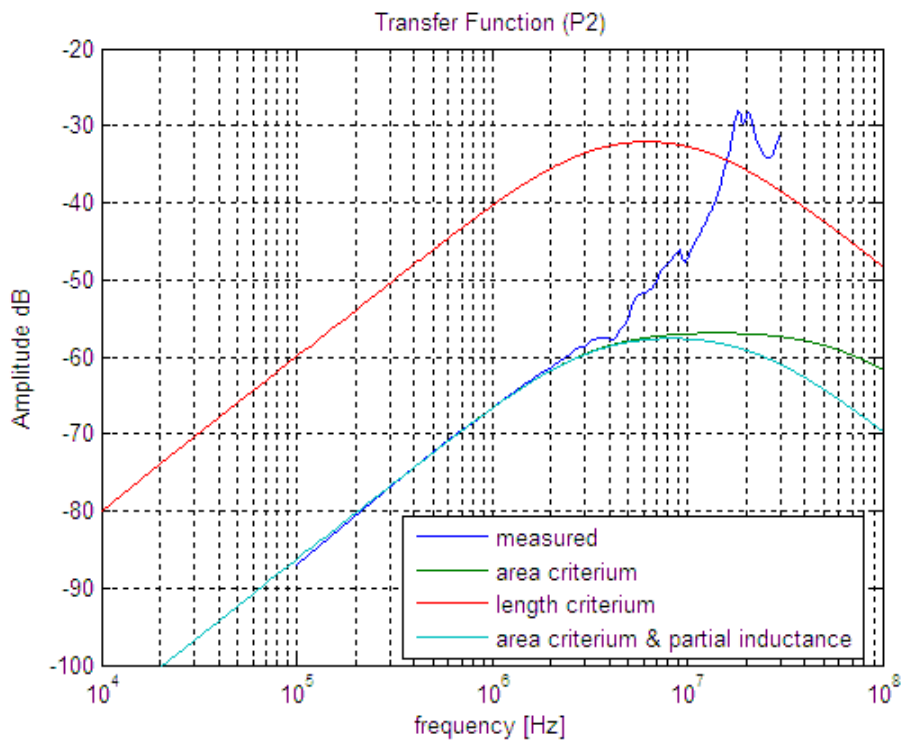


Fig. 121 Magnitude of transfer function for the test board P2.

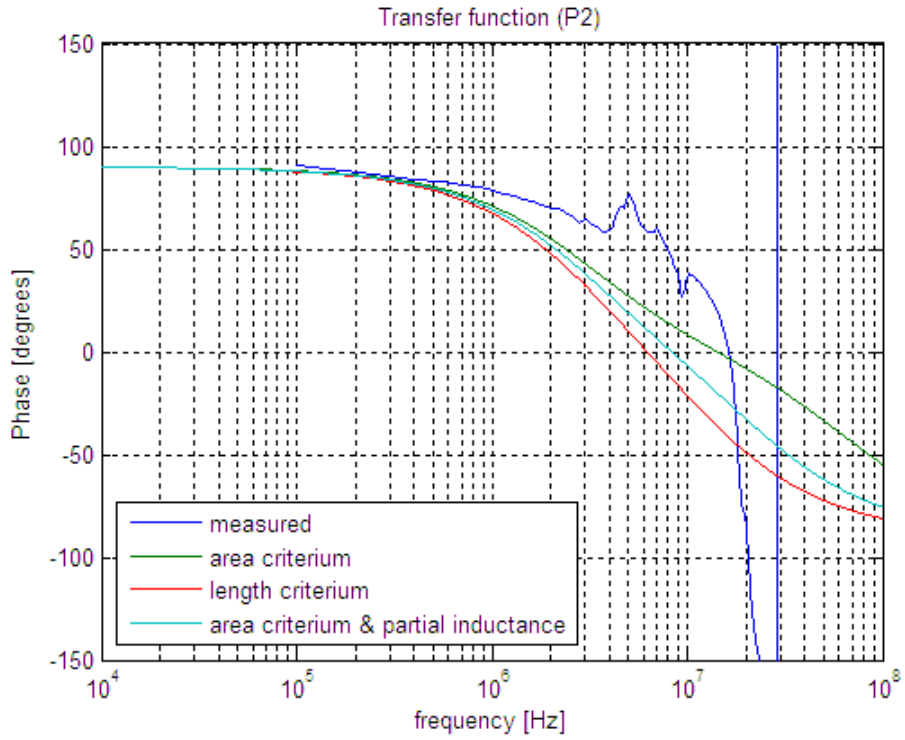


Fig. 122 Phase of transfer function for the test board P2.

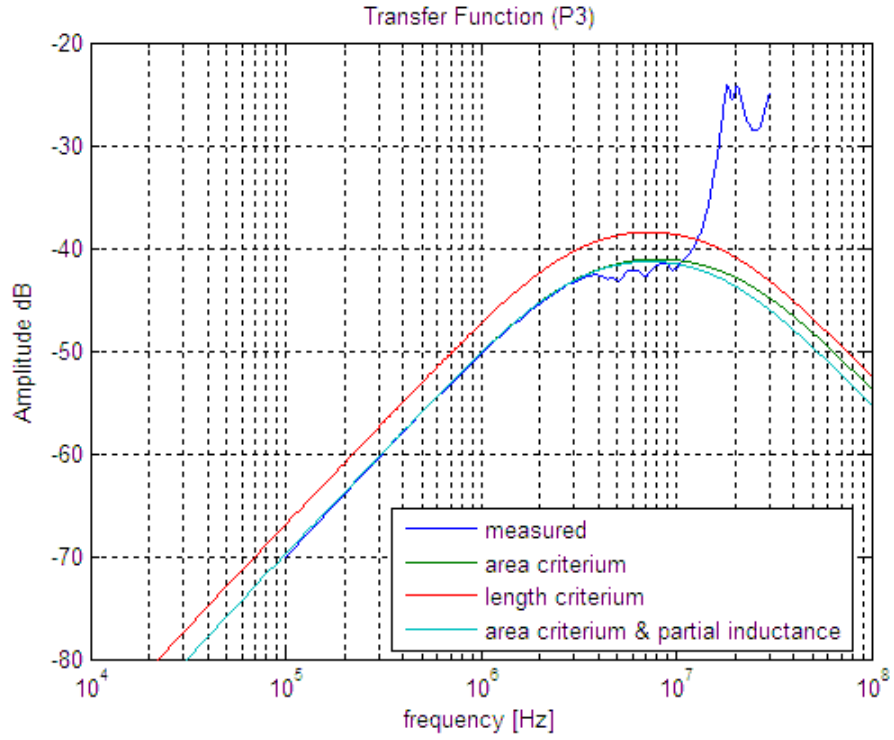


Fig. 123 Magnitude of transfer function for the test board P3.

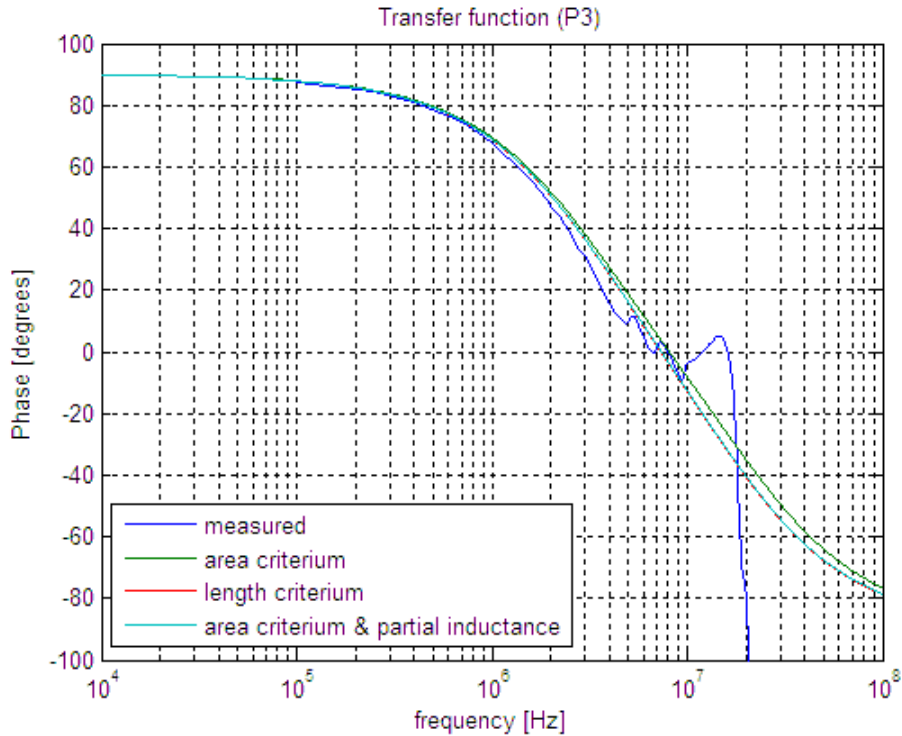


Fig. 124 Phase of transfer function for the test board P3.

The proposed model which parameters are computed using the same area criterion shows a very good agreement with experimental results for all the test boards.

For complex geometry trace, the model which parameters are calculated with the area criterium for the mutual inductance and partial inductance method for the self inductance can be either used. The model shows a very good agreement with experimental results up to 10 MHz.

For this particular configuration one point of the receiving loop is connected to ground and the loop behaves as a $\lambda/4$ resonant dipole at about 24 MHz.

Generally the loop antenna is not connected to ground and its resonance frequency ($\lambda/2$) is about 48 MHz and this allows to extend the frequency range of the model up to 30 MHz.

An intrinsic limitation to the model consists in the fact that it doesn't take into account the spatial density current and voltage distribution on the receiving loop and this doesn't allow to predict the resonant peak of the magnitude of transfer function and the shift of phase at about 20 MHz.

VI. Closed formula for mutual capacitance

The mutual capacitance between some smooth metal piece (ex: an heatsink) and the TLA can be calculated with good approximation using the formula for a spherical capacitor [10]

$$C_{12} = 4\pi\epsilon \frac{r_{eq} \cdot r_2}{r_2 - r_{eq}}, \quad (3.11)$$

being r_2 the radius of the TLA, ϵ the permeability of the medium and r_{eq} the radius of the equivalent sphere of the heatsink. Different real heatsink geometries are simulated with an electromagnetic numerical code [15] (FIT technique) and compared with the results obtained with (1.12). The self capacitance of the heatsink (source) can be computed using

$$C_1 = 4\pi\epsilon r_{eq} \quad (3.12)$$

being r_{eq} the radius of the equivalent source according to the different criteria.

Both self and mutual capacitance can be calculated using two different methodologies:

- the same surface criterion
- the same volume criterion.

For the same surface criterion, $r_{eq} = \sqrt{\frac{S}{4\pi}}$ being S the surface of the exposed metal object,

and for the same volume criterion $r_{eq} = \sqrt[3]{\frac{3V}{4\pi}}$ with V the volume of the exposed metal object.

The self capacitance of the TLA can be computed with [16]

$$C_2 = 3 \frac{2\epsilon r_2}{\left[\text{Ln}\left(\frac{16r_2}{d_2}\right) - 2 \right]} \quad (3.13)$$

being d_2 the diameter of the wire section of the loop.

Firstly, two test simulations are considered:

Test A is a single sphere in free space which self capacitance is calculated by (1.13)

Test B is a sphere inside a TLA; a voltage source is connected between sphere and TLA and the equivalent capacitance from the voltage source is calculated as

$$C_{eq} = C_{12} + \frac{C_1 \cdot C_2}{C_1 + C_2} \quad (3.14)$$

The imaginary part of the self admittance of the sphere and the equivalent admittance between the sphere and the TLA is computed and compared with the admittance computed using (1.13) and (1.15).

Tab.5 summarizes the values calculated using (1.15),(1.14),(1.13) in Test A and Test B.

Test A / Test B			
Input dimension	Value [m]	Parameter output	Value [pF]
R ₁	0.1000	C ₁	11
R ₂	0.0508	C ₂	7
D ₂	0.0240	C ₁₂	14

Tab. 18 Test A and B parameter values.

The results are shown in Figs. 29-30.

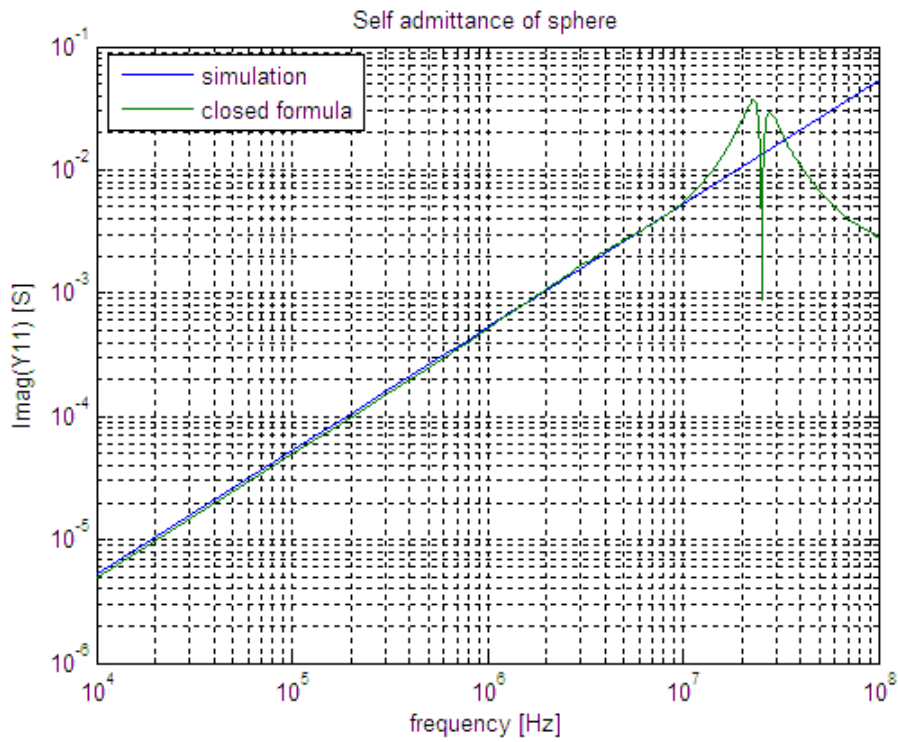


Fig. 125 Imaginary part of self admittance of the sphere in Test A

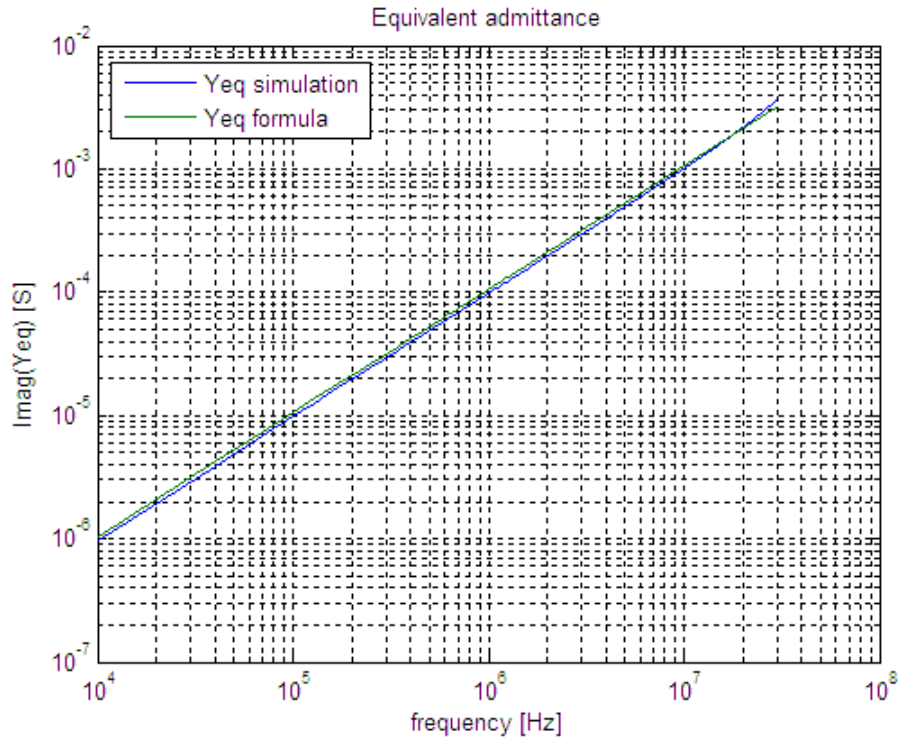


Fig. 126 Imaginary part of equivalent admittance in Test B

Different real heatsinks are simulated with numerical simulator based on a FIT technique [15]. Each of them are set in the TLA and the equivalent capacitance from the source is computed and compared with the results of (1.15).

The equivalent radius of the heatsink can be calculated using the same surface criterion or the same volume criterion as already mentioned. The simulated test heatsinks are presented in in Figs.31-33.

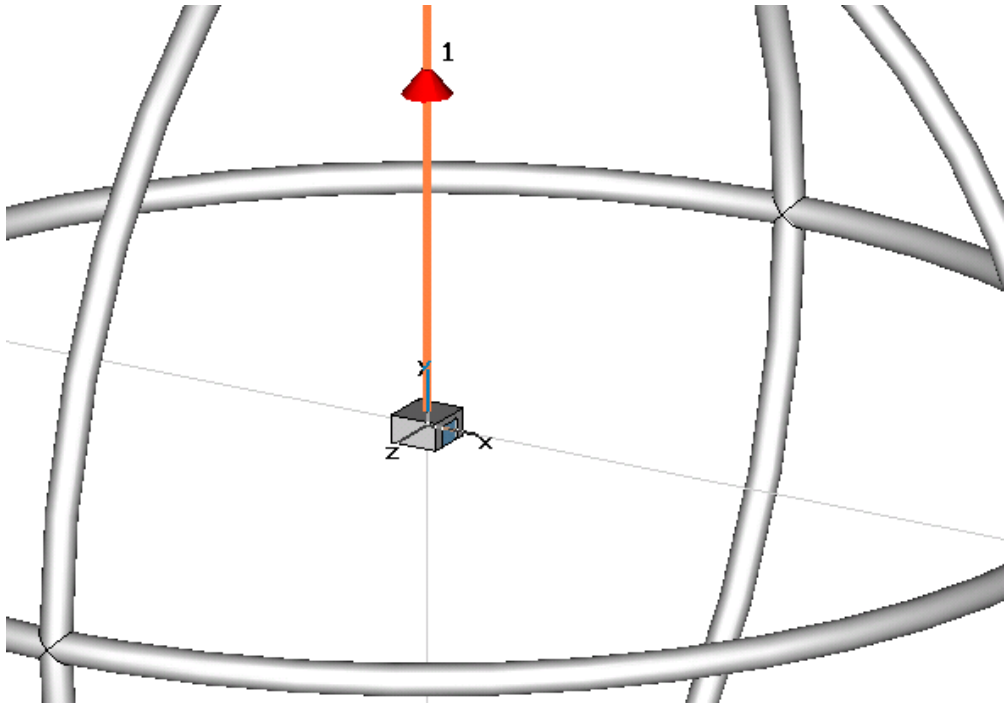


Fig.127 Test heatsink Q1

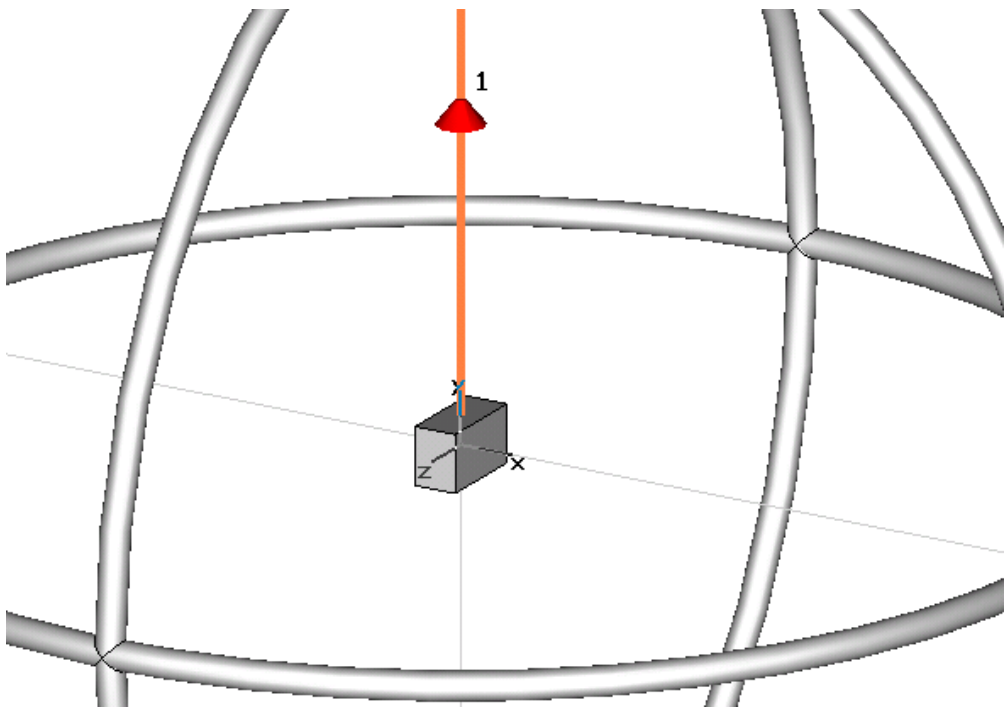


Fig.128 Test heatsink Q2

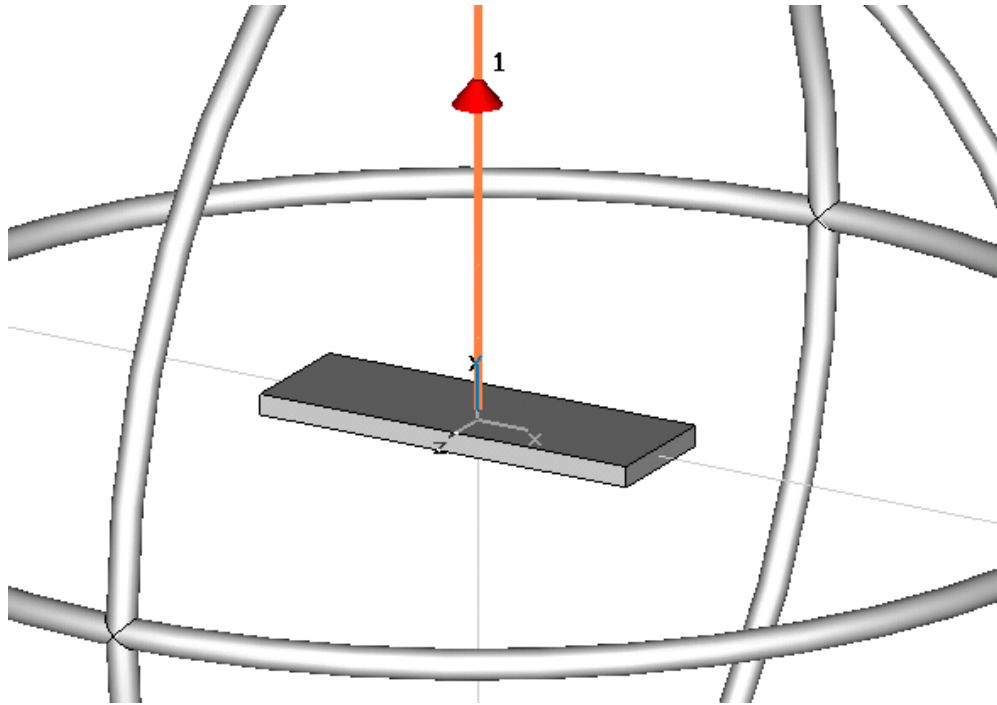


Fig.129 Test heatsink P3

The results obtained for the equivalent admittance $\hat{Y}_{eq} = j\omega C_{eq}$ are shown in Figs. 34-36.

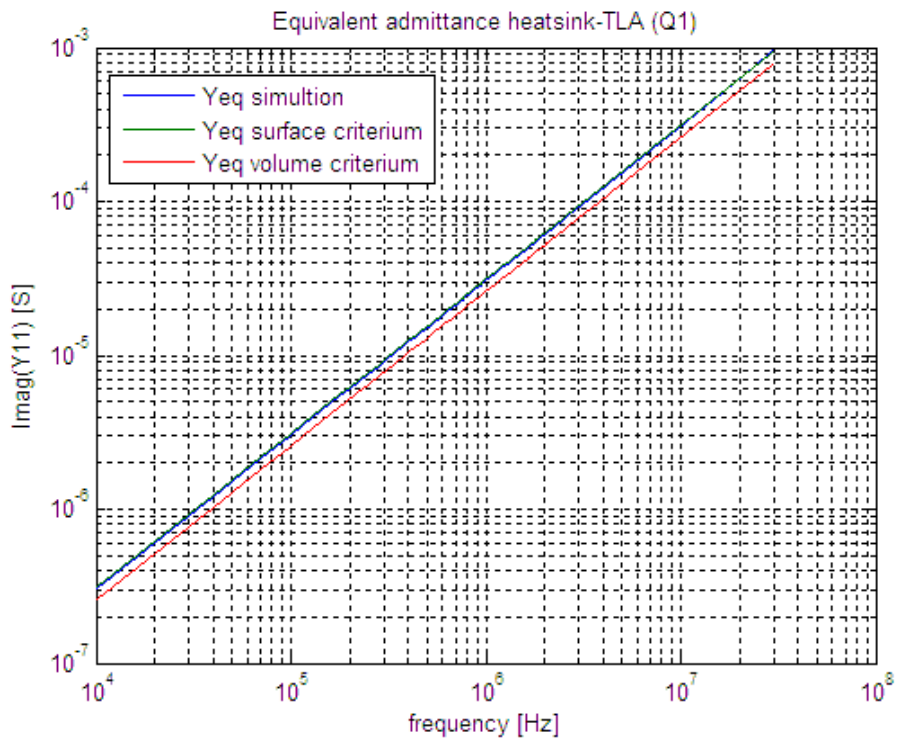


Fig. 130 Imaginary part of equivalent admittance of heatsink-TLA (Test board Q1)

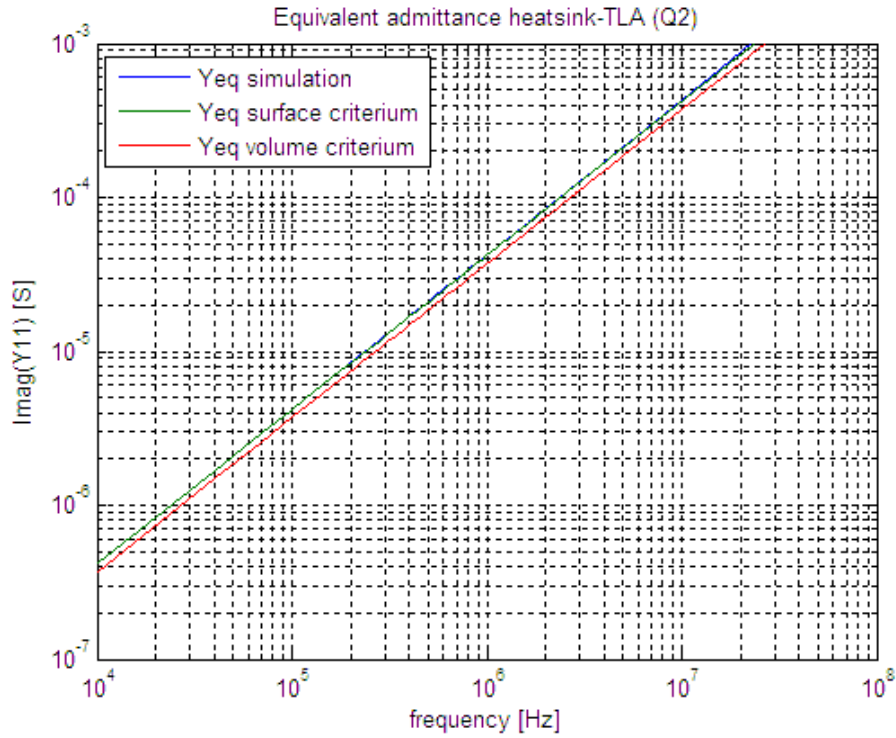


Fig. 131 Imaginary part of equivalent admittance heatsink-TLA (Test board Q2)

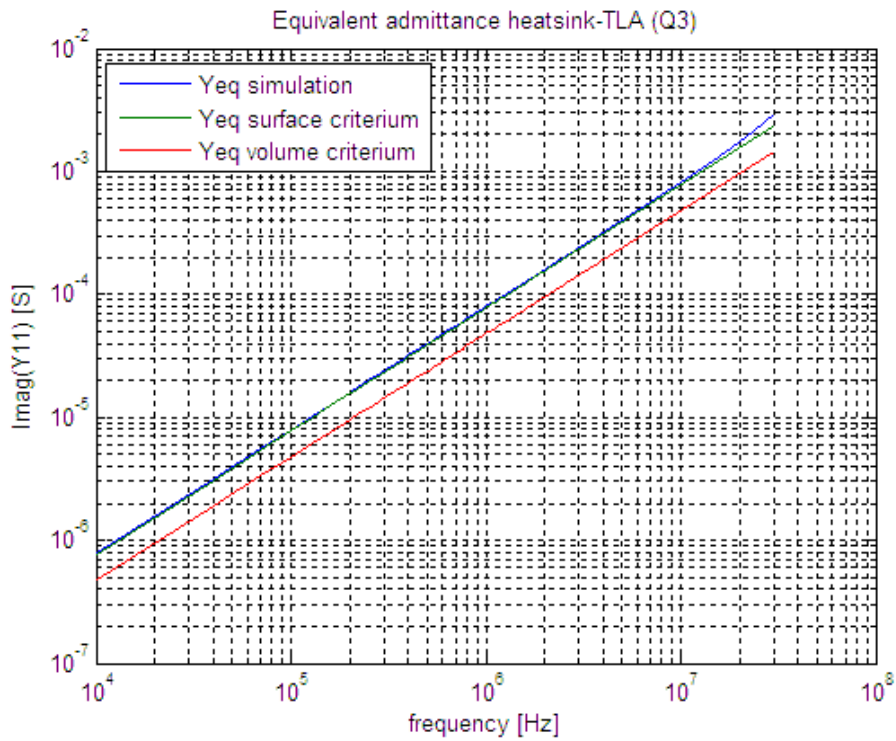


Fig. 132 Imaginary part of equivalent admittance heatsink-TLA (Test board Q3)

Tabs.6-7 summarize the input parameter values and the computed parameters for the different test heatsinks.

Input parameter values	Q1	Q2	Q3
Surface [mq]	0.004608	0.015220	0.087184
Volume [mc]	0.00001656	0.000118864	0.0004896

Tab. 19 Input parameter values for the test heatsink.

Computed parameter values	Q1	Q2	Q3
Mutual C area criterion [pF]	3	4	11
Mutual C volume criterion [pF]	2	3	6
Self C area criterion [pF]	3	4	9
Self C volume criterion [pF]	2	3	5
Self TLA C [pF]	7	7	7

Tab. 20 Computed parameter values for the test heatsink.

The results clearly show that the same surface criterion for calculation of mutual capacitance between the heatsink and the TLA get to better agreements with simulation results.

The actual values of the imaginary part of the mutual and self impedance can be considered as an apparent inductance which value depends on frequency and parasitic inductance.

VII. Experimental validation of electric coupling

A network analyser (NA) is used to measure the transfer function between one of the test heatsink Q1, Q2, Q3 and one gaped loop of the TLA. The NA RF source is terminated with a 47 Ω resistor, to minimize the reflected power at the input port; one of the resistor's termination is connected to a copper plane strictly bound to the heatsink. One gap of the loop is shorted with copper tape and the other is chosen as output port to the NA. The equivalent circuit of the test setup is presented in Fig.37.

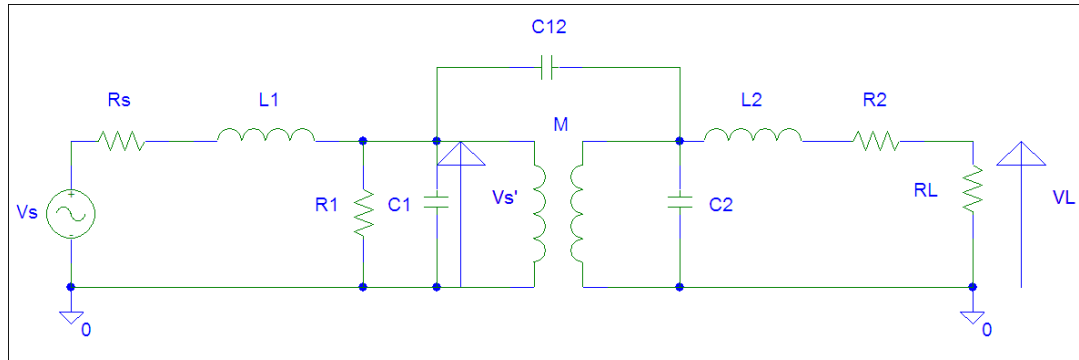


Fig. 133 Equivalent circuit for mutual capacitive coupling between test heatsink and receiving loop.

The transfer function can be simply calculated neglecting the self capacitance and self inductance of the source and the mutual inductance between heatsink and the receiving loop.

Under these assumptions $\hat{V}_S^i \approx \frac{\hat{V}_S}{2}$ and

$$\hat{H}_E = \frac{R_L}{1 + j\omega C_2(R_2 + j\omega L_2 + R_L)} j\omega C_{12} \frac{\hat{V}_S^i}{1 + j\omega C_{12} \frac{(R_2 + R_L + j\omega L_2)}{1 + j\omega C_2(R_2 + R_L + j\omega L_2)}} \quad (3.15)$$

being $R_L=50 \Omega$ the input resistance of the NA, R_2 and L_2 the resistance and self inductance of the receiving loop, R_S the Thevenin equivalent resistance of the source, R_1 and L_1 the resistance and self inductance of the test boards bound to the heatsink.

Tab.8 presents the parameter's values of the transfer function for the different test heatsinks.

Parameter values	Q1	Q2	Q3
R_L [Ω]	50	50	50

R_2 [Ω]	2	2	2
L_2 [μ H]	2.60	2.60	2.60
R_1 [Ω]	47	47	47
R_s [Ω]	50	50	50
L_1 [nH]	5	5	5
M [nH]	<5	<5	<5
C_{12} area criterion [pF]	3	4	11
C_{12} volume criterion [pF]	2	3	6
C_1 area criterion [pF]	3	4	9
C_1 volume criterion [pF]	2	3	5
C_2 [pF]	7	7	7

Tab. 21 Parameter values for the test heatsink.

The values of the self inductance in Tab.8 are computed using formula of the rectangular loop [5] and the values of the mutual inductance can be supposed to be always less than the self inductance values. Those parameters show that they can be neglected compared to the value of self and mutual capacitance in the equivalent circuit in Fig.37.

Test heatsinks Q1, Q2, Q3 are shown in Figs.38-40.

The magnitude and phase of the transfer function (1.16) are measured and compared with those computed with:

3. mutual and self capacitance computed using the same surface criterium,
4. mutual and self capacitance computed using the same volume criterium.

The results obtained are presented in Fig.41-46.



Fig. 134 Test heatsink Q1



Fig. 135 Test heatsink Q2



Fig. 136 Test heatsink Q3

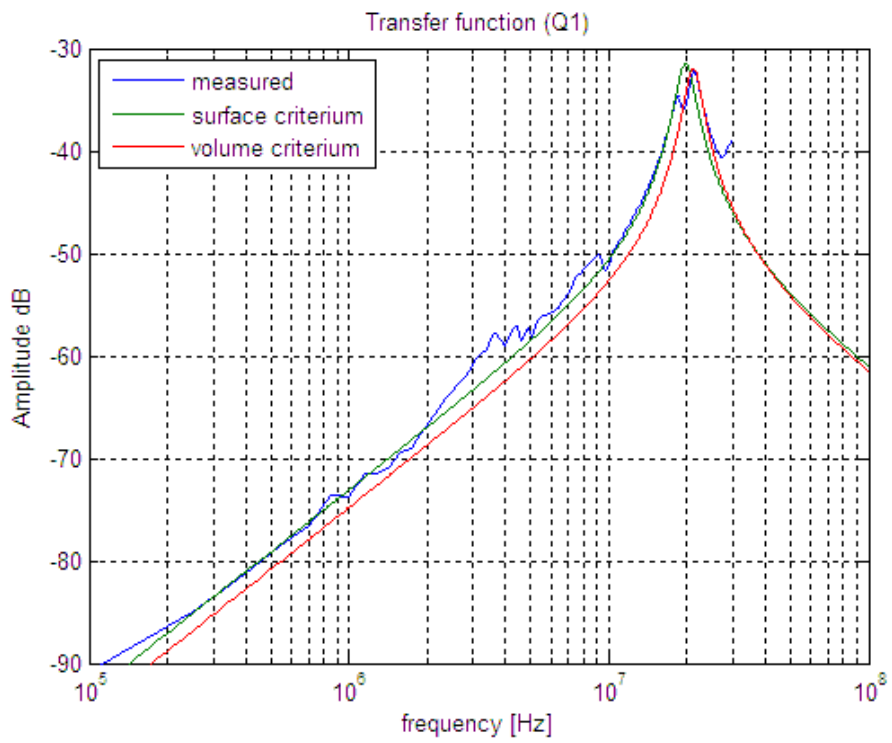


Fig. 137 Magnitude of transfer function for the test heatsink Q1.

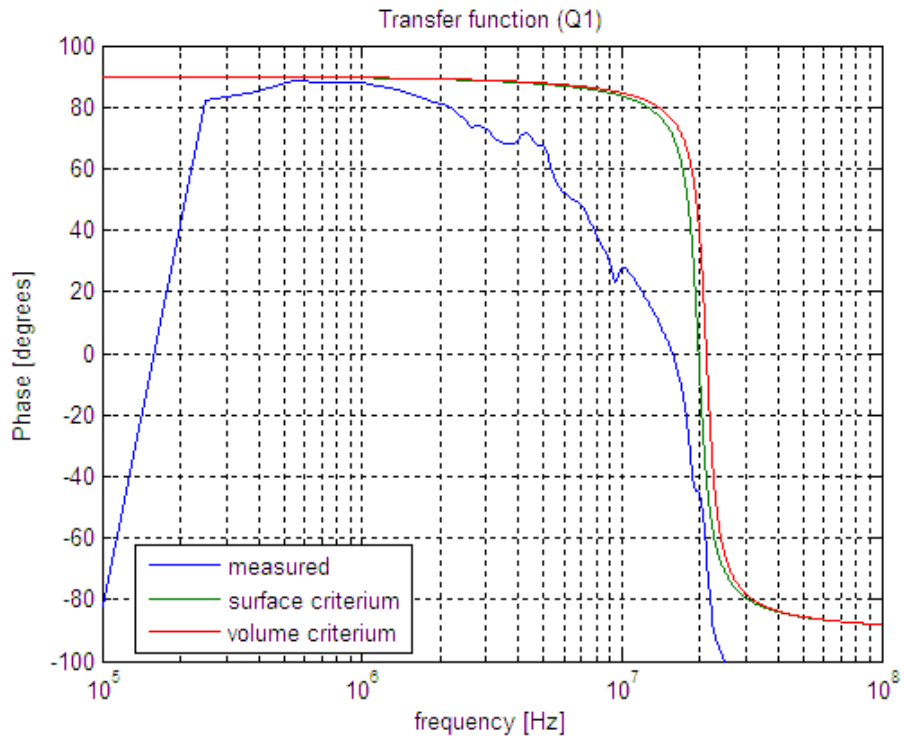


Fig. 138 Phase of transfer function for the test heatsink Q1.

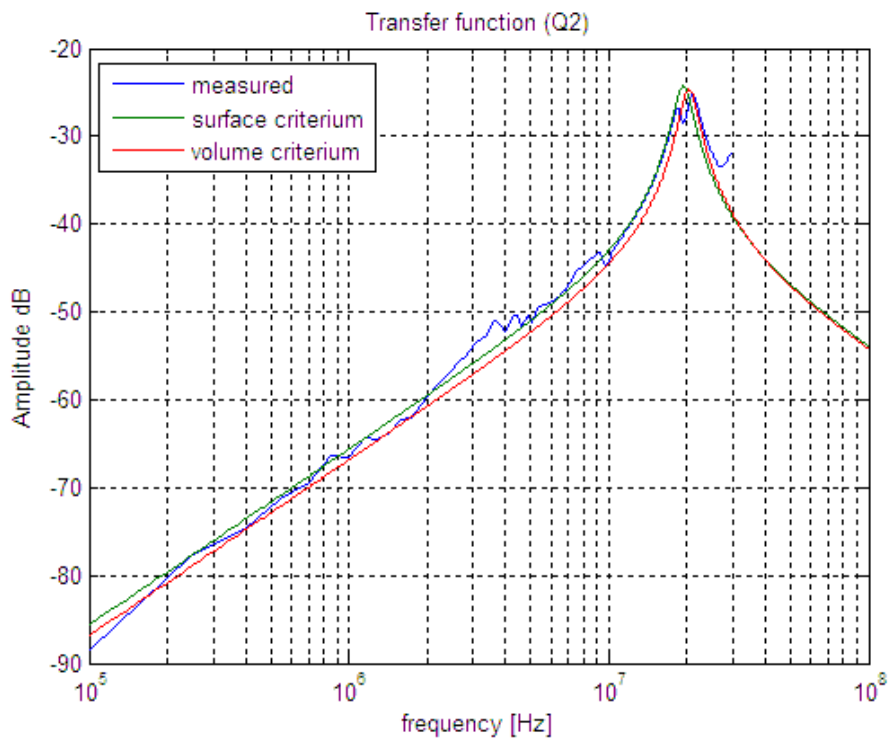


Fig. 139 Magnitude of transfer function for the test heatsink Q2.

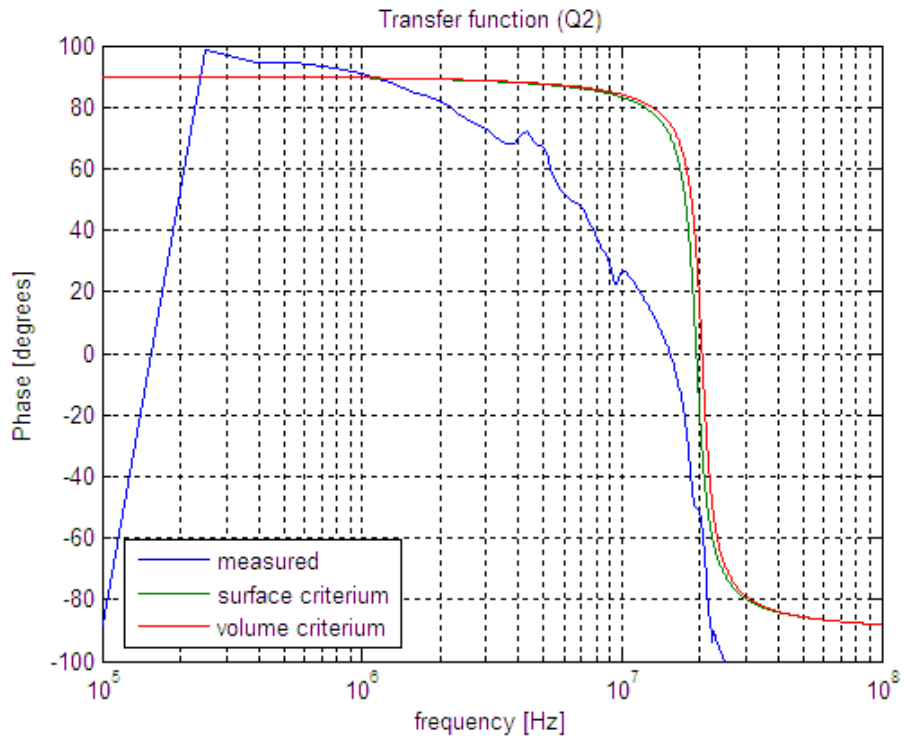


Fig. 140 Phase of transfer function for the test heatsink Q2.

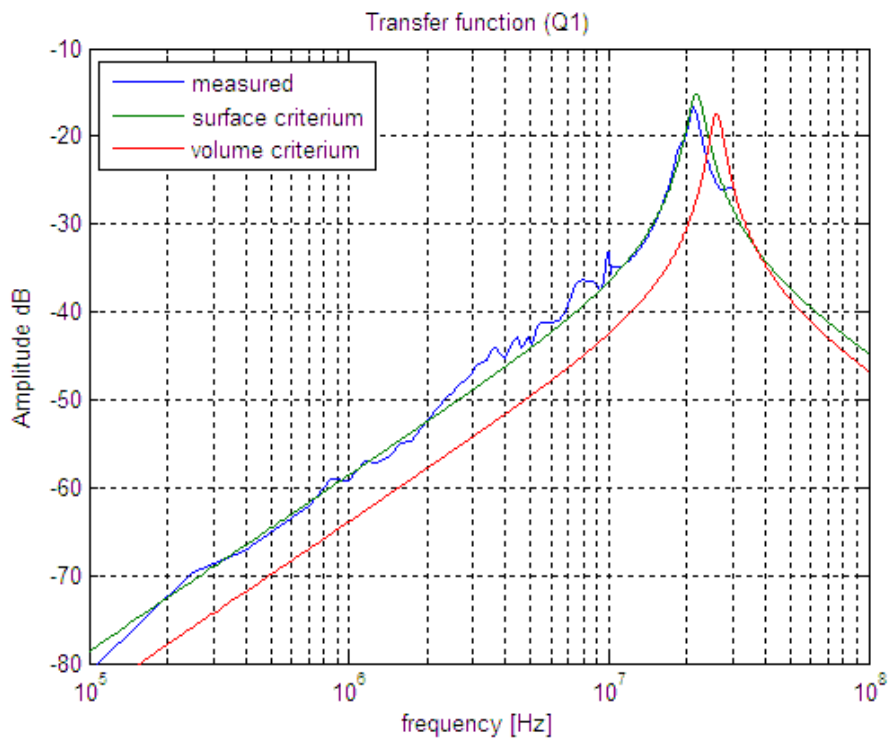


Fig. 141 Magnitude of transfer function for the test heatsink Q3.

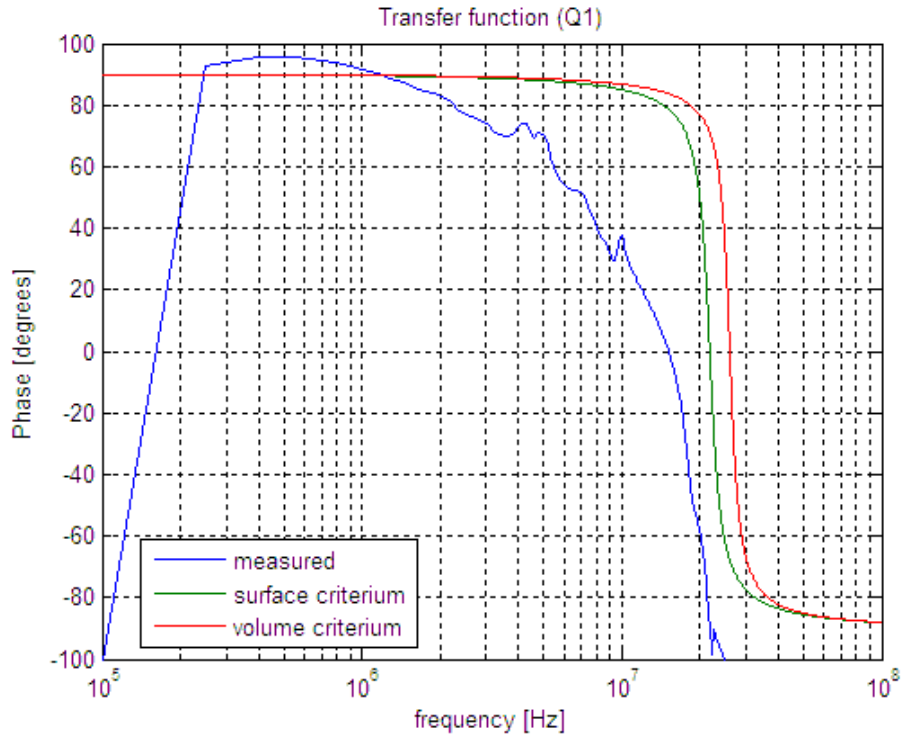


Fig. 142 Phase of transfer function for the test heatsink Q3.

The proposed model (1.16) which parameters are computed using the same surface criterion shows a good agreement with experimental results for all the test heatsinks.

Some more investigation in the phase plots differences would be necessary but so far it is possible to underline that the general behaviour of the transfer function is well represented by the proposed model.

The accuracy when measuring the amplitude and phase transfer function in is ± 1 dB and ± 6 degrees.

6 CONCLUSIONS

In this thesis, an algorithm has been developed to estimate the “radiated” emissions from SMPS.

A resistance-inductance-capacitance (RLC) model is described for estimating current waveforms in digital CMOS circuits. The model is based on parameters that are readily derived from information available in board layout files and component data sheets or IBIS files. Compared with the simpler triangular waveform traditionally used to approximate current in CMOS circuits, the RLC model more accurately estimates the shape of the current waveform in the time domain and the amplitudes of the upper harmonics in the frequency domain.

This model can be applied to estimate the current spectrum in the primary and secondary loop of the transformer in a SMPS, primary source of noise in power converters. A secondary source of noise has been also figure out for this circuits to be the voltage between the heatsinks and a ground reference point. The current noise sources are magnetically coupled to any sensible receiving loop in the surrounding and the voltage noise sources are electrically coupled to any sensible receiving in the surrounding.

In near field and in case of weak coupling between source and victim, magnetic and electrical coupling mechanisms can be described by simple equivalent circuit presented in this thesis. To validate the proposed model a TLA has been built and used. Simple closed formulas can be used to describe the mutual inductive and capacitive coupling between the source and the TLA.

The proposed algorithm is applied to a commercial SMPS for personal computer predicting the receiving voltage noise in a TLA with very good agreement.

Appendix A

NOTE on FFT

For a given signal $x(t)$, its periodic repetition $x_T(t)$ is defined as,

$$x_T(t) = \sum_k x(t - kT) ;$$

$X(f)$ and $X_T(f)$ are their Fourier transforms

$$X_T(f) = \sum_n x(f - nF)$$

being T and F respectively the periods of the functions.

The previous functions can be sampled with N sample per period and the sample steps as

$$\Delta t = \frac{T}{N} , \Delta f = \frac{F}{N} \text{ with } TF=N.$$

Now the sampled functions are

$$\hat{x}_n \triangleq x_T(n) = x_T(n\Delta t) \text{ and } \hat{X}_q \triangleq X_T(q) = X_T(q\Delta f) \text{ for } n, q=0, \dots, N-1$$

And the relationship between them is

$$\hat{X} = \Delta t \cdot DFT[\hat{x}] \text{ and } \hat{x} = \frac{IDFT[\hat{X}]}{\Delta t}$$

The DFT and IDFT are respectively defined as follows

$$X_q = \sum_{k=0}^{N-1} x_k e^{-\frac{j2\pi kq}{N}} \quad q=0, \dots, N-1$$

$$x_n = \frac{1}{N} \sum_{q=0}^{N-1} X_q e^{\frac{j2\pi nq}{N}} \quad n=0, \dots, N-1.$$

This kind of algorithm is very useful for frequency domain analysis of signals but very time consuming. The FFT are a family of efficient algorithms for computing the DFTs and IDFTs and are often use by different kind of software as Matlab and Spice

Gibbs phenomenon.

While working with time and frequency analysis remind that a truncation in frequency domain of a discrete sequence rise oscillations up in time domain, while a truncation in time domain yield to oscillations in frequency domain.

MATLAB FFT

An example of Matlab FFT routine for even and odd time vector sample is presented

Even Routine

```
x=linspace(0,12,512);
```

```
y=5*sin(0.5*2*pi*x);
```

```
N=length(x);
```

```
Tsample=x(2)-x(1);
```

```
fs=1/Tsample;
```

```
fn=fs/2;
```

```
f=[0:1:(N/2-1)]/(N*Tsample);
```

```
If=fft(y)*Tsample/(2*pi);
```

```
Iff=abs(If(1:(N/2)));
```

```
Ifff=20*log10(Iff);
```

Odd Routine

```
x=linspace(0,12,513);
```

```
y=5*sin(0.5*2*pi*x);
```

```
N=length(x);
```

```
Tsample=x(2)-x(1);
```

```
fs=1/Tsample;
```

```

fn=fs/2;

f=[0:1:(N-1)/2]/(N*Tsample);

If=fft(y)*Tsample/(2*pi);
Iff=abs(If(1:(N+1)/2));
Ifff=20*log10(Iff);

```

.....

The Matlab FFT compute the Fourier Series coefficients of a signals as shown in Fig.1-3.

SPICE FFT

SPICE simulator use a FFT algorithm to compute the Fourier spectrum coefficients with a uniform sampling in frequency domain.

The same periodic trapezoidal waveform is considered in SPICE simulator and the Spice FFT is applied using different number of period of the waveform. These are shown in Figs 4-6. Using the Spice FFT algorithm with few periods or a non integer number of period as shown in Figs.4-6 leads to amplitude and frequency inaccuracy. The time domain signal resulting from PSPICE simulation is not uniform sampled in time domain, therefore applying the Matlab FFT provide wrong results as shown in fig.7.

Both Matlab and PSPICE FFT algorithms compute the Fourier spectrum coefficients measured in [V] or [W] and require an integer number of periods in time domain (at least 3 periods). For broad-band signals, the same periodic waveform can be displayed by its Spectral density [V/Hz] or [W/Hz] $X(f)$.

The relationships between Fourier coefficients for a periodic signal and the spectral density of the same signal are

$$C_k = \frac{X(f)}{T_1} \Big|_{jk2\pi f_1} \quad \text{and} \quad C_0 = \frac{X(f)}{T_1} \Big|_{jk0}$$

The spectral density is more useful than the Fourier coefficients because is independent from pulse repetition rate and remains true for a single pulse. For a narrow-band signals the spectrum shown by a Spectrum Analyzer is

$$A_k = \frac{2C_k}{\sqrt{2}} \quad \text{and} \quad A_0 = \frac{C_0}{\sqrt{2}}$$

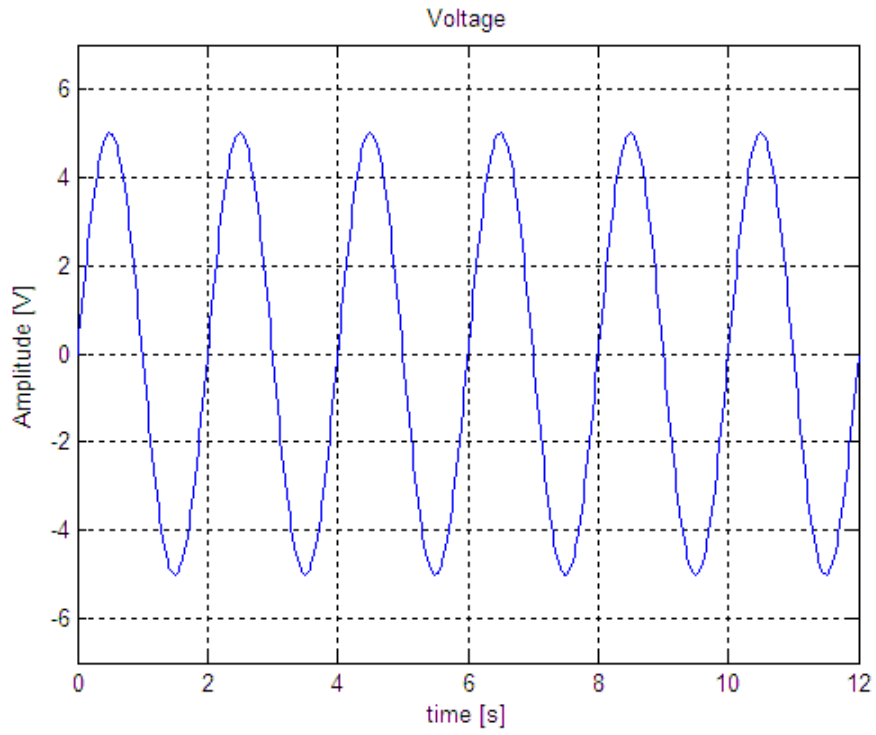


Fig. 143 Time signal 5 V amplitude and 0.5 Hz frequency.

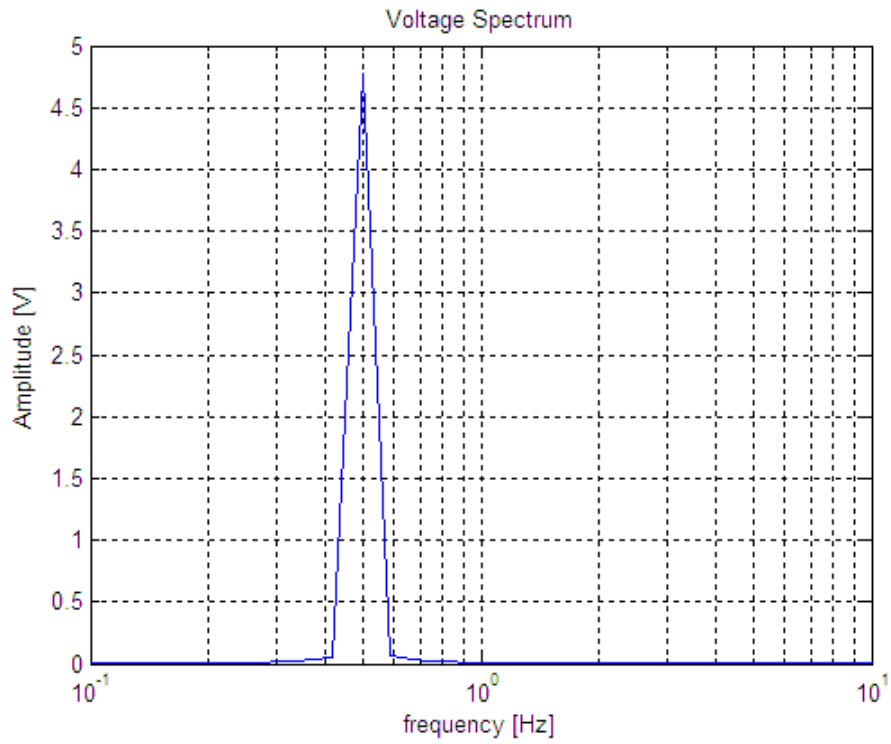


Fig. 144 Matlab FFT of the previous signal with odd or even sample.

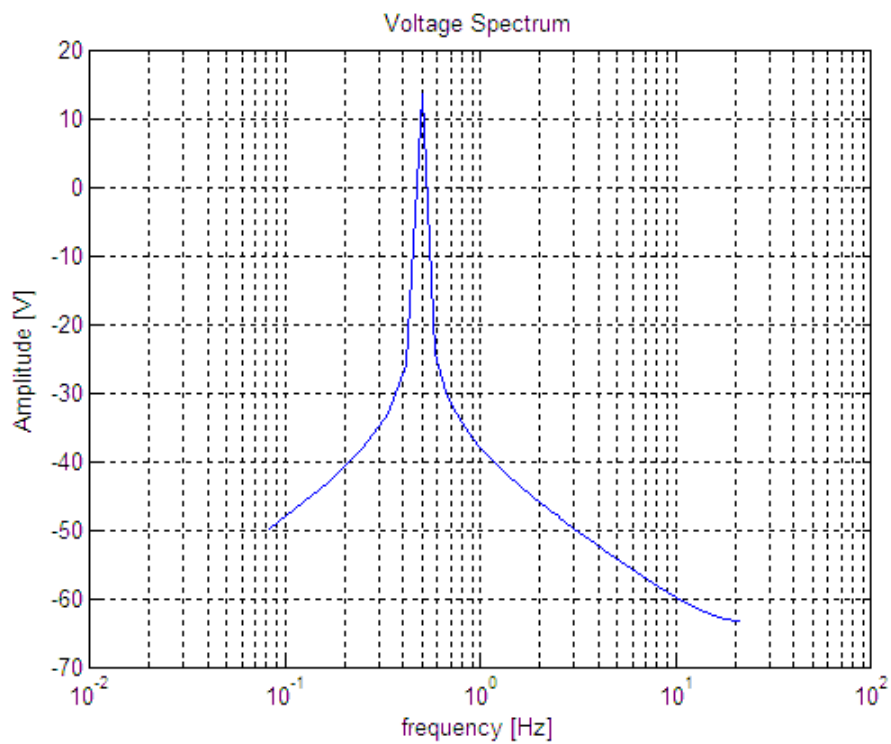


Fig. 145 Matlab FFT of the previous signal (amplitude in dB).

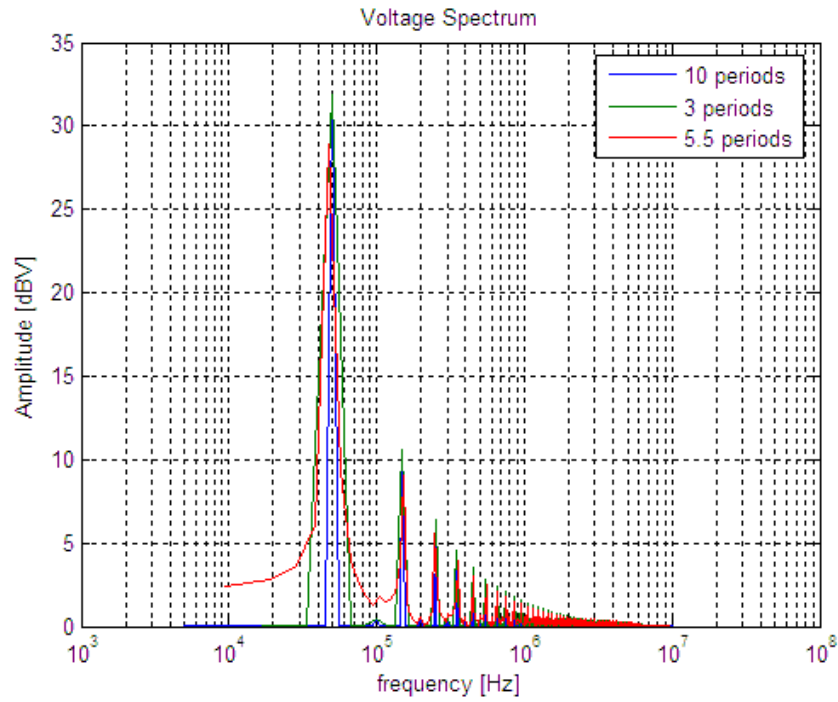


Fig. 146 Frequency Spectrum of a trapezoidal waveform computed using PSPICE FFT algorithm for different periods.

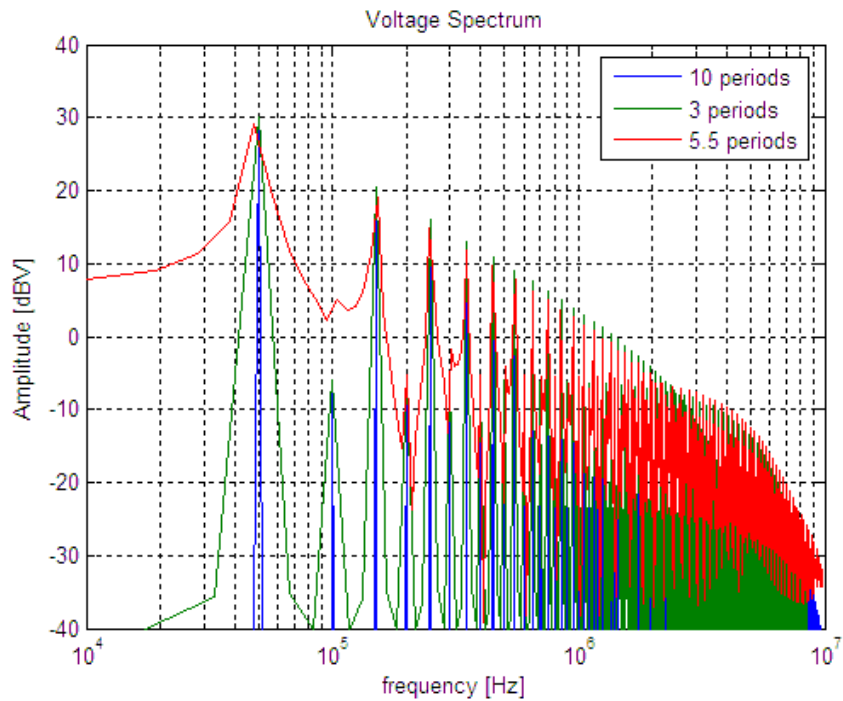


Fig. 147 Frequency Spectrum of a trapezoidal waveform computed using PSPICE FFT algorithm for different periods.

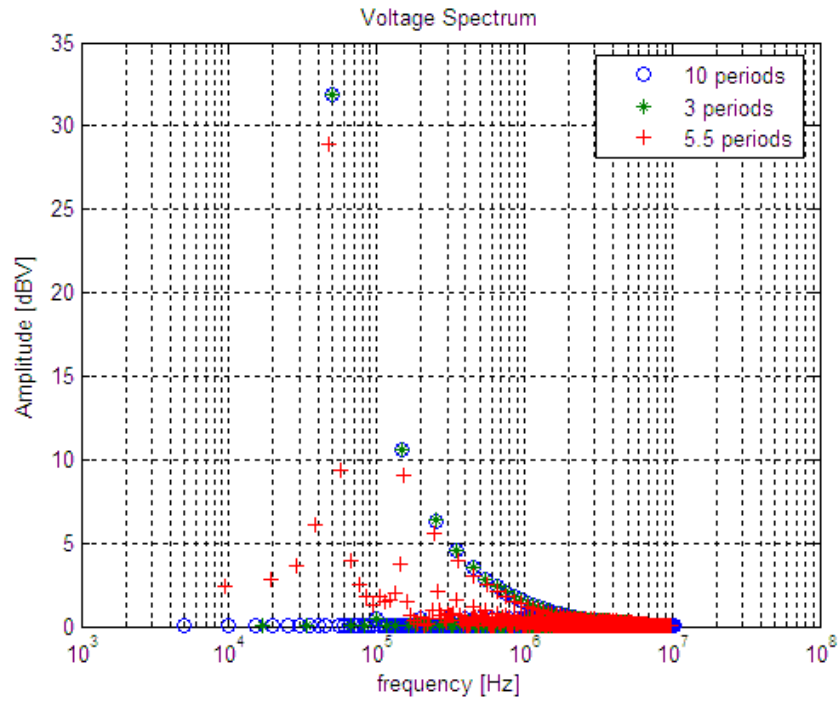


Fig. 148 Frequency Spectrum of a trapezoidal waveform computed using PSPICE FFT algorithm for different periods.

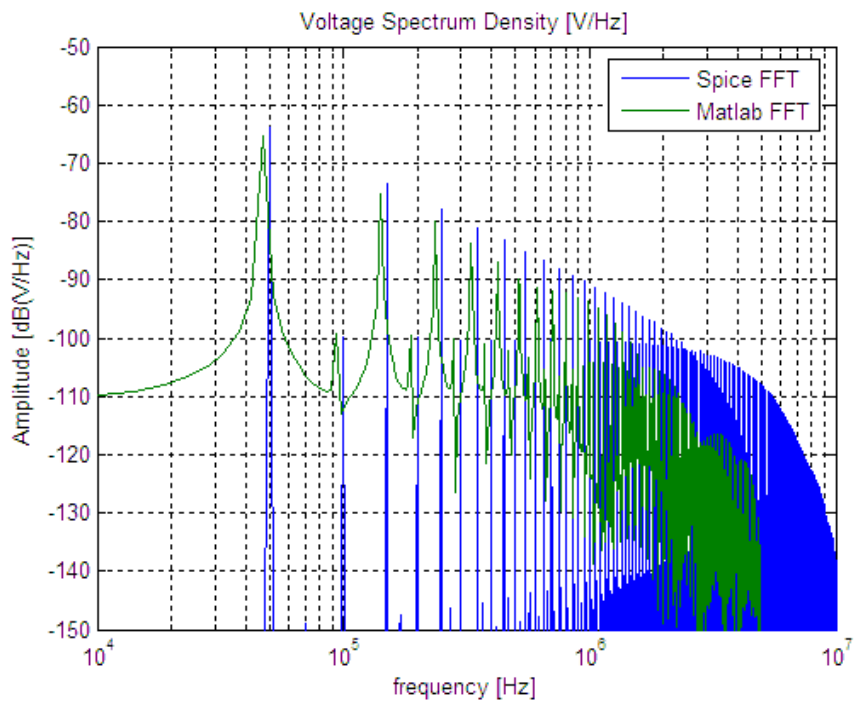


Fig. 149 Matlab FFT applied to time domain waveform obtained by PSPICE simulation.

Equation Chapter 1 Section 1 DIODE equivalent linear component

When a diode is forward biased, it begins to conduct with only a small forward voltage across it, which is on the order of 1 V. When a diode is reverse biased, only a negligibly small leakage current flows through the device until the reverse break-down voltage is reached. The i - v characteristic for the diode can be idealized, as shown in Fig.1. This idealized characteristic can be used for analyzing the converter topology but should not be used for the actual converter design.

At turn-on, the diode can be considered as an ideal switch because it turns on rapidly compared to the transients in the power circuit. However, at turn-off, the diode current reverses for a reverse-recovery time, before falling to zero. Fast recovery diodes are designed to be used in high-frequency circuits in combination with controllable switches where a small reverse-recovery time is needed. At power levels of several hundred volts and several hundred amperes, such diodes have reverse recovery time ratings of less than a few microseconds.

In the on state the equivalent series resistance of the diode can be simply calculated as

$$R_{DIODE} = \frac{V_F}{I_F} \quad (1.1)$$

being V_F and I_F the forward voltage and the correspondently average forward current available from datasheets. In off state the equivalent series capacitors of the diode C_{DIODE} can be obtained from datasheets at the reverse voltage.

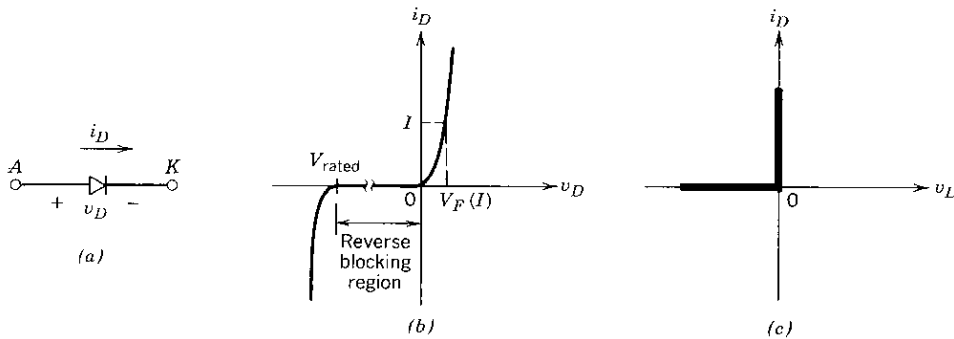


Fig. 150 Diode (a) symbol, (b) i - v characteristic, (c) idealized characteristic.

BJT equivalent linear component

The circuit symbol for an NPN BJT is shown in Fig.2a, and its steady-state $i-v$ characteristics are shown in Fig.2b. As shown in the $i-v$ characteristics, a sufficiently large base current (dependent on the collector current) results in the device being fully on. This requires that the control circuit provide a base current that is sufficiently large so that

$$I_B > \frac{I_C}{h_{FE}} \quad (1.2)$$

being h_{FE} is the DC current gain of the device simply readable from datasheet.

The on-state voltage $V_{CE(sat)}$ of the power transistors is usually in the 1- 2 V range, so that the conduction power loss in the BJT is quite small. The idealized $i-v$ characteristics of the BJT operating as a switch are shown in Fig.2c.

Bipolar junction transistors are current-controlled devices, and base current must be supplied continuously to keep them in the on state. In the on state the equivalent resistance between collector and emitter can be computed by

$$R_{CE} = \frac{V_{CEsat}}{I_C} \quad (1.3)$$

being V_{CEsat} the collector-emitter saturation voltage for given I_B available from datasheets. In the off state the capacitance C_{CE} between collector and emitter can be measured or found out from datasheet. Typical switching times are in the range of a few hundred nanoseconds to a few microseconds.

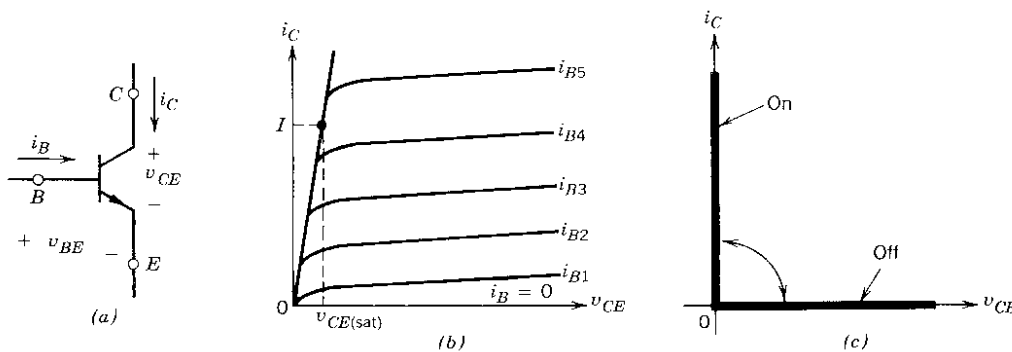


Fig. 151 BJT: (a) symbol, (b) $i-v$ characteristics, (c) idealized characteristics.